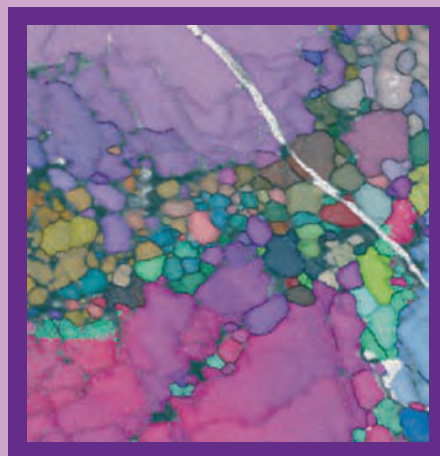


SEMINARIOS DE LA SOCIEDAD ESPAÑOLA DE MINERALOGÍA

VOLUMEN 5

Instrumental Techniques Applied to Mineralogy and Geochemistry

Zaragoza, 16 de septiembre de 2008



S.E.M.

Editores:

Ignacio Subias y Blanca Bauluz
Universidad de Zaragoza



Patrocinadores:



**SEMINARIOS DE LA SOCIEDAD ESPAÑOLA
DE MINERALOGIA**

VOLUMEN 5

**INSTRUMENTAL TECHNIQUES APPLIED TO
MINERALOGY AND GEOCHEMISTRY**

Editores:

Ignacio Subías y Blanca Bauluz

© Ignacio Subías y Blanca Bauluz (Editores)
© Sociedad Española de Mineralogía

Depósito legal: CA-602-2004
ISSN: 1698-5478
Impreso en España- Printed in Spain

2008

Impresión: Gráficas Lema s.l.
Monasterio de la Oliva, 4
Teléfono: 976 298 320 – Zaragoza

FOREWORD

On the occasion of the Spanish Society of Mineralogy (SEM) and Spanish Society of Clays (SEA) joint meeting in Zaragoza on September 16th-19th, a workshop on *Instrumental techniques applied to Mineralogy and Geochemistry* is held with the aim of updating the knowledge of young and also senior researchers.

The scope of this workshop includes the most common analytical techniques used in geological and material sciences research mainly covering details of analytical practice and representative and new applications. The treatment is designed to be of interest to the graduate student, as well as the research scientist whose involves the use of analytical techniques and/or the interpretation of analytical results. Consequently, it is hoped that this volume will provide a valuable source for researchers in their respective fields and stimulate future development.

This volume is divided into four topical sections: Electron Microscopy, X-ray absorption Spectroscopy (XAS), Isotope Geology and Fluid Inclusions. The volume follows the same pattern; after a general introduction to the subject, an overview of the technique and its practical applications to understanding geological processes. It is clear that some techniques are further along than others in terms of specific applications, but all of them are promising and have high potential for making important contributions to knowledge.

Accounts of Electron Microscopy include two contributions reflecting the basics and the progress that have been achieved at present. These techniques appear to be useful for solving problems in traditional areas as well as in other fields, such as nanotechnology. The next session, XAS, describes methods involving in detection and characterization of even trace amounts of atoms that are dispersed within minerals. This has been recently exploited also by Environmental scientists working on the understanding of mineralogical and biogeochemical processes. Specific aspects of different techniques and instrumentation will be highlighted on the basis of few examples of their use in mineralogy and geochemistry. The following section deals with

Isotope Geology a discipline, like the already mentioned, capable of contributing significantly to the solution of a wide variety of problems. This is the reason why the first volume of the *Seminarios de la SEM* series was devoted to principles and applications of isotope geochemistry mainly to use this information in all geological branches. In this volume, the aim is to illustrate not only the geological application but also other areas of significant activity. Finally, a session devoted to Fluid Inclusion studies will be useful for workers in any field: the principles, philosophy and procedures expressed herein are applicable to any study, no matter what the emphasis.

In a collective work, such as this volume, the first acknowledgement must go to the invited authors for their willingness to participate and for all their hard work (timely efforts) in the production of the workshop and the resulting volume. We are indeed grateful to the institutions that helped to make both this volume and the *Instrumental techniques applied to Mineralogy and Geochemistry* workshop possible. The University of Zaragoza along with the Faculty of Science strongly support the whole organization of the workshop. The Ciencia y Tecnología department (Gobierno de Aragón), the Instituto Geológico y Minero de España, Colegio Oficial de Geólogos and SAMCA mining company provided generous financial support to the organization and printing of this volume, making possible to the same time its distribution to all SEM and SEA members and to the libraries of the main universities and research institutions.

Ignacio Subías
Blanca Bauluz
Universidad de Zaragoza
July 2008

INDEX

Electron back-scattered diffraction (EBSD) in
the SEM: applications to microstructures in minerals
and rocks and recent technological advancements 7

Elisabetta Mariani

TEM in Geology. Basics and applications21

Fernando Nieto García

X-ray absorption spectroscopy in Mineralogy and
in the Earth and Environmental sciences 43

Jesús Chaboy Nalda

Raman, conventional infrared and synchrotron infrared
spectroscopy in Mineralogy and Geochemistry: basics
and applications 57

Biliana Gasharova

Alike as two water drops: distinguishing one source
of the same substance from another 83

Clemente Recio Hernández

Radiogenic isotopes and their applications within
a range of scientific fields 111

Kjell Bilström

Analytical techniques applied to fluid inclusions studies:
basics and applications133

Salvador Morales Ruano

Electron backscatter diffraction (EBSD) in the SEM: applications to microstructures in minerals and rocks and recent technological advancements

Elisabetta Mariani^a, D. J. Prior^a, D. McNamara^a, M. A. Pearce^a, N. Seaton^b, G. Seward^c, D. Tatham^a and J. Wheeler^a

^aDepartment of Earth and Ocean Sciences, University of Liverpool, Liverpool L69 3GP, UK

^bDepartment of Geology and Geophysics, University of Minnesota, Minneapolis, MN 55455, USA

^cDepartment of Geology, University of California, Santa Barbara, CA 93106-9630 USA

Abstract

Electron backscatter diffraction (EBSD) is based on the principle that a beam of electrons generated in the scanning electron microscope (SEM) is the source of randomly scattered electrons in a specimen. The backscattered electrons (BSE) that escape the sample generate a Kikuchi pattern on a phosphor screen, which is linked to the specimen crystal structure. Different crystal orientations generate different EBSPs. EBSD provides orientation, misorientation and boundary measurements from a small area (>1 μm) in a crystal and automated EBSD analysis is applied to an increasingly large number of rock-forming minerals. Excellent results are obtained for example on calcite and quartz and recent achievements include successful automated indexing of low symmetry minerals such as feldspars and omphacite. The effective application of EBSD to mineralogy and petrology has increased and includes detailed studies of microstructures, twin boundaries, deformation mechanisms and metamorphic processes. A technique for in-situ high temperature tensile deformation of minerals and rocks is currently being developed.

Introduction

The analysis of 1) crystallographic orientations and misorientations and 2) the geometry and structure of subgrain and grain boundaries is fundamental to a comprehensive petrographic study of any rock sample. In the past quantitative information on 1) and 2) was gathered using the optical microscope combined with the universal stage. However such measurements were time consuming and limited to a few crystal symmetries. More recently new techniques have been developed which provide high resolution (few 10s of nm) qualitative and quantitative 2D and 3D microstructural data. These include computer-integrated polarization microscopy (CIP) (van Daalen et al. 1999), electron backscatter diffraction (EBSD) (Prior et al. 1999), serial sectioning using a focused-ion-beam (FIB) system in the SEM (Groeber et al. 2006) and synchrotron X-Ray tomography (Mikulik et al. 2003). Of these techniques EBSD is the more widely used in the Earth Sciences. It is fully automated, fast and allows collection of accurate, reproducible and statistically meaningful crystallographic orientation data of minerals belonging to any of the seven crystal systems (from cubic to triclinic). EBSD is a very important tool to the mineralogist and petrologist as it allows testing of microstructural models based on the distribution of crystallographic orientations (Prior et al. 1999).

In this short contribution we review the basic principles of EBSD, analytical procedures that are specific to mineral and rock samples and some applications to mineralogy and petrology. Recent progress on in-situ heating and deformation experiments is also addressed.

Basic principles of EBSD

High energy electrons from an electron beam interact with the target specimen in many different ways. Broadly we may distinguish between 1) elastic interactions and 2) inelastic interactions. In 1) the scattered electrons do not lose significant energy compared to the primary electrons, whilst in 2) considerable energy is lost due to the activation of a variety of physical processes in the specimen. A thorough review of specimen-beam interactions is given in the software package MATTER (www.matter.org.uk). The incident electron beam diameter is always larger than the atomic spacing, thus, by interaction with a population of nuclei in the specimen, incident

primary electrons will be scattered within the sample in all directions. High energy electrons which exit the specimen via the surface of incidence after one or more scattering events are backscatter electrons. Of these, those that satisfy the Bragg equation for diffraction describe conical trajectories for each lattice plane. Such diffraction cones approximate planes and may be imaged on a phosphor screen as sub-parallel diffraction lines (bands). A network of diffraction lines forms an electron backscatter diffraction pattern (EBSP) or Kikuchi pattern. Intersecting bands result in bright spots on the EBSP which correspond to zone axes. Thus elements of symmetry can be recognized in EBSPs. Kikuchi patterns may be imaged in the transmission electron microscope (TEM) as well as in the SEM (e.g. by electron channelling (Lloyd et al. 1987)). In this contribution we focus on EBSD in the SEM (Randle 1992 and Prior et al. 1999). The resolution of EBSD is a function of the accelerating voltage, which controls the depth of penetration of the electrons in the specimen (activation volume). The smaller the activation volume, the higher the resolution. Also, an angle of incidence of 70° between the electron beam and the specimen normal results in a statistically higher number of BSE emitted from within few tens of nm of the sample surface and thus in a clearer EBSD signal. In a field emission (FE) SEM, at 70° tilt angle and 20 kV accelerating voltage the resolution of EBSD is $< 1 \mu\text{m}$ and sometimes as low as 30-100 nm. The quality of EBSPs is controlled by the beam current (or spot size). A large spot size is required to obtain sharp EBSPs, however this reduces spatial resolution. Thorough descriptions of the principles of EBSD are given by Randle (1992) and Prior et al. 1999.

Problems with resolution and quality of EBSPs mainly due to charging in non-conductive materials such as rocks and minerals have been largely overcome by coating with a very thin layer of carbon the specimen surface.

Using EBSD

Sample preparation

The surface of interest must be smooth to avoid shadowing caused by topography. This can be achieved by mechanical polishing. The amorphous layer produced during mechanical polishing may be removed using chemo-mechanical polishing. The latter results in a surface of pristine lattice that is required for orientation analyses by EBSD. A large number of rock forming minerals can be chemo-mechanically polished

successfully. Nevertheless particular care must be taken when polishing hydrophilic minerals such as for example NaCl or gypsum. Ion-beam milling techniques may be explored for polishing phyllosilicates, EBSD analysis of which is currently limited to the basal planes due to difficulties in achieving satisfactory polishing of any other orientation.

EBSD geometry

The specimen and the phosphor screen are positioned in the chamber so that a large ($\sim 90^\circ$) angular range can be obtained on EBSPs. The projection of the source of BSE on the phosphor, along a trajectory at 90° to it, generates the pattern centre (PC). The closer the phosphor and the specimen (i.e. the shorter the distance, DD, between the source point and the pattern centre) the larger the angular range of the EBSP imaged. This yields better quality pattern images that are then easier to index. A digital camera, with axis orthogonal to the phosphor screen, is positioned behind the latter.

The positioning of the phosphor is generally restricted by chamber geometry, number of existing detectors and in-situ experimental requirements. To date only 2 SEMs (at Liverpool and Montpellier) have been purposely built to optimize EBSD data acquisition, both standard and during in-situ experiments.

Data acquisition set-up

EBSD data can be acquired using dedicated software packages supplied by Oxford Instruments HKL and TSL Crystallography.

In order to index EBSPs it is necessary to calculate the solid angle between the cones that project as bands on the phosphor screen. Thus a calibration of the EBSD geometry is needed where the position of the pattern centre and the detector distance may be obtained from the EBSP image of a known material (e.g. Si) in a known orientation. Refinement of the initial calibration should be performed before any manual or automated EBSD work is carried out.

The polychromatic component of electron scattering generates a background signal that affects the quality of EBSPs. Correction for the background signal can be applied within the dedicated software packages. This involves collecting the signal at very low

magnification in scanning mode and then averaging and subtracting it from the EBSP signal.

Indexing an EBSP involves calculating the position and orientation of bands with respect to the PC thus obtaining the specimen crystallographic orientation at the source point. Indexing algorithms require knowledge of the crystal symmetry, the lattice parameters and the number of lattice planes that give bands on EBSPs (refractors). Correct indexing by the software can be assessed by rigorous comparison of the simulation bands with the live EBSP bands (Winkelmann et al. 2007). Whilst interactive (manual) indexing is available in the software, fully automated EBSD (e.g. Juul Jensen and Schmidt 1990) has become common practice on a large number of rock forming minerals. Very recent advancement in the EBSD detector and software technology allow faster data collection than was ever possible before, at top speeds of 600 data points per second. Additionally combined acquisition of EBSD and EDS data is now possible, although this hampers the speed of the acquisition.

EBSD provides us with orientation and misorientation distribution datasets for a given crystalline material (Wheeler et al 2001). Knowledge of the relationship between the specimen surface and the microscope, kinematic and geographic reference frames allows interpretation of data from rock samples at the regional scale. Also, information on the 2D geometry of grain boundaries can be obtained from EBSD data. Recently developed non-standard data processing analysis enables calculation of the distribution of grain boundary planes from EBSD data in cubic materials (Randle 2006).

Applications of EBSD in mineralogy and petrology

A comprehensive review of a number of different applications of the EBSD technique in petrology is given by Prior et al. 1999. Since then significant progress in sample preparation and in both EBSD hardware and software technology has occurred and the effective application of EBSD to mineralogy and petrology has increased exponentially (e.g. Storey and Prior 2005, Halfpenny et al. 2006, Pennock et al. 2006, Barrie et al. 2007). Excellent to satisfactory EBSD datasets (depending on the quality of polishing, material characteristics and working conditions) can be acquired from a large

number of rock forming minerals of different crystal symmetry including calcite, quartz, feldspars, pyroxenes, amphiboles and many others.

The good EBSD results obtained for calcite and quartz (>78% successful indexing and statistical significance resulting from full automation) have allowed focussing on the detailed study of microstructural features and dauphine twin boundaries in quartz and curved twin boundary in calcite that cannot be recognised using the optical microscope. A case study is reported below.

Detailed EBSD analyses of cold-worked and then statically recrystallized Carrara marble show that, although little or no variation of the lattice preferred orientation (LPO) is observed throughout a wide range of testing conditions, significant microstructural changes have occurred (see pattern quality maps and pole figures in Fig. 1 a, b and c) (Mariani work in progress). In order to reconcile these observations we investigate textural evolution locally, within the microstructure. Strain free, incipient lattice nuclei form during the initial deformation and subsequently develop, during annealing, predominantly along existing grain boundaries and deformation twin lamellae. The newly formed grains preserve LPOs similar to those of the pre-existing grains. They also show high angle misorientation relationships to their parent grains and twin lamellae. Recurrent misorientation angles of $\sim 30^\circ$, 60° and 90° are interpreted to be generated by initial subgrain rotation recrystallization, followed by grain boundary migration, of both parent and deformation twin grain boundaries. Thus twin boundaries play an important role in both the static and dynamic recrystallization behaviour of some rock-forming minerals and should be accounted for in microphysical models of recrystallization.

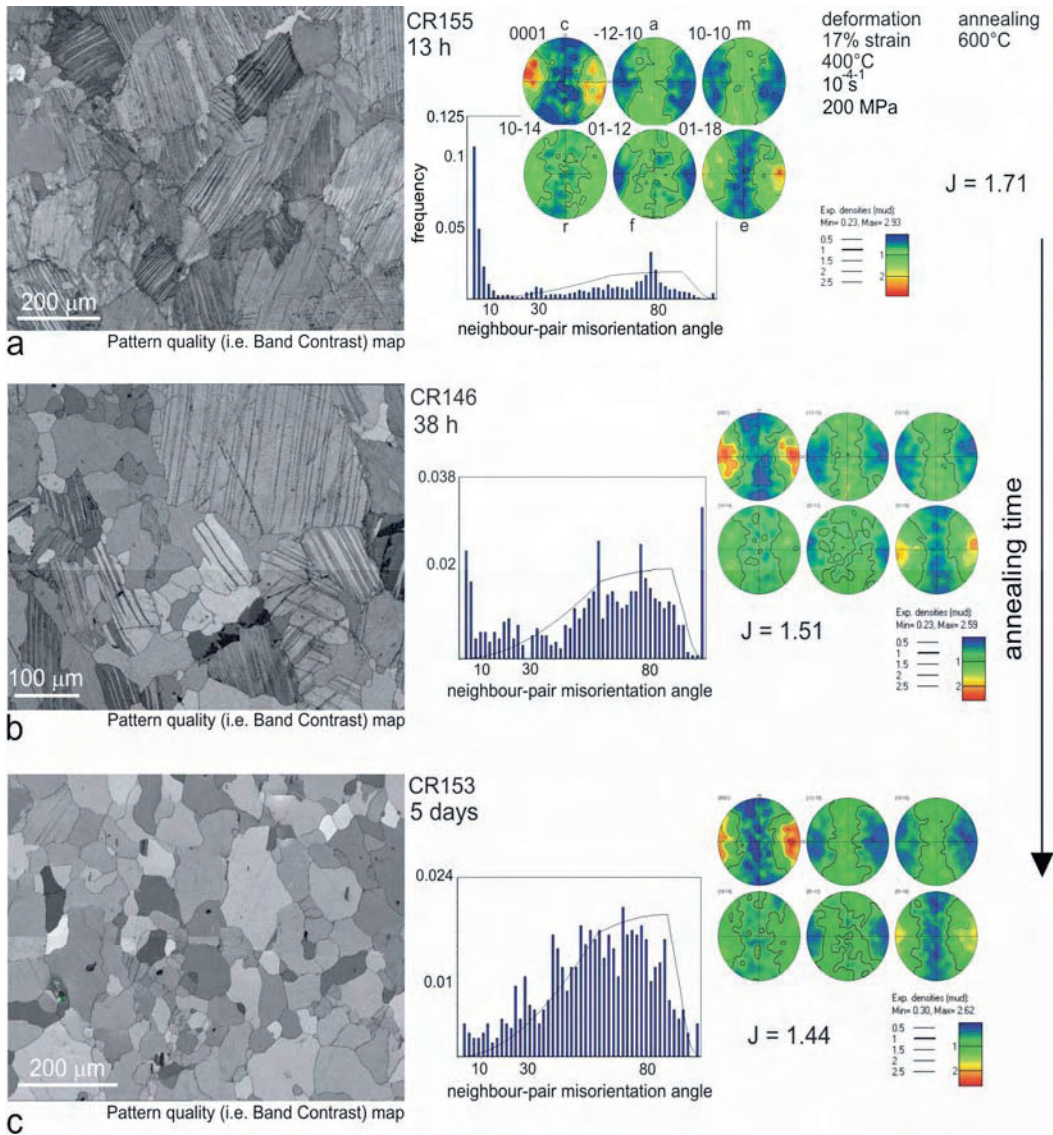


FIGURE 1. Lattice preferred orientations (LPOs) (pole figures on the right) and microstructural variations (pattern quality maps on the left) as a function of annealing period, a) 13 h, b) 38 h and c) 5 days, in cold-worked and then statically recrystallized Carrara marble. Calcite c-axes are aligned perpendicular to the stress direction (horizontal). Little variation of the LPO is observed. However, EBSD show that significant microstructural changes have occurred.

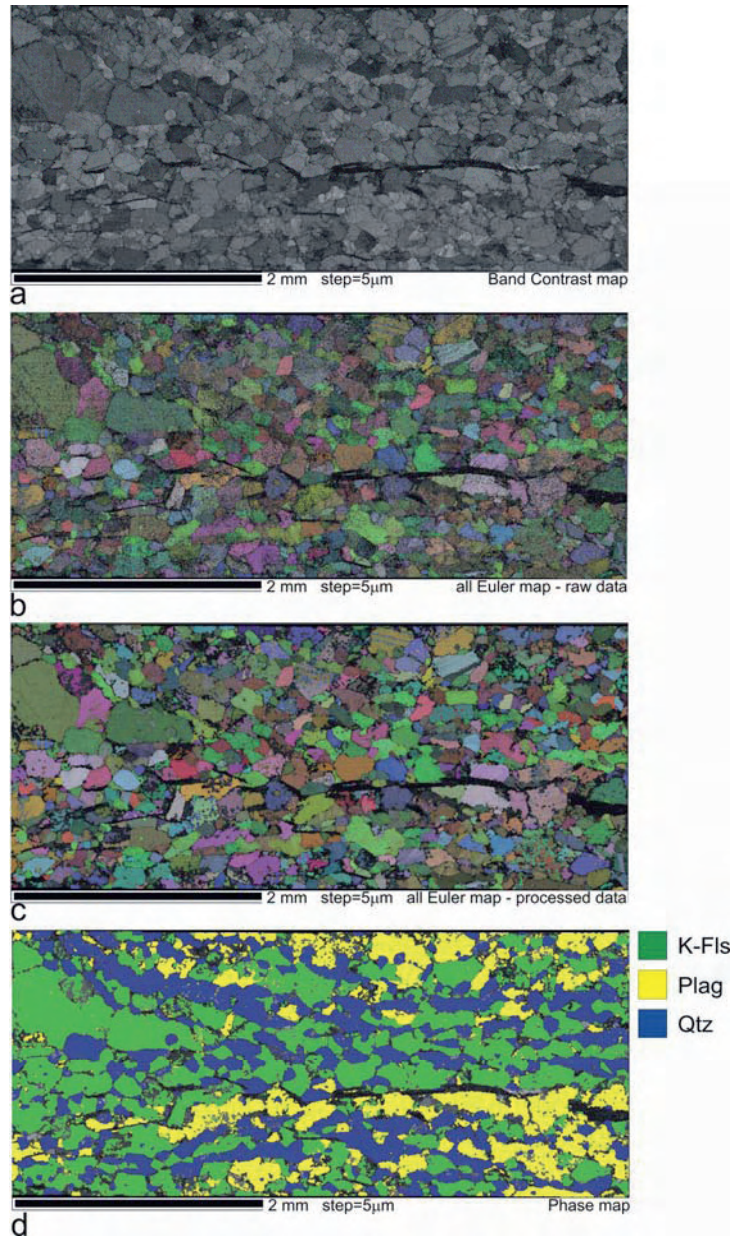


FIGURE 2. Amphibolite facies quartzo-feldspathic gneiss from the Lewisian Complex, NW Scotland. The section is cut parallel to lineation and perpendicular to foliation (kinematic x - z section) and show elongated aggregates dominated by K-feldspar but with subsidiary plagioclase, quartz and biotite. EBSD data was acquired on a Philips XL30 W-filament SEM, at 6.5 nA and 20 keV. The acquisition settings in Flamenco were 7 bands (the minimum needed to give a low level of misindexing –usually 8 are needed), 120 Hough resolution, 75 reflectors, band edges and 4x4 binning.

One of the recent achievements in EBSD is successful automated analysis of very low symmetry minerals (triclinic and monoclinic) such as feldspars and some pyroxenes (e.g. omphacite). In Fig. 2 we report an EBSD case study of an amphibolite facies quartzo-feldspathic gneiss from the Lewisian Complex, NW Scotland (Pearce work in progress). In this specimen elongated aggregates dominated by K-feldspar with subsidiary plagioclase, quartz and biotite can be observed in the ‘tails’ of large porphyroclasts. Both K-feldspar and plagioclase were indexed using triclinic crystal symmetry. Lattice parameters for the two minerals are very similar only differing significantly in the α angle. However this appears to be enough for the software to distinguish between the minerals in a statistically significant number of cases (Fig. 3). It is observed that misindexing in feldspars is more common than in other minerals. Orientations that are misoriented by 180° (pericline and albite twin laws) have very similar patterns that may differ only by one band. Thus certain orientations may be significantly affected by systematic misindexing problems. Some phase misidentification may also occur in feldspars. Misidentification and misindexing can be carefully processed out of the dataset in the post-processing stage thus allowing LPOs and boundary analysis for the whole mineral assemblage and interpretation the deformation/recrystallization mechanisms.

EBSD combined with chemical analysis of omphacite from the Streaked Eclogite, Sesia-Lanzo Zone, NW Italian Alps, is a key tool to understanding how this mineral forms strong LPOs and what is the role of mechanisms such as dislocation creep, pressure solution and grain growth (McNamara work in progress) (Fig. 4). Comparison of the EBSD and EDS results on the omphacite from the Streaked Eclogite with results from omphacite fans growing in an undeformed eclogite from the same locality, suggest that the pronounced subgrain structure observed may originate during grain growth and not during deformation. Chemical analysis show subtle or no chemical variations in the omphacite (Fig 4).

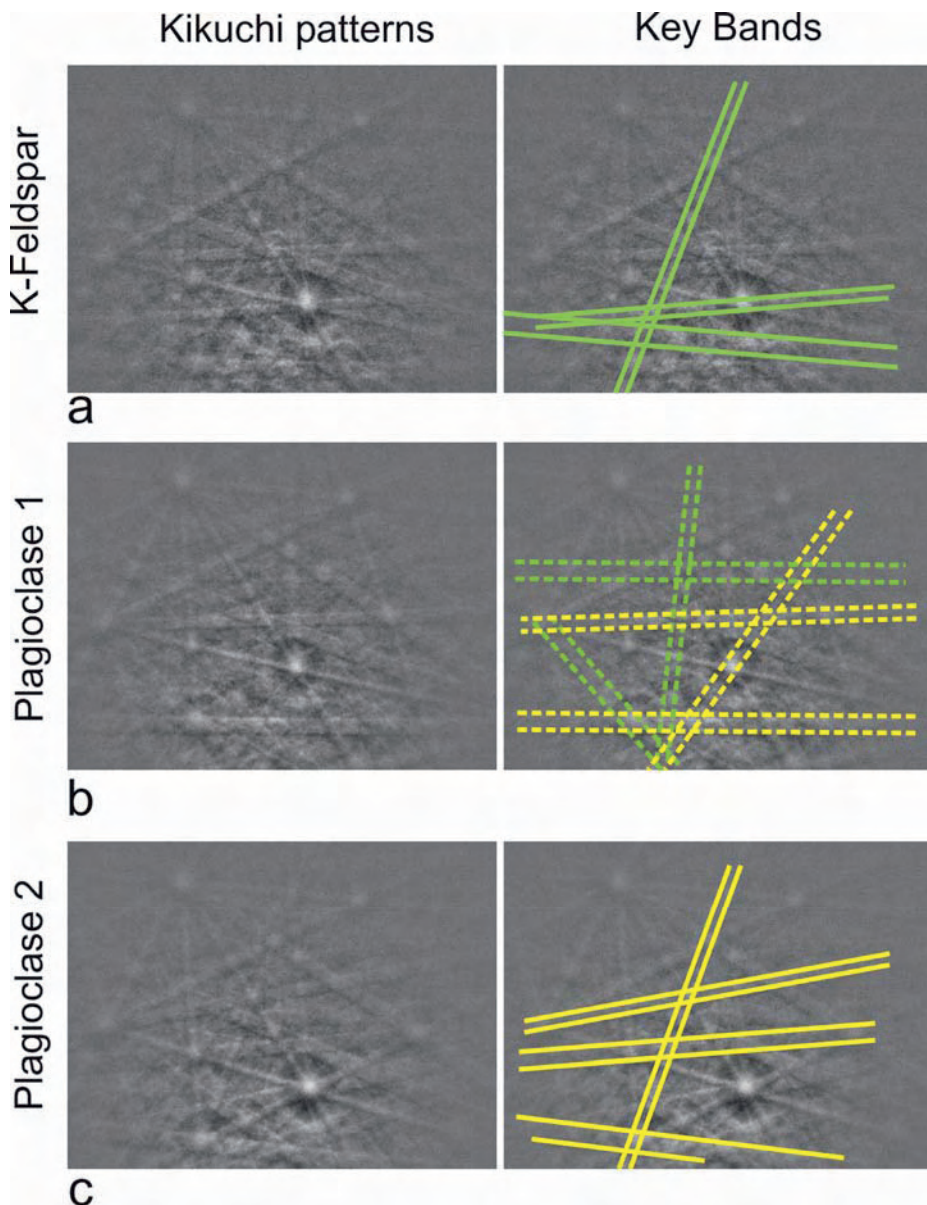


FIGURE 3. Three feldspar patterns, a), b) and c) from a perthite grain indexed manually using Channel 5 Flamenco. Plagioclase 1 and K-Feldspar are the same orientation, plagioclase 2 exhibits an albite twin relationship with plagioclase 1 (180° around $[201]$). Also shown are the key differences from plagioclase 1 (on the right). Bands highlighted on plagioclase 1 are those that are not present in K-feldspar (green dashed) and plagioclase 2 (yellow dashed).

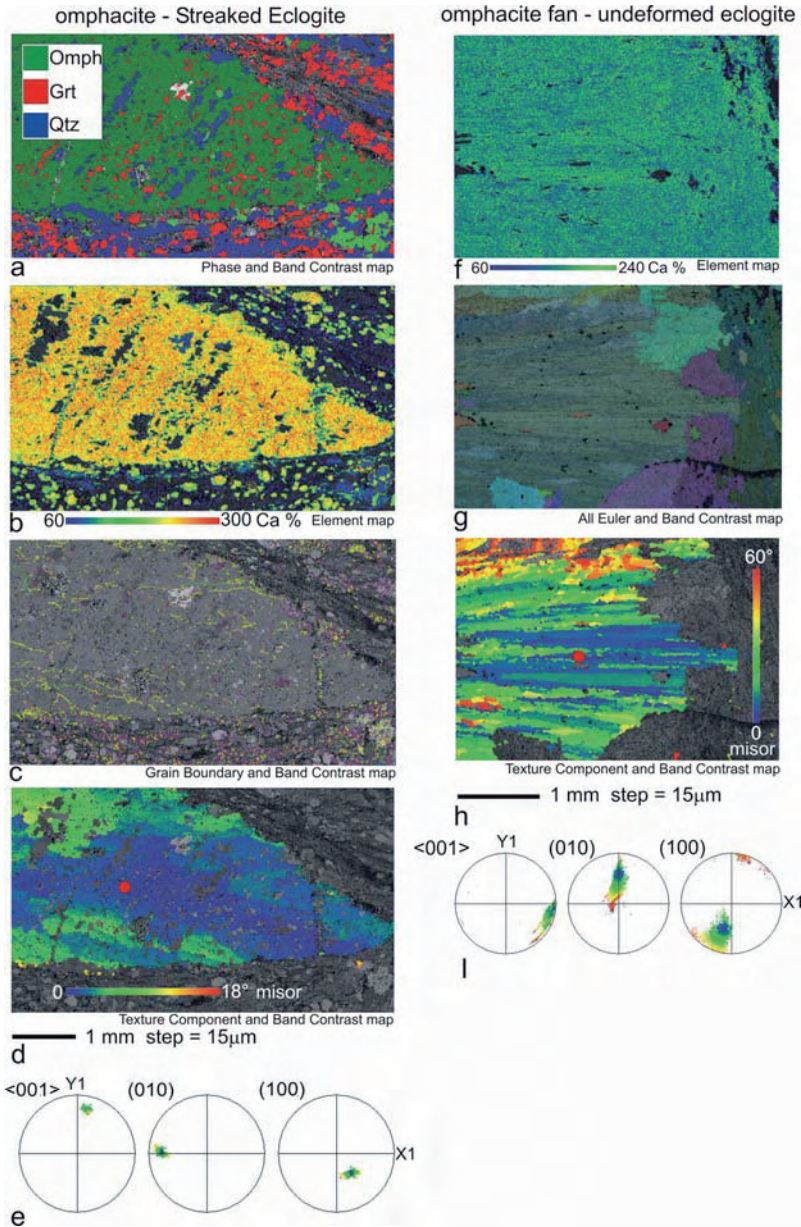


FIGURE 4. a), b), c), d) and e) Omphacite in Streaked Eclogite and f), g), h) and i) omphacite fan in undeformed eclogite, Colle della Barme d'Oropa, Sesia-Lanzo Zone, NW Italy. The Streaked Eclogite has a strong foliation defined by shape (omphacite and muscovite grains) and location (alternating bands of garnet and omphacite, plus quartz and muscovite) fabrics. Lineation is defined by quartz. Omphacite fans show large misorientations (up to 60°) across them (h). Pole figures show one single misorientation axes for the sub-grain boundaries (e and i). Only subtle chemical changes are observed (b and f).

In-situ heating and deformation experiments

Static in-situ high-temperature EBSD and SEM imaging experiments on metals and rock-forming minerals have proved successful in the observation and quantification of recrystallization and phase transformations up to $\sim 1000^{\circ}\text{C}$ (e.g. Seward et al. 2004 and Bestmann et al. 2005). The range of samples that can be analysed is somewhat limited by the material properties and the operating conditions of the SEM. An interplay exist between 1) the attainment of temperatures suitable for studying recrystallization processes on experimental timescales, 2) preserving the integrity of lattice structure at temperature, and 3) avoiding sample deterioration by heating (e.g. calcite) or reduced grain boundary mobility (e.g. quartz) at reduced pressure conditions in the SEM.

A custom-designed sample stage for the CamScan X500 FEG-SEM at Liverpool incorporates a high-temperature heating system with a deformation rig, permitting simultaneous heating and tensile deformation of samples with real-time EBSD analysis and conventional SEM imaging (Tatham work in progress). Although the deformation stage is undergoing significant hardware and software development in order to optimise the assembly for crystal-plastic deformation of geological materials, preliminary deformation experiments on copper samples have provided useful results and are promising for future work.

Summary

Electron backscatter diffraction is now a commonly used analytical tool in the Earth Sciences. It provides a measure of the full crystallographic orientation of crystalline materials $> 1 \mu\text{m}$ in size and fully automated EBSD can be successfully applied to a large number of rock-forming minerals. In-situ high temperature tensile deformation capability for rocks and minerals is being developed at Liverpool.

References

- Barrie, C. D., Boyle, A.P. et al. (2007). *Jour. Structural Geol.*, 29, 1494-1511.
Bestmann M., Piazzolo, S. et al. (2005). *Jour. Structural Geol.* 27, 447-457.
Groeber, M. A., Haley, B.K. et al. (2006). *Materials Characterization* 57(4-5), 259-273.
Halfpenny, A., Prior, D.J. et al. (2006). *Tectonophysics* 427(1-4), 3-14.

- Juul Jensen, D. and Schmidt, N.H. (1990). An automatic on-line technique for determination of crystallographic orientation by EBSP. In P. Chandra, Ed., Proceedings, Recrystallization 90. 219-224.
- Lloyd, G. E., C. C. Ferguson, et al. (1987). *Tectonophysics*, 135, 243-249.
- Mikulik, P., Lubbert, D. et al. (2003). *Jour. Physics D-Appl. Physics*, 36(10A), A74-A78.
- Pennock, G. M., Drury, M.R. et al. (2006). *Jour. Structural Geol.*, 28(4), 588-601.
- Prior, D. J., Boyle, A.P. et al. (1999). *Amer. Mineral.*, 84, 1741-1759.
- Randle, V. (1992). *Microtexture determination and its applications*. London, The Institute of Materials. pp 174.
- Randle, V. (2006). *Jour. Microscopy* 222, 69-75.
- Seward, G. G. E., Celotto, S. et al. (2004). *Acta Materialia* 52(4), 821-832.
- Storey, C. D. and Prior, D.J. (2005). *Jour. Petrol.* 46(12), 2593-2613.
- van Daalen, M., Heilbronner, R. et al. (1999). *Tectonophysics* 303(1-4), 83-107.
- Wheeler J, Prior D.J. et al. (2001). *Contrib. Mineral. Petrol.*, 141 (1) 102-124.
- Winkelmann, A., Trager-Cowan, C. et al. (2007). *Ultramicroscopy*. 107, 414-421.

TEM in Geology. Basics and applications

Fernando Nieto García

Departamento de Mineralogía y Petrología and IACT, Universidad de Granada-CSIC,
18002 Granada, Spain

Introduction

In general a microscope is capable of producing an enlarged image of an object through a combination of lenses. The fundamental lens is the objective lens, which produces a diffraction pattern of the object in its back-focal plane. If these diffracted beams are focused and magnified again by additional lenses, we finally obtain the enlarged image of the object. This is the normal means of operation of an optical microscope (Fig. 1). The resolution of the microscope depends on the wavelength of the radiation used. Therefore, the resolution of an optical microscope is limited to textural relationships between crystalline objects, but it is unable to provide information about the atomic structure of these crystalline objects. In theory, X-rays and electrons have wavelengths small enough to produce such information. Consequently, these two types of radiation are usually employed to study the crystalline structure of matter. Nevertheless, no lenses exist for X-rays; therefore, they cannot be focused to produce an image and X-rays microscopes do not exist. An X-ray “image” can only be generated by crystallographers by calculating the intensity of the diffracted beams; however, in the electron microscope, the Fourier transform of the diffracted beams is physically carried out by the electromagnetic lenses and a real image can be obtained. The geometry and optical paths of the rays in optical and electron microscopes are exactly equivalent (Fig. 1).

A significant difference between these two types of microscopes is that electromagnetic lenses can continuously change their focal length, and thus their magnification, in contrast to glass lenses. Some consequences are easily deduced, but perhaps the fundamental one is the possibility of bringing to the image plane the back focal plane of the objective lens—that is, the diffraction pattern instead of the

intermediate image (Fig. 1). In modern microscopes, the change from image to diffraction can be accomplished instantly by pressing a button.

When electrons interact with matter, other signals (in addition to various types of electrons) such as electromagnetic waves are produced. Analytically, X-rays are the most important, as their wavelength contains the fingerprint of the chemical elements present in the sample. This is the basis of all the modern *in-situ* analytical techniques. Although electron microprobe and scanning electron microscopes with EDX are the best-known examples of such techniques, this possibility is also present in the transmission electron microscope (TEM).

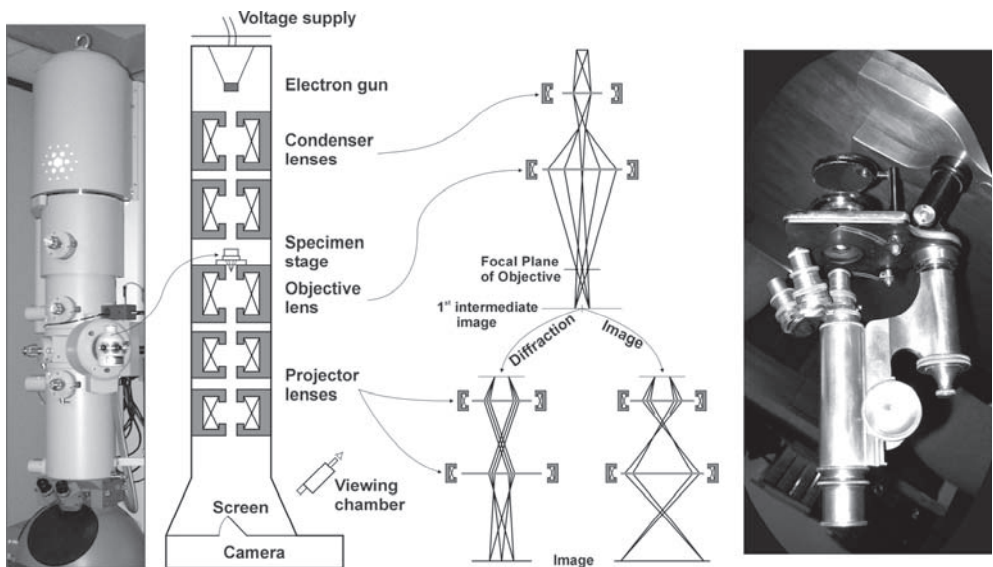


FIGURE 1. Schematic of the column of a transmission electron microscope (left) and optical path of the rays valid for both electron and optical microscopes (right). Two different field strengths of the projector lenses allow the production of two different ray paths after the first intermediate image. Thus, it is possible to bring to the image plane the back focal plane of the objective lens (diffraction pattern) or the intermediate image to obtain diffraction or an image, respectively. Modified from Buseck (1992) and Putnis (1993).

In conclusion, a TEM is a complex machine that simultaneously combines a powerful microscope with crystalline-lattice resolution, a diffractometer, and a chemical-analysis device. More than its high spatial resolution, this combination of techniques is the real reason for its powerful capability for geological research.

Samples

Although a universal electron microscope is possible, transmission and scanning/microprobe capabilities are, in practice, separate techniques. One of the reasons is the different characteristics of the samples involved. TEM samples must be as thin as possible. Three means of preparation are the most common for geological samples:

1) Ion milling. This technique allows the extraction of a small area from a thin section, prepared with adhesive easily melted by heat. A copper ring is affixed to the selected area with the aid of a microscope, the rock is cut around the ring, and the round piece of sample removed from the thin section by heating. The copper ring with the attached piece of rock is placed into the ion mill, which bombards the centre of the ring with a beam of ions or uncharged atoms (Fig. 2). The area surrounding the hole produced in the centre of the sample contains sectors thin enough to be studied by TEM.

2) Fine powder deposited on a holey-carbon film. This is the simplest method, very useful when neither a particular orientation of the sample nor especially thin areas are necessary. The disadvantage for petrographic studies is that information on the location of the studied grain in the rock is lost. It is a very useful method for chemical analysis of fine-grained materials.

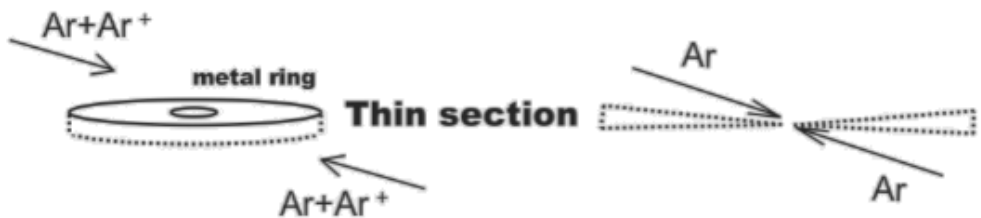


FIGURE 2. Basics of ion-milling preparation of samples. A round piece of rock, removed from the thin section by heating, is placed in the ion mill, which bombards the centre of the ring with a beam of ions or uncharged atoms (left). Sectors thin enough to be studied by TEM surround the hole thus produced (right).

3) Ultramicrotomy. This is a method widely used in bio-medical sciences. Suitable minerals either have to be relatively soft, like many layer silicates, or very fine-grained. The sample can be encased within a suitable epoxy and then sliced, like ham in a delicatessen, producing extremely thin wafers, which are deposited in a grid.

Electron diffraction

The Ewald sphere, which allows prediction of the directions of the diffracted beams, is far larger for electrons than for X-rays as a consequence of the difference in wavelength between the two kinds of radiations (Fig. 3a). Therefore, the radius of the sphere with TEM is so large and the crystal so thin (causing the diffraction spots to become spikes) that the pattern is essentially tangent over a large region of the reciprocal space and many diffraction spots can be recorded without any sample motion. In combination with the strong diffraction effects that occur with electrons, this means that planes through reciprocal space can be viewed in real time. In contrast to X-ray diffraction, diffracted electrons have a greater probability of themselves being scattered as they pass through the sample. Dynamical diffraction gives rise to diffracted intensities that are difficult to interpret quantitatively. Another consequence of dynamical effects is that weak reflections such as those “forbidden” by symmetry commonly appear. These dynamical effects are commonly undesirable, particularly if we want to extract any information from the intensities of the spots, but in some cases may be welcome as they allow easy identification of the symmetry from the “forbidden” reflections.

By simple geometric considerations, it can be demonstrated that the d_{hkl} spacing of a given spot can be calculated by dividing a constant by the distance to the central spot in the diffraction pattern. This camera constant is the product of the wavelength of electrons by the so-called camera length, which, in diffraction, plays a role equivalent to magnification in the images. Nevertheless, the camera constant can be affected by a number of factors, including distortions, and it is far from its theoretical value; therefore, precision and accuracy are clearly worse than for X-ray diffraction, but can be approximated to 0.1% if distortion is corrected by the Capitani *et al.* (2006) method and some basic guidelines are respected (Mugnaioli *et al.* 2008). As a diffraction pattern is a representation of the reciprocal space, in a similar way to X-ray diffraction, shorter distances represent longer d spacings.

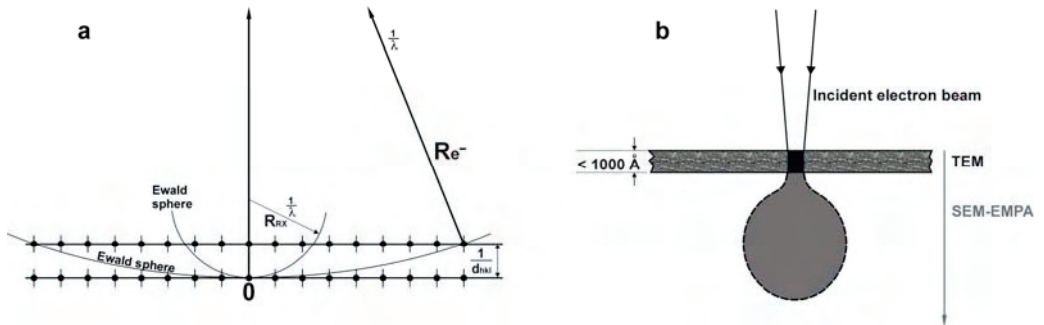


FIGURE 3. a) Schematic diagram of the Ewald sphere for electrons and X-rays. The radius ($R=1/\lambda$) is far greater for electrons, and therefore more reciprocal-lattice points (which represent the crystallographic planes) are intersected for a given orientation. Consequently, the pattern is essentially tangent over a large region of the reciprocal space and many diffraction spots can be recorded without any sample motion. The effect is accentuated by the extremely thin samples, which produce extended reciprocal lattice spikes (vertical lines superposed on the spots). λ = wavelength, d_{hkl} = spacing between crystallographic planes. Modified from Buseck (1992). b) Comparison of the electron-excited areas between thick (grey area) and thin (black area) samples.

Lattice images

A surplus of the electron diffraction facility in the microscope is the possibility of acting on the images, selecting the rays used to construct the images using appropriate apertures. If we use only one diffracted or transmitted ray, we obtain amplitude contrast, producing respectively dark or bright field images. They do not have lattice resolution and consequently this technique is termed conventional TEM.

By contrast, if we select a combination of rays with d_{hkl} spacing higher than the nominal resolution of the microscope, we allow the rays to interfere each other, thereby producing phase contrast images, which contain information about the crystallographic structure of the sample. They are usually termed high-resolution images (HRTEM), but in most cases give information only about lattice periodicity—including local defects—due to which their correct name would be lattice (fringe) images in contrast to structure images. A structure image would be directly interpretable without previous knowledge of the crystal structure; only in this case an atom produce black spots and voids white ones.

One of the basic conditions to obtain structure images is that the microscope focus be adjusted to the value in which the contrast transfer function has its greatest trough, that is, the so-called Scherzer focus, which is specific to each particular TEM. The contrast transfer function describes the imperfections in the lens system that result in modifications to the amplitudes and phases of the electron beams, producing distortions of the images due to the prevention of proper interference of the waves.

Electron crystallography

X-ray diffraction produces structural information in which the crystallographic characteristic of all the cells of the diffracting crystal are mediated; in this way, we obtain an average structure in which individual defects are ignored and potentially avoided. By contrast, TEM concentrates its power on the proper identification of such defects. This has, in part, been the reason for the great success of TEM in geology in recent years. Nevertheless, electron microscopists are exploring the possibilities of HRTEM and electron diffraction to determine the crystallographic structure of fine-grained and defective materials.

A high-resolution image is a more-or-less distorted representation of the atomic distribution in the sample. Two basic methods have been employed to properly interpret such information. The first one is image simulation, which calculates expected images from the structure of the sample and the technical conditions of TEM. In this manner, the experimental images can be compared with a limited number of hypothetical structures. The second method is the direct interpretation of the images. Electron crystallography software is able to produce Fourier transforms of the experimental images, producing something like virtual electron diffraction. A second Fourier transform would give the original image again, but with all the cells and symmetric parts of the each cell mediated; finally, the effects of the contrast transfer function can be subtracted, thereby mathematically producing a virtual structural image.

The other way in which electron crystallography works is to use the intensities of electron diffraction in a similar way to those of X-ray diffraction. Here also two different methods have been employed. One method tries to minimize dynamical effects by obtaining the electron diffraction from very thin areas, hence it uses the same software as X-ray diffraction. The other method assumes the presence of dynamical effects and uses

a completely different system of structural analysis based on the dynamical diffraction theory.

Analytical electron microscopy (AEM)

The intensity of a given emission line is proportional to the concentration of the corresponding element. In thick samples, the beam penetrates to considerable depth (Fig. 3b). The resulting X rays emitted are subject to absorption and fluorescent effects. Nevertheless, in the thin electron-transparent films generally used in TEM, the paths of emitted X-rays are so short that absorption and fluorescence can be neglected. This is the so-called Cliff-Lorimer (Cliff and Lorimer, 1975) approximation. The ratio of atomic concentrations of two elements (c_a/c_b) is directly proportional to the ratio of the intensities of the emission lines of those elements (I_a/I_b). Only a proportionality factor K_{ab} is necessary to calculate the relative amount of the elements from the measured intensities. Therefore, it is a relative method in which the concentration ratios of elements can be known, but not their absolute quantities. This is a basic limitation of the technique, but it is not particularly limiting in mineralogy as mineral compositions are usually normalized to their formulae. To present an analysis in the form of oxides in the traditional fashion is artificial and may be misleading. It is the concentration ratios (formulae) that should normally be presented as the basic AEM data.

The software of EDX equipment contains theoretical K factors, calculated from first principles (Goldstein et al., 1986) to be used in the so-called *standardless analyses*. Nevertheless, the K factors need to be experimentally determined for a standard of known composition, as they are valid only for values obtained under specific conditions for a specific instrument. In fact, should the counter window or crystal be replaced, large changes in K-values are possible. Therefore, *standardless analyses* produce only approximate results very far from being considered quantitative.

Electron energy-loss spectroscopy (EELS)

The energy lost by beam electrons during inelastic interactions is converted into secondary signals as X-rays, cathodoluminescence, and Auger electrons. In addition to these signals, the changes in energies of the beam electrons also provide information about both the types of atoms in the specimen and about their chemical states (bonding,

valence, coordination). Electron energy-loss spectroscopy, or EELS for short, is the measurement of the energy distribution of electrons that have passed through a specimen.

EELS reflects a primary event of energy change, in contrast with EDX, which reflects a secondary event, the energy of radiation released upon relaxation during the return of the atom to its ground state. Since most electrons that cause ionization can be collected by the EELS spectrometer, the method has high detection efficiency. In comparison to EDX, EELS is better suited for light elements, with the possibility of measuring up to Li. In general, quantification of EELS spectra is more difficult and the results less accurate than for EDX because of the broad shapes of the EELS edges and the high background.

Elemental and chemical analysis is probably the major application of EELS for mineralogy, but the spectra contain far more information. Valence states and local environments of atomic species can be determined from EELS spectra by using EXELFS (extended energy-loss fine structure) and ELNES (energy-loss near-edge fine structure). Small changes in the edge energy are caused by differences in valence state. These chemical shifts can be used to determine the valence states of elements in a specimen; this technique has been successfully applied to a variety of minerals. It is difficult to obtain such information at such a fine spatial resolution by any other technique. Nevertheless, while it is easy to see changes in oxidation states, one limitation is that it is difficult to quantify their fractions.

Applications

The scales for the observation of geological phenomena range from 10^6 m for plate tectonics to 10^{-10} m for mineral lattices. Many characteristics may be recognized in such a wide range of dimensions with similar meaning (e.g. folds). The various sub-techniques included in TEM, presented above, allow the observation and study of a plethora of phenomena—among them the following can be mentioned as examples.

- Electron diffraction

Identification, orientation, and cell parameters of minerals.

- Images (low or high resolution)

Mosaic crystal, twins, dislocations, strain, polytypism, polysomatism, phase transformation, antiphase domains, nanotextures, nanocrystals, exsolution, non-stoichiometry.

- Analytical electron microscopy

Quick mineral identification, high-spatial resolution quantitative analysis.

The frequent use of TEM in the geological sciences has revealed that many of these phenomena are more the rule than the exception. Mellini (1985) proposed the concept of microstructure to define “defects of various types and origins inside a monomineral grain (definable as real structure in a strict sense) or the diverse associations of several minerals in a polyphasic grain, homogeneous on a macroscopic scale” The first part of the definition has been a well-known concept in crystallography for decades, even considered in some definitions of crystals (Navrotsky, 1994), while the second part begins to point to a redefinition of the concept of mineral itself. The occurrence of a given microstructure mainly depends on the nucleation conditions and/or on the post-crystallization sub-solidus evolution. They may be important indicators of the thermobaric evolution of minerals and rocks.

TABLE 1 refers to some representative examples, ordered according to the type of phenomenon studied. In addition, some significant cases are presented below.

PHENOMENON	REFERENCE
POLYMORPHISM	
Reconstructive transformations	
-Three different polymorphs of wollastonite in the Allende meteorite	Brenker and Krot (2004)
-Biogenic nanocrystalline sphalerite and wurtzite growing on degraded wood	Moreau <i>et al.</i> (2004)
-Berthierine and chlorite: stability relationships; are they true polymorphs?	Abad-Ortega and Nieto (1995)
-Microstructures of polygonal serpentines	Baronnet and Devouard (2005)
-Martensitic transition due to decompression in α -PbO ₂ -type TiO ₂ in ultra-high-pressure metamorphic rock	Shen <i>et al.</i> (2005)
Displacive transformations	
-Antiphase domains in pigeonite	Moore <i>et al.</i> (2001)
-Twin walls in anorthoclase enriched in alkali and depleted in Ca and Al	Camara <i>et al.</i> (2000)
Order-disorder transformations	
-Antiphase domains in omphacites	Brenker <i>et al.</i> (2003)
-Antiphase domains in scapolite solid solutions	Seto <i>et al.</i> (2004)
-Niocalite. False disordered distribution of Nb and Ca, due to polysynthetically twinned domains	Mellini (1982)
Fe/Cu ordered superstructure of bornite	Ding <i>et al.</i> (2005)
Fe/Mg ordering in low-calcium actinolite	Driscall <i>et al.</i> (2005)
POLYTYPISM	
-Micas	Amouric <i>et al.</i> (1981)
-Kaolinite-dickite	Kogure and Inoue (2005)
-Chlorites	Spinkler <i>et al.</i> (1984)
-Lizardite-chlorite transformation and high-pressure lizardite polytype	Dodony and Buseck (2004)
-Disorder across the interlayer region in sodium mica wonesite	Kogure <i>et al.</i> (2005)
-Parallel intergrowths in cronstedtite	Durovic <i>et al.</i> (2004)

POLYSOMATISM	
-Structural modulation of antigorites	Viti and Mellini (1996)
-Pyribole evolution during tremolite synthesis (non-amphibole chain multiplicity faults)	Bozhilov <i>et al.</i> (2004)
-Polysomatic faults and structural imaging in antigorite	Capitani and Mellini (2005)
-Chain multiplicity faults in deformed and recovered omphacite	Muller <i>et al.</i> (2004)
Interstratified minerals	
-Interstratification of 2:1 layer-silicates studied by alkylammonium ion treatment	Vali and Köster (1986)
-Illite-smectite mixed-layering	Olives <i>et al.</i> (2000)
-Interstratification of Na/K interlayers in aspidolite, the Na analogue of phlogopite	Kogure <i>et al.</i> (2004)
STRUCTURAL DEFECTS	
-Deformation microstructures in eclogites	Muller and Franz (2004)
-Dislocations and plasticity of experimentally deformed coesite	Idrissi <i>et al.</i> (2008)
-Deformation and recrystallisation mechanisms in naturally deformed omphacites	Buatier <i>et al.</i> (2004)
Alteration and deformation microstructures of biotite	Sanchez-Navas and Galindo-Zaldivar (1993)
TRANSFORMATIONS WITH CHEMICAL CHANGE	
Exsolution	
-Augite and pigeonite lamellae in meteorites. Thermal histories of basaltic eucrites from Vesta	Schwartz and McCallum (2005)
-Topotaxially concordant amphibole exsolution lamellae in garnet from ultrahigh-pressure rocks	Song <i>et al.</i> (2005)
-Exsolution microstructures in a complex amphibole assemblage from metabasalts	Ruiz Cruz <i>et al.</i> (2007)
Non-stoichiometry	
- Massive and lamellae amphiboles within clinopyroxenes of Coronas in anorthosites	Mellini <i>et al.</i> (1983)
-Invisible gold in As-rich overgrowths on pyrite	Palenik <i>et al.</i> (2004)

False stoichiometry	
-Native copper inclusions in biotites of porphyry copper deposits	Ilton and Veblen (1988)
-Iron in rutile	Banfield and Veblen (1991)
ELECTRON CRYSTALLOGRAPHY	
-Basics	Zou (1995)
-Crystallographic Image-Processing of high-resolution images of bannisterite	Ferrow and Hovmoller (1993)
-Crystal structure of parsettensite determined using electron diffraction patterns	Eggleton and Guggenheim (1994)
-Crystal structure of “iscorite” described anew from Fourier-filtering analyses of HRTEM images in combination with SAED data	Van Aken <i>et al.</i> (2005)
-Electron-Diffraction of Textures	Zvyagin (1994)
NANOCRYSTALS	
-Syntheses of magnetite nanocrystals: morphology, crystal size, and shape ratio. Implications for formation conditions	Faivre <i>et al.</i> (2005)
-Exclusively inorganic formation of magnetite in Martian meteorite	Golden <i>et al.</i> (2004)
-Vaterite precipitation in the microenvironment around bacterial cells	Rodriguez-Navarro <i>et al.</i> (2007)
-Irreversible colloidal behavior of Ca(OH) ₂ in lime mortars and plasters	Rodriguez-Navarro <i>et al.</i> (2005)
-Spherical aggregates of kaolinite crystallized via in-situ transformation of gels	Huertas <i>et al.</i> (2004)
-Bacterially-mediated authigenesis of clays phosphate stromatolites	Sánchez Navas <i>et al.</i> (1998)

PETROGRAPHY OF FINE-GRAINED MATERIALS	
-Smectite-illite diagenetic transformation	Ahn and Peacor (1986)
-Prograde and retrograde diagenetic and metamorphic evolution in metapelitic rocks	Abad et al (2003)
-Nanometer-sized meteorite impact-derived glass	Bauluz <i>et al.</i> (2004a)
-Mineral composition and genetic relationships in impactite	Ding and Veblen (2004)
-Direct transformation of andalusite to kaolinite in strongly deformed areas	Jimenez-Millan <i>et al.</i> (2007)
-Submicroscopic intergrowths of K biotite, Na biotite, and intermediate Na-K biotite	Ruiz Cruz (2004)
-Nanometric intergrowths of graphite within ultramafic phlogopite	Ferraris <i>et al.</i> (2004)
-Mineralogical characterisation of archaeological pottery	Giorgetti <i>et al.</i> (2004)
-Environmentally important, poorly crystalline Fe/Mn hydrous oxides	Hochella <i>et al.</i> (2005)
-Mineral transformations in fired carbonated clays	Bauluz <i>et al.</i> (2004b)
-Evolution of textures and mineral assemblages from sediment to metamorphic rock in open hydrothermal systems	Giorgetti <i>et al.</i> (2003)

The polymorphs of TiO₂

Seven known polymorphs of TiO₂ exist. Rutile, anatase, and brookite had been previously found in nature. Nevertheless, in anatase Bandfield *et al.* (1991) found lamellae of a second mineral, ranging in size from a few nm to hundreds of a nm across. Both minerals showed a well-defined orientation relationship but the interplanar spacings of lattice parallel to the interphase were not exactly equal. They interpreted high-resolution electron micrographs to determine the positions of columns of Ti cations within the unit cell. The model structure was tested by comparing computer-generated images with experimental micrographs and refined using a distance-least-squares program to adjust interatomic distances to those previously known in anatase and rutile. The unnamed mineral had been reported previously as the synthetic polymorph TiO₂ (B). In this way, they were able to model the structure of anatase, TiO₂ (B), and their

boundaries. Heating experiments carried out with the electron microscope showed that TiO₂ (B) was converted to anatase at a furnace temperature of ~700 °C (~100 °C below the anatase-rutile transformation).

The most common form of TiO₂ in nature is rutile, which is an important accessory mineral in metamorphic rocks, particularly high-pressure ones. Wu *et al.* (2005) described a natural high-pressure phase of titanium oxide with α -PbO₂-structure. It occurred as (<20 Å) lamellae between multiple twinned rutile crystals in coesite-bearing eclogite at Shima in the Dabie Mountains, China. These lamellae presented an orthorhombic lattice, corresponding to α -PbO₂-type TiO₂ with space group Pbcn. The α -PbO₂-type TiO₂ could be an extremely useful index mineral for ultrahigh pressure. Diamond in the mineral assemblage of Dabie Mountains indicates the metamorphic conditions to be greater than a pressure of 4 GPa (Xu *et al.* 1992). Based on the TiO₂ phase boundary reported by Withers *et al.* (2003), the α -PbO₂-type nanophase of TiO₂ in rutile records a minimum pressure of 7 GPa (depth of more than 200 kilometres).

Antiphase domains

High pigeonite has symmetrically equivalent Si-O tetrahedral chains, but in low pigeonite there are two symmetrically distinct chains, each with a different degree and sense of rotation. With a decrease in temperature, the polymorphic change produces the two types of chains, which lose their equivalence (Putnis, 1993); as the change does not match up in the different areas of the mineral, there is the possibility of the formation of an interface across which the sequence of chains is incorrect. Such domains are called antiphase domains.

Since they involve only translational differences, antiphase domains cannot be seen by optical microscopy. However, the loss of symmetry between the two types of chains produces the change from a C-centred to a primitive unit cell (Putnis, 1993). Dark-field electron micrographs using reflections of the type $h+k = \text{odd}$, which are present in P lattice but absent in C lattice, allow the antiphase domains to be identified and their boundaries to be recognised.

In omphacites, and in many other minerals (e.g. plagioclases), two cations, or more, share a site. With a decrease in temperature, each cation “chooses” its own exclusive site. Such a differentiation of crystallographic sites may even produce a change in the

space group. The low-temperature polymorph is a sub-group of symmetry of the high-temperature one. The loss in translational symmetry in order-disorder transformations can also produce antiphase domains (Brenker *et al.* 2003).

The mean antiphase domain size and form depend on peak temperature, duration of peak metamorphism, cooling rate, and composition. They therefore provide very useful information about the geological history of the minerals.

Retrograde intergrown phyllosilicate grains

Phyllosilicate grains, showing optical characteristics identical to biotite, are frequent. They differ in mineral nature, composition, and origin, and may be grains corresponding to a single mineral or a combination of two or more mineral species. One of the most significant cases was described in the Alps by Chatterjee (1966), who gives it the name “oxidized chlorites” due to its basically chloritic composition. Grains with the same optical and chemical characteristic are rock-forming minerals in the graphite schists of the Nevado-Filabride Complex in the Internal Zones of the Betic Cordillera. Based on Chatterjee’s description in the Alps, the Nevado-Filabride grains were also considered as oxidized chlorites. Nevertheless, Mellini *et al.* (1991) recognised that most of the area was dominated by 14 Å lattice fringes, with chlorite composition, but smectite was also present as individual 10Å layers interlayered in the chlorite or as packets a few layers thick. In other areas, a poorly crystalline 16Å phyllosilicate with chlorite composition, interpreted as hydrated chlorite, was recognised in addition to semi-amorphous material showing hematite spacings and composition.

All these supergenic-origin materials were interpreted as the result of fluid-mediated processes in relation to the uplift of the Nevado-Filabride rocks, due to erosion and/or post-metamorphic extension. A similar process was later described in the overlying Malaguide Complex by Nieto *et al.* (1994). These two cases were some of the first retrograde alteration processes, which, together with numerous other examples, were employed some years later (Nieto *et al.* 2005) to define *retrograde diagenesis*.

Serpentine minerals

The serpentine tetrahedral and octahedral layers present partially different dimensions along the **a** and **b** directions. The various serpentine minerals display

different mechanisms that provide solutions to their fitting. For example, a rolled microstructure producing cylinders is a characteristic in TEM for recognising chrysotile. In contrast, the antigorite structure results from a structural modulation of the serpentine layers along the **a** direction. The shorter tetrahedral layers change their polarity every given number of sub-cells, passing from upper to lower position in relation to the longer octahedral layers (Capitani and Mellini, 2004). A selected area electron diffraction (SAED) pattern consists of the main diffraction spots from the sub-cell, which are surrounded by satellite diffraction spots from the modulated structure of antigorite. The *m*-values, representing the number of tetrahedra in one modulation, range from 13 to 50 and can be determined from the respective spacings of the sub-cell and the modulated structure. Antigorite microstructures vary from highly ordered to lower periodic structures in the *c* direction (Auzende *et al.* 2006). TEM is a convenient tool for investigating and characterising antigorite variability at such a scale. Serpentine microstructures can potentially preserve information on metamorphic conditions.

The deformation processes of serpentinites during subduction are complex. According to microstructural evidence, shearing is accommodated by brittle and/or ductile deformation mechanisms. With increasing metamorphic grade, the brittle behaviour gives way to pressure solution, which persists up to eclogite-facies conditions. Once the partial dehydration reaction is reached, antigorite may recrystallise, mainly by a pressure-solution mechanism. The required fluids would derive from the progressive dehydration of antigorite (Auzende *et al.* 2006). Pressure solution is an effective mechanism to accommodate deformation; according to these authors, serpentinites could localize the deformation within a subduction/exhumation channel, thus making it possible to preserve eclogites from depths of about 100 km below the Earth's surface.

Ammonium micas

The common interlayer cations in low-grade metapelite micas are K and Na. In addition, since the late 1950s, ammonium has been recognised as an important interlayer constituent in white micas associated with organic matter. This third important interlayer component had not been thoroughly studied due, in part, to the intrinsic difficulty of analyzing NH_4 by *in-situ* methods and, in part, to the typically defective character and

small grain size of minerals in very low-grade metamorphic rocks, since most natural tobelites have been described in subgreenschist-facies rocks.

Nieto (2002) was the first to describe, using TEM, the textural characteristics of NH_4 micas in very low-grade metapelites with associated coal seams (from the *Bacia Carbonífera do Douro-Beira*, N Portugal), and he established their chemical and genetic relationships with coexisting K micas. NH_4 and K micas and berthierine form small subparallel packets of a few layers separated by low-angle boundaries, exhibiting all the characteristics commonly described for subgreenschist-facies, which includes a lack of textural and chemical equilibrium. In the Douro-Beira samples, the simultaneous presence of two groups of compositions of micas, one K-rich and the other K-poor, was demonstrated by XRD, lattice fringe images, electron diffraction, and analytical electron microscopy data (Fig. 4). The textural relationship between the two micas was the usual one between paragenetic phyllosilicates in very low-grade shales, like the one described for the muscovite/paragonite system by Shau *et al.* (1991). NH_4 - and K-dominated micas were segregated into well-separated packets with scarce intergrowth and almost no mixed-layers. Hence, they showed a solvus relationship. The compositional gap is narrow (Fig. 4), possibly near closure.

The presence of N in the micas was also confirmed by electron energy loss spectroscopy (EELS) of powdered portions dispersed on holey-carbon grids (Livi *et al.* 2006). The method involves a simultaneous acquisition of EELS spectra over the energy-loss range 275–475 eV and the acquisition of energy dispersive X-ray spectra (EDS). The EELS spectra contain the core-loss edges for K L_{2,3} (296.3 eV) and N K (400.9 eV). Thus, the N/K ratio can be calculated. Analysis of ammonium in white micas from the Central Alps, Switzerland, indicated that concentrations of N down to 0.01 atoms per formula unit could be detected.

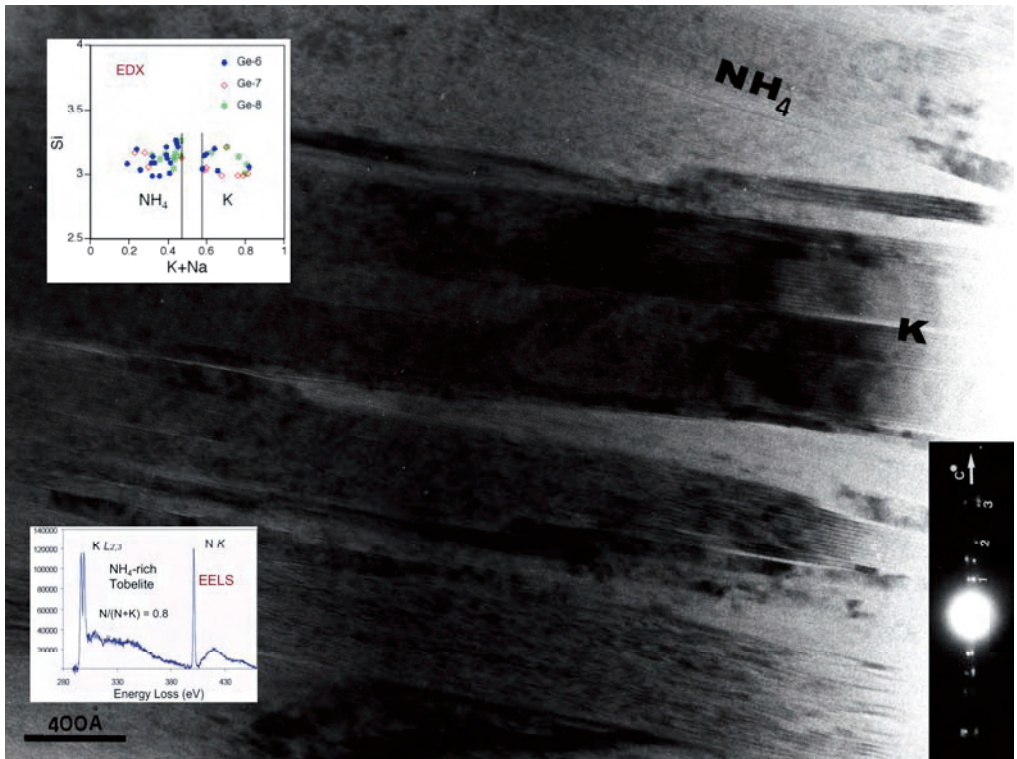


FIGURE 4. Lattice-fringe image showing textural relationships between packets of muscovite (K) and tobelite (NH_4) in an organic-rich shale. Insets: Chemical contents of three samples determined by EDX, showing the gap between the two kinds of micas; K/N ratio of a tobelite crystal determined by EELS; electron diffraction pattern (bottom right) in which the existence of two slightly different (00l) spacings is evident in the third (3) order. The intermediate spot between second (2) and first (1) order corresponds to a minor local muscovite/tobelite mixed-layer (not visible in the image). From Nieto (2002) and Abad *et al.* (2007).

Genesis of Mn oxides from marine sediments

Mn oxy-hydroxides form as a result of diagenetic, hydrogenous, or hydrothermal processes along mid-ocean ridges or on the sea floor, using reduced dissolved Mn^{2+} provided by springs. These oxides, which have a +3 or +4 valence state, are largely controlled by redox and pH conditions. Precipitation of Mn oxy-hydroxide in natural environments could result from microbial processes, which accelerate the rate of Mn^{2+} oxidation. Buatier *et al.* (2004) studied Mn deposits and partially altered sediments from the flank of the Juan de Fuca Ridge. At SEM scale, samples exhibited abundant

encrustations of detrital grains and fossils by Mn oxy-hydroxides, suggesting that the oxides formed from the interaction of fluids with sediments.

Well-crystallised Mn-oxide phases were todorokite and birnessite, based on XRD, TEM, and SAED analyses of Mn crusts. TEM and SAED allowed the identification of poorly crystallized and amorphous phases with small crystal size that could correspond to poorly crystallized birnessite and amorphous Mn-rich nanocrystallites, also containing Si and Fe.

To determine the valence of Mn in the different types of particles, the MnL_3 to MnL_2 area ratio was measured and compared with that of three standard samples containing Mn^{2+} , Mn^{3+} , and Mn^{4+} respectively. The valence of Mn was then calculated from the calibration curve. The chemical shift of the MnL_3 edge was also measured for the different types of particles and compared to standard samples. The shape of the oxygen K-edge spectra of the samples was also observed and compared with that of standard compounds. EELS analyses gave an average oxidation state for Mn of about 3.7 for birnessite and a lower average valence state for veil-like particles and aggregates of small veil-forming cellular structures of filament.

Buatier *et al.* (2004) concluded that todorokite was the final product requiring a several-step mechanism for formation. This implies that reactants included intermediate lower-valence state and poorly crystallized minerals, with progressive increases in the size and crystallinity of Mn oxide and a progressive oxidation of Mn.

References

- Abad, I., Livi, K., Nieto, F., Árkai, P. and Judik, K. (2007). Analysis of ammonium in micas by Electron Energy-Loss Spectroscopy, in "Diagenesis and Low-Temperature Metamorphism. Theory, Methods and Regional Aspects", F. Nieto and J. Jiménez-Millán, eds. Seminarios SEM 3, 99.
- Abad, I., Nieto, F., Peacor, D.R. and Velilla, N. (2003). Clay Miner., 38, 1-23.
- Abad-Ortega, M.A. and Nieto, F. (1995). Contrib. Mineral. Petrol., 120, 327-336.
- Ahn, J.H. and Peacor, D.R. (1986). Clays Clay Miner., 34, 165-179.
- Amouric, M., Mercurio, G. and Baronnet, A. (1981). Bull. Miner., 104, 298-313.
- Auzende, A.L., Guillot, S., Devouard, B. and Baronnet, A. (2006). Eur. J. Mineral., 18, 21-33.
- Banfield, J.F., Veblen, D.R. and Smith, D.J. (1991). Am. Mineral., 76, 343-353.
- Banfield, J.F. and Veblen, D.R. (1991). Am. Mineral., 76, 113-127.
- Baronnet, A. and Devouard, B. (2005). Can. Mineral., 43, 513-542.

- Bauluz, B., Mayayo, M.J., Yuste, A., Fernandez-Nieto, C. and Gonzalez Lopez, J.M. (2004a). *Clay Miner.*, 39, 333-344.
- Bauluz, B., Peacor, D.R. and Hollis, C.J. (2004b). *Earth Planet. Sci. Lett.*, 219, 209-219.
- Bozhilov, K.N., Jenkins, D.M. and Veblen, D.R. (2004). *Am. Mineral.*, 89, 74-84.
- Brenker, F.E. and Krot, A.N. (2004). *Am. Mineral.*, 89, 1280-1289.
- Brenker, F.E., Muller, W.F. and Brey, G.P. (2003). *Am. Mineral.*, 88, 1300-1311.
- Buatier, M.D., Guillaume, D., Wheat, C.G., Herve, L. and Adatte, T. (2004). *Am. Mineral.*, 89, 1807-1815.
- Buseck, P.R. (1992). Principles of transmission electron microscopy, in "Minerals and reactions at the atomic scale: transmission electron microscopy", P.R. Buseck, ed. *Min. Soc. Amer. Reviews in Mineralogy* 27, 1-35. Washington, D.C.
- Camara, F., Doukhan, J.C., Domeneghetti, M.C. and Zema, M. (2000). *Eur. J. Mineral.*, 12, 735-748.
- Capitani, G. and Mellini, M. (2004). *Am. Mineral.*, 89, 147-158.
- Capitani, G. and Mellini, M. (2005). *Am. Mineral.*, 90, 991-999.
- Capitani, G.C., Oleynikov, P., Hovmoller, S. and Mellini, M. (2006). *Ultramicroscopy*, 106, 66-74.
- Chatterjee, N.D. (1966). *Contrib. Miner. Petrol.*, 12, 325-339.
- Cliff, G. and Lorimer, G.W. (1975). *Journal of Microscopy*, 103, 203-207.
- Ding, Y. and Veblen, D.R. (2004). *Am. Mineral.*, 89, 961-968.
- Ding, Y., Veblen, D.R. and Prewitt, C.T. (2005). *Am. Mineral.*, 90, 1265-1269.
- Dodony, I. and Buseck, P.R. (2004). *Am. Mineral.*, 89, 1631-1639.
- Driscoll, J., Jenkins, D.M., Dyar, M.D. and Bozhilov, K.N. (2005). *Am. Mineral.*, 90, 900-911.
- Durovic, S., Hybler, J. and Kogure, T. (2004). *Clays Clay Miner.*, 52, 613-621.
- Eggleton, R.A. and Guggenheim, S. (1994). *Am. Mineral.*, 79, 426-437.
- Faivre, D., Menguy, N., Guyot, F., Lopez, O. and Zuddas, P. (2005). *Am. Mineral.*, 90, 1793-1800.
- Ferraris, C., Grobety, B., Fruh-Green, G.L. and Wessicken, R. (2004). *Eur. J. Mineral.*, 16, 899-908.
- Ferrow, E.A. and Hovmoller, S. (1993). *Eur. J. Mineral.*, 5, 181-188.
- Giorgetti, G., Gliozzo, E. and Memmi, I. (2004). *Eur. J. Mineral.*, 16, 493-503.
- Giorgetti, G., Mata, M.P. and Peacor, D.R. (2003). *Clay Miner.*, 38, 113-126.
- Golden, D.C., Ming, D.W., Morris, R.V., Brearley, A., Lauer, H.V., Treiman, A.H., Zolensky, M.E., Schwandt, C.S., Lofgren, G.E. and McKay, G.A. (2004). *Am. Mineral.*, 89, 681-695.
- Hochella, M.F., Kasama, T., Putnis, A., Putnis, C.V. and Moore, J.N. (2005). *Am. Mineral.*, 90, 718-724.
- Huertas, F.J., Fiore, S. and Linares, J. (2004). *Clay Miner.*, 39, 423-431.
- Idrissi, H., Cordier, P., Jacob, D. and Walte, N. (2008). *Eur. J. Mineral.*, in press.
- Ilton, E.S. and Veblen, D.R. (1988). *Nature*, 334, 516-518.
- Jimenez-Millan, J., Velilla, N. and Vazquez, M. (2007). *Clay Miner.*, 42, 273-286.
- Kogure, T., Banno, Y. and Miyawaki, R. (2004). *Eur. J. Mineral.*, 16, 891-897.
- Kogure, T. and Inoue, A. (2005). *Eur. J. Mineral.*, 17, 465-473.
- Kogure, T., Miyawaki, R. and Banno, Y. (2005). *Am. Mineral.*, 90, 725-731.

- Livi, K., Abad, I., Nieto, F. and Veblen, D. (2006). Geophysical Research Abstracts, 8, 09739.
- Mellini, M. (1982). *Tschemaks Min. Petr. Mitt.*, 30, 249-266.
- Mellini, M. (1985). *Rend. Soc. Ital. Min. Petrol.*, 40, 229-240.
- Mellini, M., Nieto, F., Alvarez, F. and Gómez-Pugnaire, M.T. (1991). *Eur. J. Mineral.*, 3, 27-38.
- Mellini, M., Oberti, R. and Rossi, G. (1983). *Periódico di Mineralogia. Roma.*, Anno 52, 538-615.
- Moore, K.T., Veblen, D.R. and Howe, J.M. (2001). *Am. Mineral.*, 86, 1314-1318.
- Moreau, J.W., Webb, R.I. and Banfield, J.F. (2004). *Am. Mineral.*, 89, 950-960.
- Mugnaioli, E., Capitani, G., Nieto, F. and Mellini, M. (2008). *Am. Mineral.*, in press.
- Muller, W.F., Brenker, F.E., Barnert, E.B. and Franz, G. (2004). *Eur. J. Mineral.*, 16, 37-48.
- Muller, W.F. and Franz, G. (2004). *Eur. J. Mineral.*, 16, 939-944.
- Navrotsky, A. (1994) *Physics and Chemistry of Earth Materials*. Cambridge University Press, 417 pp.
- Nieto, F. (2002). *Am. Mineral.*, 87, 205-216.
- Nieto, F., Mata, M.P., Bauluz, B., Giorgetti, G., Árkai, P. and Peacor, D.R. (2005). *Clay Miner.*, 40, 93-104.
- Nieto, F., Velilla, N., Peacor, D.R. and Ortega-Huertas, M. (1994). *Contrib. Mineral. Petrol.*, 115, 243-252.
- Olives, J., Amouric, M. and Perbost, R. (2000). *Clays Clay Miner.*, 48, 282-289.
- Palenik, C.S., Utsunomiya, S., Reich, M., Kesler, S.E., Wang, L.M. and Ewing, R.C. (2004). *Am. Mineral.*, 89, 1359-1366.
- Putnis, A. (1993). *Introduction to mineral sciences*. Cambridge University Press. Cambridge. 457 pp.
- Rodriguez-Navarro, C., Jimenez-Lopez, C., Rodriguez-Navarro, A., Gonzalez-Munoz, M.T. and Rodriguez-Gallego, M. (2007). *Geochim. Cosmochim. Acta*, 71, 1197-1213.
- Rodriguez-Navarro, C., Ruiz-Agudo, E., Ortega-Huertas, M. and Hansen, E. (2005). *Langmuir*, 21, 10948-10957.
- Ruiz Cruz, M.D. (2004). *Clays Clay Miner.*, 52, 603-612.
- Ruiz Cruz, M.D., Puga, E. and De Federico, A. (2007). *Eur. J. Mineral.*, 19, 547-556.
- Sánchez Navas, A., Martín Algarra, A. and Nieto, F. (1998). *Sedimentology*, 45, 519-533.
- Sanchez-Navas, A. and Galindo-Zaldivar, J. (1993). *Eur J Mineral*, 5, 245-256.
- Schwartz, J.M. and McCallum, I.S. (2005). *Am. Mineral.*, 90, 1871-1886.
- Seto, Y., Shimobayashi, N., Miyake, A. and Kitamura, M. (2004). *Am. Mineral.*, 89, 257-265.
- Shau, J.H., Feather, M.E., Essene, E.J. and Peacor, D.R. (1991). *Contrib. Mineral. Petrol.*, 106, 367-378.
- Shen, P.Y., Hwang, S.L., Chu, H.T., Yu, T.F., Pan, C.N. and Huang, W.L. (2005). *Eur. J. Mineral.*, 17, 543-552.
- Song, S.G., Zhang, L.F., Chen, J., Liou, J.G. and Niu, Y.L. (2005). *Am. Mineral.*, 90, 814-820.

- Spinkler, G.E., Self, P.G., Lijama, S. and Buseck, P.R. (1984). *Am. Mineral.*, 69, 252-263.
- Vali, H. and Köster, M. (1986). *Clay Min.*, 21, 827-859.
- Van Aken, P.A., Mische, G., Woodland, A.B. and Angel, R.J. (2005). *Eur. J. Mineral.*, 17, 723-731.
- Viti, C. and Mellini, M. (1996). *Eur. J. Mineral.*, 8, 423-434.
- Withers, A.C., Essene, E.J. and Zhang, Y.X. (2003). *Contrib. Mineral. Petrol.*, 145, 199-204.
- Wu, X.L., Meng, D.W. and Han, Y.J. (2005). *Am. Mineral.*, 90, 1458-1461.
- Xu, S.T., Okay, A.I., Ji, S.Y., Sengor, A.M.C., Wen, S., Liu, Y.C. and Jiang, L.L. (1992). *Science*, 256, 80-82.
- Zou, X. (1995). Thesis Univ. of Stockholm, 523 pp.
- Zvyagin, B.B. (1994). *Kristallografiya*, 39, 283-290.

X-ray Absorption Spectroscopy in Mineralogy and in the Earth and Environmental Sciences

Jesús Chaboy Nalda

Instituto de Ciencia de Materiales de Aragón (ICMA) and Departamento de Física de la Materia Condensada, CSIC-Universidad de Zaragoza, 50009 Zaragoza (Spain)

Introduction

X-ray absorption spectroscopy (XAS) has proven to be an outstanding structural tool by allowing the determination of the local environment around a selected atomic species in a great variety of systems. An important advantage of this technique is its utility for heterogeneous samples in such a way that a wide variety of solid and liquids, including whole soils and liquids, can all be examined directly and non-destructively. Additionally, since the local structure does not depend on long-range crystalline order, the structure of amorphous phases (and that of dissolved species) is easily achieved.

XAS is useful for concentrations from about 10 ppm to major elements. As such, it is useful to speciate trace elements such as contaminants adsorbed to pure minerals, soils and sediments, and is also a valuable tool for studying the mineralogical composition of the soil or sediment (especially when used in conjunction with other techniques such as X-ray diffraction).

Our purpose here is to present a brief review of the principles underlying x-ray absorption spectroscopy. The main strengths of this technique mainly focused on Mineralogy and in the Earth and Environmental Sciences are highlighted and illustrated by showing different selected examples.

X-ray Absorption Spectroscopy (XAS): basic principles

The basic process of X-ray absorption is the excitation of electrons from deep core levels of a selected atom by the absorption of a photon. When X-rays pass through any sort of material, a proportion of them will be absorbed. The absorption of x-rays by atoms is smoothly varying with photon energy except at some discrete energies where

abrupt increases occur, called absorption edges. These edges correspond to the x-ray photon attaining enough energy to free or excite a bound electron in the atom.

The absorption of x-rays on the high energy of the absorption edges does not vary monotonically in condensed matter but has a complicated behavior which extends past the edge by an amount typically of the order of 1 keV. The small oscillations can superimposed on the edge step gradually die away as the X-ray energy increases. The oscillations are known as EXAFS (Extended X-ray Absorption Fine Structure) are due to the interaction of the photoelectron with the surrounding atoms.

Usually the x-ray absorption spectrum is divided in several regions depending on the energy of incoming photons:

- * the pre-edge, edge and the near-edge (XANES) regions, which extend about 20 eV below the edge to 30-100 eV beyond the edge.
- * the EXAFS region which extends from 30-100 eV to 600-1000 eV beyond the edge.

The physical origin of the absorption features in the pre-edge and edge regions depend on the material, i.e. Rydberg states in free atoms, bound valence states or bound multiple scattering resonances in molecules, unoccupied local electronic states in metals and insulators. Thus, analysis of these near-edge features in the spectrum of a particular sample can provide information about vacant orbitals, electronic configuration and the site symmetry of the absorbing atom.

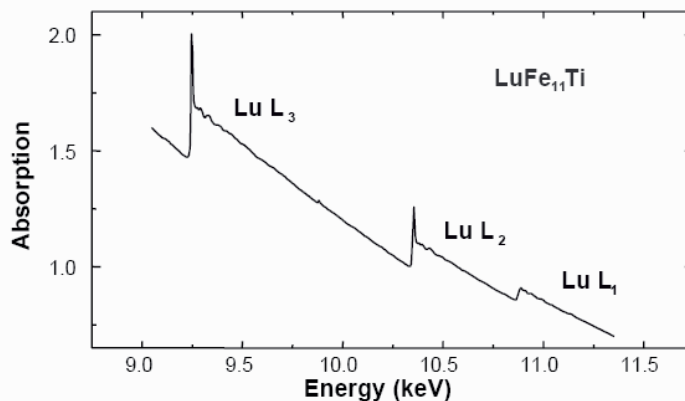


FIGURE 1. X-ray absorption spectra of $\text{LuFe}_{11}\text{Ti}$ at the Lu L-edges, involving different final state symmetry: L_3 ($2p_{3/2} \rightarrow \epsilon\{d_{3/2}, d_{5/2}\}$), L_2 ($2p_{1/2} \rightarrow \epsilon d_{3/2}$), L_1 ($2s_{1/2} \rightarrow \epsilon\{p_{1/2}, p_{3/2}\}$).

The underlying physics of the processes that occur to produce the XANES and EXAFS structures in the x-ray absorption spectra is easy to understand. The photon is completely absorbed and kicks out a core photoelectron from the absorbing atom leaving behind a core hole. This photoelectron will be ejected with an energy equal to energy of the incoming photon less its binding energy, when in the core. This photoelectron will interact with the surrounding atoms. Considering the wave nature of the ejected photoelectron and regarding the atoms as point scatterers a simple picture can be seen in which the backscattered waves interfere with the forward wave to produce either peaks or troughs. This is an interference effect on the final state. Since the transition probability is given by a matrix element between the final and initial states and the absorption coefficient is related to the transition probability, this interference affects the absorption coefficient which is the value that is measured in an XAS experiment.

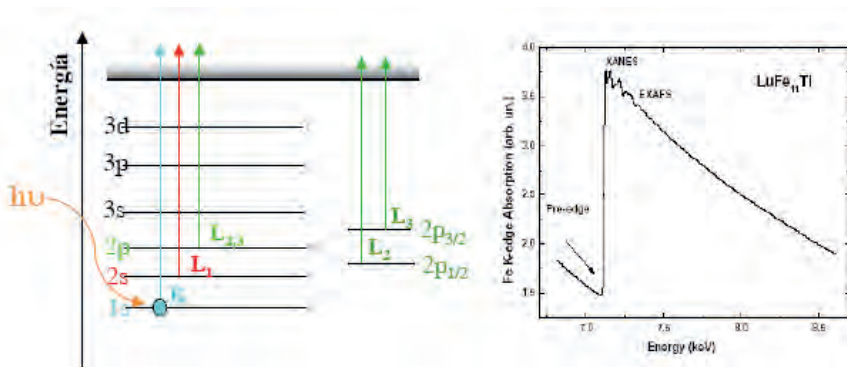


FIGURE 2. Schematic of the excitation of an electron by the absorption of an x-ray photon.

The wavelength of the photoelectron is dependent on its energy and thus the phase of the back-scattered wave at the central atom will change with the energy of the incoming photon. This leads to the oscillatory nature of the interference effect. Since backscattering amplitude and phase are dependent on the type of atom doing the backscattering and the distance it is from the central atom, information regarding the coordination environment of the absorbing atom can be obtained by analyzing the XANES and EXAFS.

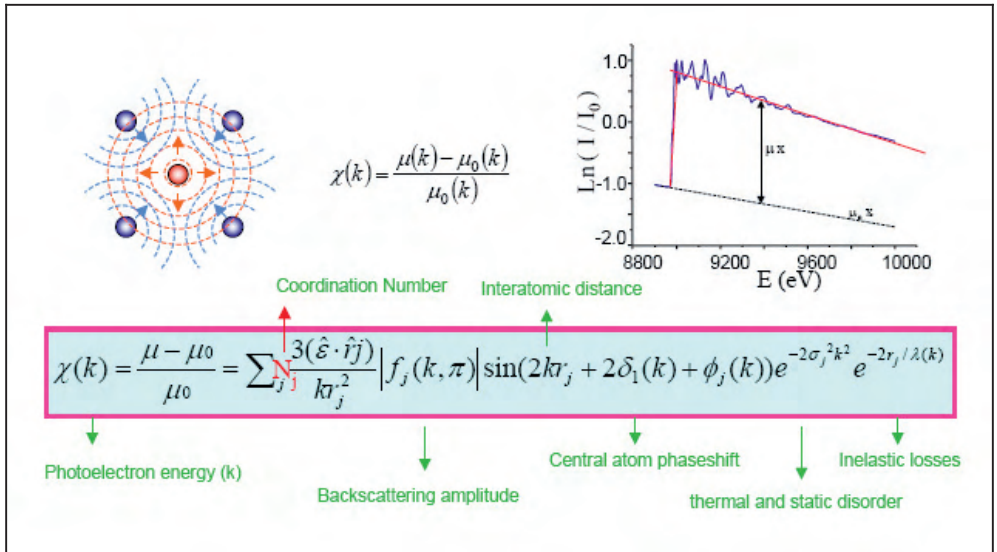


FIGURE 3. Schematic illustration of the interference phenomena giving rise to the modulations (EXAFS) in the x-ray absorption cross-section.

The only distinction between XANES and EXAFS regions is the relative weight of the multiple scattering processes of the excited photoelectron. Usually it is considered that in the EXAFS region only single-scattering processes are important contrary to the XANES region in which due to the low kinetic energy of the ejected photoelectron multiple scattering processes are dominant. Consequently, through careful analysis of the oscillating part of the spectrum after the edge, information relating to the coordination environment of a central excited atom can be obtained.

As outlined above, the near-edge and XANES parts of the x-ray absorption spectrum are sensitive to bonding environment as well as oxidation state. The position of the edge and the assignment of peaks near or on the edge give information about oxidation state, covalency (increasing ligand character of metal d orbitals), molecular symmetry of the site, and thereby coordination number. XANES spectra are commonly compared to standards to determine which species are present in an unknown sample. Once species are identified, their relative abundance is quantified using linear-combination fitting (or other curve-fitting algorithms) using XANES standards to reconstruct the experimental data.

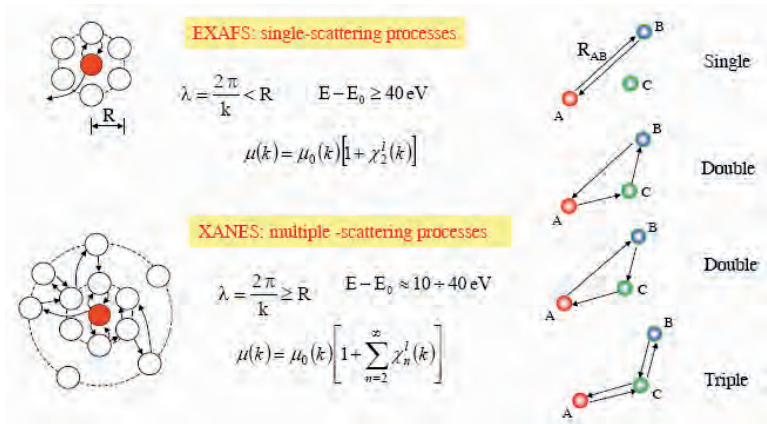


FIGURE 4. Single and multiple-scattering processes in x-ray absorption.

Often these features are diagnostic of coordination and are of use for geochemistry. For example, the toxic chromate anion is tetrahedral and as a result has a large absorption feature just below the absorption edge (the so-called pre-edge) that is not present in the more benign Cr(III). As a result, the presence of this feature is diagnostic for the more toxic form of chromium.

It is important to note that XANES is sensitive not only to the oxidation state, but also to the bonding geometry. The symmetry of the absorbing site strongly affects the pre-edge transition and, thus, XANES is capable of discriminating species of similar formal oxidation state but different coordination.

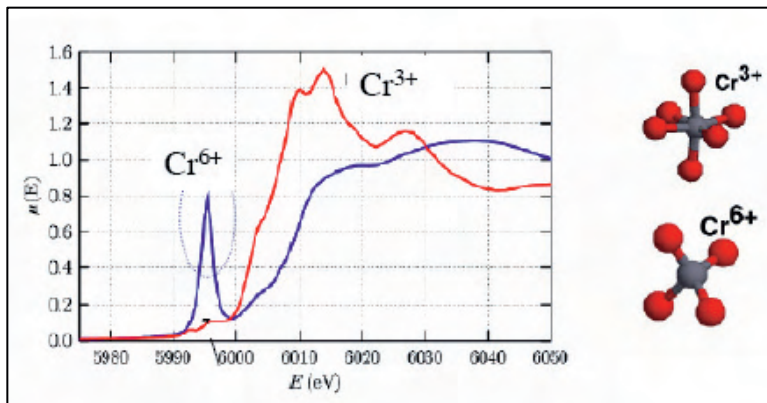


FIGURE 5. Cr K-edge XANES of Cr^{3+} and Cr^{6+} in octahedral and tetrahedral environments.

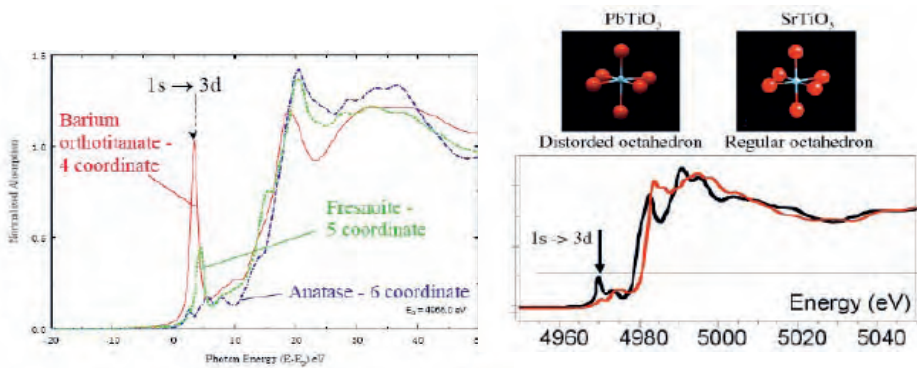


FIGURE 6. Ti K-edge XANES spectra of reference compounds in which Ti ion shows the same oxidation state but different coordination.

The more distant region of the X-ray absorption spectrum is termed the extended X-ray absorption fine structure (EXAFS) region. EXAFS spectra are best described as a series of periodic sine waves that decay in intensity as the incident energy increases from the absorption edge. These sine waves result from the interaction of the ejected photoelectron with the surrounding atomic environment. As such, their amplitude and phase depend on the local structure of excited atom and, consequently, the EXAFS provides direct, local structural information about the atomic neighborhood of the element being probed. The information content consists of the identity of neighbouring atoms, their distance from the excited atom, the number of atoms in the shell, and the degree of disorder in the particular atomic shell. These distances and coordination numbers are diagnostic of a specific mineral or adsorbate-mineral interaction; consequently, the data are useful to identify and quantify major mineral phases, adsorption complexes, and crystallinity.

Although the EXAFS formula (see Fig. 3) provides a complete description of the EXAFS oscillations, it is not a particularly convenient form for visualizing the information content of an EXAFS spectrum. Fourier transformation can be used to decompose a frequency-space signal into its different constituent frequencies. This is illustrated for crystalline and amorphous Germanium in Fig. 7. The Fourier transform

(FT) of an EXAFS spectrum gives a pseudo-radial distribution function. It is pseudo in that the FT amplitude cannot be related directly to electron density around the absorber due to the backscattering amplitude and the damping factors, and because the apparent distances in the FT are shifted by about 0.5 Å, due to the phase shifts. However, the FT is a useful way of judging qualitatively what shells may be present in a system and for comparing a fit to the data.

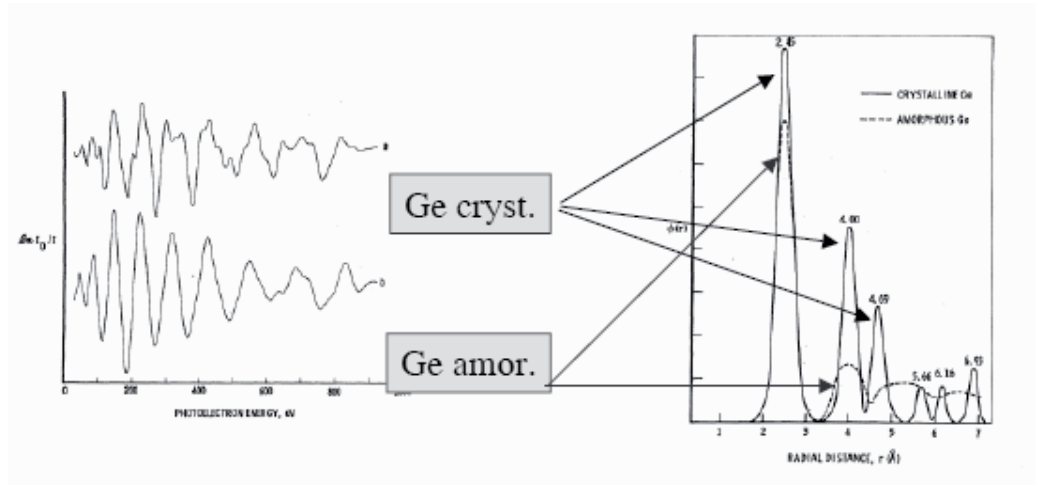


FIGURE 7. Ge K-edge EXAFS spectra and their Fourier transforms in the case of crystalline and amorphous Germanium.

X-ray Absorption Spectroscopy in Mineralogy and in the Earth and Environmental Sciences.

X-ray absorption spectroscopy has become a common technique in mineral studies suited to extend structure determination down to an atom local environment, thus some three orders of magnitude less than the structure volume, best inspected by methods based on X-ray diffraction.

The unique capabilities offered by XAS are due to its main general features:

i) the absorption spectrum is element specific: the inner-shell absorption steps occur at x-ray energies characteristic of the absorbing element, so that individual element absorption spectra can be picked up out in samples containing a complex chemical mixture of different elements simply by changing the x-ray wavelength;

ii) by tuning the x-ray energy one can not only select specific elements in the sample but to select different absorption edges for the same atom, i.e. select the final-state symmetry.

iii) the principal advantage of XAS as a structural probe is that it is a local structure probe and the presence of long-range order is not required. This means that XAS can be used to study non-crystalline samples or to compare solution structure with solid state structure. In ideal circumstances EXAFS data can be analysed to determine the absorber–scatterer distance with an accuracy of 0.02 Å (and a precision that is substantially better, 0.004 Å, and perhaps even better under carefully controlled conditions). Coordination numbers can be determined with accuracy better than 20% and scatterer identity can typically be defined to the nearest row of the periodic table.

iv) Flexible detection mode. Different detection schemes are available for XAS measurements. The detection system depends on the concentration of the absorbing atom, on the photon flux of the beam line and on the energy of the absorption edge to be investigated. Transmission and fluorescence modes are typically used for XAS detection. For bulk experiments using hard X-rays on atoms with $Z > 20$ present with concentrations greater than 0.1% in the sample (atomic ratio), standard X-ray transmission techniques are used, under gas (He, N) or in air. Indeed, the Transmission mode is the preferred one when there are no experimental constraints that suggest another. Limiting conditions are excessive thickness of the sample that forbids the beam to pass through, and diluteness of the absorber species (< 1 wt.%), when the XAS features become comparable with the statistical noise. Transmission through the sample assures that the whole bulk content of absorber present in the sample is probed and it is relatively independent upon the matrix effect, although the signal to noise ratio (S/N) may be somewhat reduced in the case of matrices having an average Z close to that of the absorber. On the other hand, recording a spectrum in the fluorescence yield (FY) mode is a highly efficient experimental method for high- Z atoms and highly diluted samples. Using appropriate filters, only the photons emitted by the excited absorbing atom are recorded. This detection mode crosscuts all problems of sample thickness that affect the transmission mode, thus even very thick samples (> 1 mm) can be probed, and is particularly effective when the absorber is diluted, as it increases detection by at least

two orders of magnitude. Consequently, S/N is enhanced and XANES spectra on even very diluted heavy atoms can be measured proficiently.

v) Finally, it should be noted that XAS experiments can be performed on a highly flexible sample environment. In this way, XAS experiments can be performed under extreme conditions of temperature, different gas atmospheres, and even under high-applied pressure on solid, liquid and gaseous samples.

These characteristics make XAS an incomparable tool to face different problems in Mineralogy and in the Earth and Environmental Sciences. Indeed, the flexible sample environment allows approach the temperature and pressure conditions of the Earth's interior where phase transitions in minerals under high pressure are known to govern some of the major geophysical properties. In a similar way, XAS provides an unique insight into the accurate knowledge of trace-element behaviour in rock-forming and accessory minerals that results fundamental to understand and model petrologic and geochemical processes. These rock-forming minerals are always complex solid solutions and, therefore, the only approach capable of characterising the local coordination of the individual substituents is the use of element-selective spectroscopic methods like XAS.

This is for example the case of the characterization of trace Nd and Ce site preference and coordination in natural melanites. The identification of the crystal-chemical parameters controlling trace-element partitioning between minerals and silicate melts is a topic of considerable interest. Garnets represent an important group of rock-forming minerals in this regard, since they are stable over a wide range of physico-chemical conditions and are able to incorporate several trace elements commonly used in geochemical modeling. For these reasons, aluminosilicate garnets ($X_3Al_2Si_3O_{12}$, $X = Fe^{2+}$, Mn^{2+} , Mg, Ca) have received much attention, regarding their complex crystal chemistry, their thermodynamic properties or trace-element behaviour. Despite the importance of the geochemical behavior of REE in garnets, little work has been done to decipher their site preference and local coordination in trace or minor amounts. Indeed, there are no examples in the literature of direct structural investigations on the site location and geometry of REE in natural garnets, possibly due to their low concentrations. A recent work by Quartieri et al. has reported the XAS study of the site location and geometry of trace amounts of neodymium (from 176 to 1074 ppm) and

cerium (791 ppm) in natural garnets. The comparison of the experimental spectra recorded at high energy (Nd K-edge, 43569 eV; Ce K-edge 40443 eV) with theoretical ab-initio computations demonstrate that, in all the samples, the trace elements are located in the dodecahedral X site and not in extended structural defects or interstitial sites. The local geometry around the two rare-earth elements is compatible with their ionic radius and is compared with that of Ca, the major element at the X site, as determined by single-crystal X-ray diffraction data. This work represents the first example of direct investigation of trace-level REE coordination in natural garnets, and confirms the great relevance for the Earth Sciences of the use of fluorescence XAS at high energy.

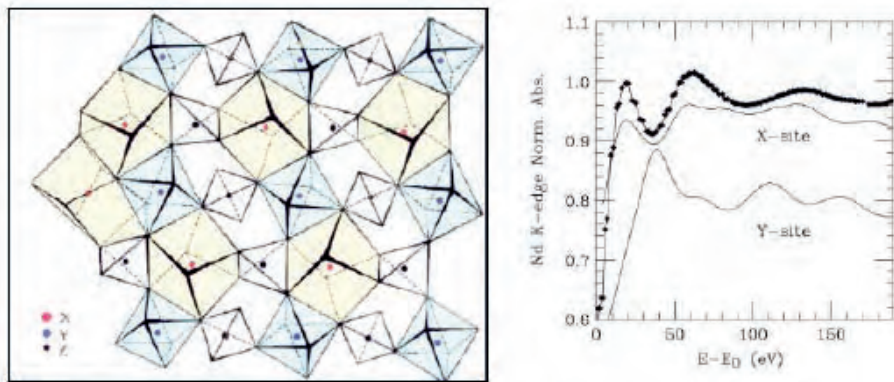


FIGURE 8. Schematic view of the crystal structure of $X_3Y_2(ZO_4)_3$ garnets and the comparison between the experimental Nd K-edge XANES signal of a natural garnet (A204) and those calculated on the basis of the FMS theory assuming Nd in the dodecahedral (X) or in the octahedral (Y) site of garnet structure. This garnet contains traces of Nd (1125 ppm) and Ce (830 ppm) being its composition $(Ca_{2.9}Mg_{0.06}Mn_{0.02}Na_{0.02})(Mg_{0.08}Ti_{0.89}Zr_{0.04}Al_{0.28}Fe^{3+}_{0.71})(Si_{2.33}Fe^{3+}_{0.62})$.

The capability of XAS to detect and characterize even trace amounts of atoms that are dispersed within minerals has been recently exploited also by Earth and Environmental scientists working on the understanding of the mineralogical and biogeochemical processes and interactions associated with environmental pollution. Within this scenario XAS is the main experimental weapon supplying information on the speciation of toxic materials. Understanding the transport and deposition of metals is crucial to both predicting toxic metal bioavailability and the accumulation of economic concentrations of metals to form mineral deposits. Toxic metals at the Earth's surface are

often present as non-crystalline forms either as sorbates on mineral species or fixed in amorphous phases. Therefore, XAS is the perfect probe for identifying those species, which are key components in the cycling of these metals.

Moreover, certain living organisms can concentrate and tolerate high amounts of heavy metals and determining the reasons for their adaptability provides strategies for remediation of contaminated land. Studies of metal take-up by biological samples have included investigation of the speciation of nickel, zinc and manganese in hyper-accumulator plants. The Ni hyper-accumulator plant *Berkheya coddii* has nickel complexed with histidine, while zinc in *Cardaminopsis halleri* and manganese in *Grevillea exul* are co-ordinated to oxygen probably as carboxylic acid anions. These relationships point to considerable selectivity in the metal-binding ligands in different classes of hyper-accumulator plants. Similarly, arsenic, lead and zinc have been found in earthworms and *Lumbricus rubellus* has adapted to living on arsenic contaminated soils with no observed deleterious effects. XAS shows that As(III)-S-thiol complexes are present in the intestines and body walls of this earthworm. As an example of the XAS capabilities in this field, we summary here the work on the changes of chemical states of toxic metals in aquatic sediments by bacteria reported by Fujiwara et al.

The implementation of Pollutant Release and Transfer Register (PRTR) obliged to report the total amount of chemical substances, such as toxic metals, released into the atmosphere, hydrosphere and soil. The total amount of these substances that have been released into the environment due to human activity is now becoming clear. However, the chemical state changes of toxic metals have not been clarified. Therefore, it is customary to clarify the behaviour of toxic metals in the environment to ensure safety against damage due to toxic metal contamination, because the toxicity of a metal depends on its valence or combined states. In many cases, microorganisms have assumed a vital role in the chemical state changes of metals.

The use of microorganisms is expected to lead to the development of environmental restoration technologies by revealing the biological reaction pathway of metals. Recently, a selenate reduction bacterium, *Sulfurospirillum barnesii*, was isolated from a freshwater sediment (R.S. Oremland *et al.*: Appl. Environ. Microbiol. **65** (1999) 4385). *S. barnesii* has the ability to reduce selenic acid [Se(VI)] under anaerobic conditions, using organic acid as an electron donor.

X-ray absorption spectroscopy allows one to monitor the change of the chemical state observed for selenium in a biological reactive process in connection with the reduction ability of *S. barnesii*. Shigeki Fujiwara, Norizo Saito and Yasuhiro Konishi used a DSM 10660 strain for *S. barnesii*, cultivated in a 500 ml sealed bottle with *Sulfurospirillum* II medium containing 83 mg/l Se(VI). Cultivation was carried out at constant temperature (30 C) under anaerobic conditions with the injection of inert gases (N₂/CO₂). XAFS spectra of *S. barnesii* culture were collected in the fluorescence mode using a Ge 19-element solid-state detector.

Figure 9 shows Se *K*-edge XANES spectra of *S. barnesii* culture and reference materials. A peak due to metallic selenium [Se(0)] was clearly observed in the spectra after 28, 37, 43, 53 and 66 hours. Also, a peak due to tetravalent selenium [Se(IV)] was observed in the same spectra. This result shows that the reduction pathway from Se(VI) to Se(0) by *S. barnesii* goes through Se(IV). In addition, the chemical composition of selenium in each moment was estimated from the ratio of each chemical states calculated by the curve-fitting method using the spectra of the reference materials. The change of the chemical composition of selenium indicates that Se(VI) constantly decreases with increasing *S. barnesii* growth rate. In this case, although a rate-limiting step of the reduction pathway from Se(IV) to Se(0) occurred for 20 hours after seeding, the reduction of Se(VI) to Se(IV) proceeded constantly. Thus, from the above finding, it is assumed that the reduction of Se(VI) to Se(IV) by *S. barnesii* is faster than that of Se(IV) to Se(0) under such a high selenium concentration (83 mg/l selenium). The results also indicate that selenium released in to the hydrosphere is immobilized as metallic selenium by anaerobic bacteria, such as *S. barnesii*, which have the ability to reduce selenium. Figure 9 shows pattern diagrams of dynamics of selenium in aquatic sediments. If we can accelerate the growth of selenium reduction bacteria, and keep them in high density, we will be able to effectively render selenium harmless.

This work illustrates how researchers using synchrotron radiation are now able to establish the mobility and bioavailability of toxic metal in contaminated land and can play a crucial role in developing methods for environmental 'clean up'.

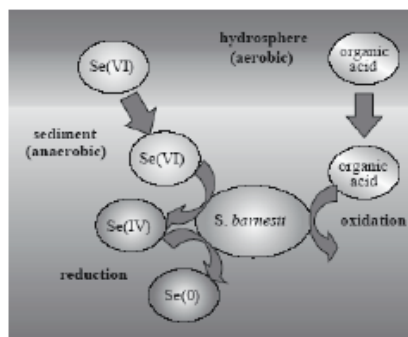
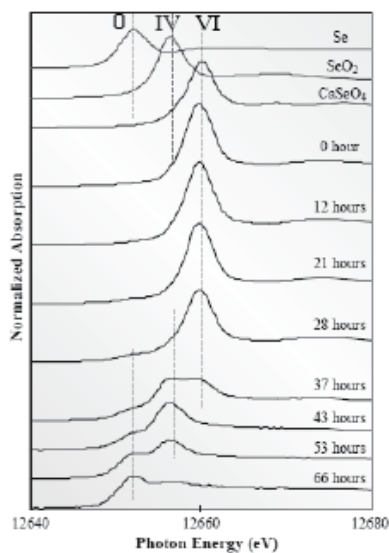


FIGURE 9. Left: Se K-edge spectra of culture after 0, 12, 21, 28, 37, 43, 53 and 66 hours from seeding *S. barnesii*, along with Se, SeO_2 and CaSeO_4 for reference. Right: Pattern diagrams of dynamics of selenium in aquatic sediments.

References

- Henderson, G.S. and Baker, D.R. (eds.) (2002). Mineralogical Association of Canada Short Course Series, Vol. 30.
- Prins, R. and Koningsberger, D. (1988). X-Ray Absorption: Principles, Applications, Techniques of EXAFS, SEXAFS, XANES.
- Brown, G.E. Jr and Sturchio, N. C. (2002). An overview of synchrotron radiation applications to low temperature geochemistry and environmental science". In Fenter, P.A., Rivers, M.L., Sturchio, N.C. & Sutton, S.R. (eds.): "Applications of synchrotron radiation in low-temperature geochemistry and environmental science /Rev Mineral. Geochem.", 49/. Washington (D.C.): Mineral. Soc. Am., 1–115 (2002).
- Brown, G.E. Jr., Calas, G., Waychunas, G. A., Petiau, J. (1988). X-ray absorption spectroscopy: Applications in mineralogy and geochemistry. In Hawthorne, F.C. (ed.): *Spectroscopic methods in mineralogy and geology* /Rev. Mineral., 18/. Washington (D.C.): Mineral. Soc. Am., 431.
- Calas, G. and Petiau, J. (1983). Solid State Comm. 48, 625.
- Calas, G., Brown, G.E. Jr, Waychunas, G. A., Petiau, J. (1987). Phys. Chem. Minerals 15, 19.
- Calas, G. Manceau, A., Combes, J. M., Farges, F. (2002). Applications of EXAFS in Mineralogy. In Mottana, A. & Burrigato, F. (eds.): "Absorption spectroscopy in Mineralogy", Amsterdam, Elsevier, 171.

- Chaboy, J. and Quartieri, S. (1995). *Phys. Rev. B* 52, 6349.
- Chaboy, J. Cotallo, E. Quartieri, S., Boscherini, F. (2002). *Journal of Synchrotron Rad.* 9, 86.
- Fujiwara, S. Saito, N., Konishi, Y. (2003). *Springer Research Frontiers* 2003, pp 97-98 (http://www.spring8.or.jp/en/support/download/publication/research_frontiers)
- Mottana, A. (2004). *EMU Notes in Mineralogy*, Vol. 6, Chapter 12, 465.
- Penner-Hahn, J. E. (1999). *Coordination Chemistry Reviews* 190-192, 1101.
- Quartieri, S., Dalconi, M. C., Boscherini, F., Oberti, R., D'Acapito, F. (2004). *Phys Chem Minerals* 31, 162 .
- Quartieri, S. Chaboy, J., Merli, M., Oberti, R., Ungaretti, L. (1995). *Phys. Chem. Minerals* 22, 159.
- Quartieri, S., Chaboy, J., Antonioli, G. and Geiger, C.A. (1999). *Phys. Chem. Minerals* 27, 88.
- Quartieri, S. Boscherini, F. Chaboy, J., Dalconi, M.C. Oberti, R., Zanetti, A. (2002). *Phys. Chem. Minerals* 29, 495.
- Iwasawa, Y. (1996). *X-Ray Absorption Fine Structure for Catalysts and Surfaces*, World Scientific, Singapore.

Raman, Conventional Infrared and Synchrotron Infrared Spectroscopy in Mineralogy and Geochemistry: Basics and Applications

Biliana Gasharova

ANKA Synchrotron Light Source / Institute for Synchrotron Radiation, Research Center Karlsruhe, P.O. Box 3640, 76021 Karlsruhe, Germany

Both vibrational spectroscopy methods, Raman and infrared (IR), have proved a useful tool for fingerprint analysis, structural characterization, *in-situ* monitoring of reaction kinetics / pressure / temperature dependence, quantitative analysis, as a probe of interatomic forces, and for calculation of thermodynamic and elastic properties. Over the past decades the development of microbeam techniques has had a major impact on vibrational studies and thus these techniques are enjoying a growing popularity in the geosciences. As with any experimental approach some theoretical understanding of the physical phenomena underlying the experiment as well as some knowledge about the principles and performance of the instrumentation are essential for a meaningful analysis of vibrational spectra. Examples of applications of Raman and IR spectroscopy in mineralogy and geochemistry will follow a brief introduction to the basics of both methods and the corresponding instrumentation.

There are a number of excellent summaries of both theory and applications available in the literature. For example, books as those of Nakamoto (1996, first published in 1963) describing fundamental theories of vibrational spectroscopy and illustrating their applications to inorganic and coordination compounds; Farmer (1974) providing an excellent description of theory, instrumentation and techniques related to mineralogy along with very extensive and valuable summary of vibrational studies across all mineralogical fields; Hawthorne (1988) summarizing theory and applications in mineralogy and geology. Some more recent books of interest could be Mirabella (1992), Putnis (1995), Turell and Corset (1996), McCreery (2000), Chalmers and Griffiths

(2001), Beran and Libowitzky (2004). The content of the theoretical part in this article is based on the literature mentioned above, which has not been further cited throughout the text.

Spectroscopic methods

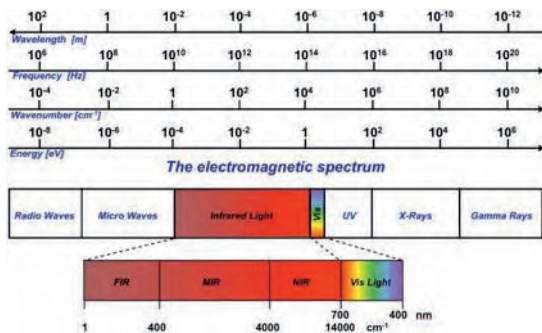


FIGURE 1. Regions of the EM spectrum with ΔE indicated in eV (energy), cm^{-1} (wavenumber), Hz (frequency) and m (wavelength).

Spectroscopic methods are complementary techniques or some times even an alternative to the traditionally applied diffraction methods. In terms of the interaction of radiation with matter, diffraction involves a change in direction of the incident radiation, without change in its energy.

The determination of structure by diffraction depends largely on the periodicity of the structure and therefore produces a long-range or average picture. Spectroscopic methods on the other hand provide information about the local structure of a material like local chemical and crystallographic environment, coordination number, site symmetry, etc. and do not depend on long-range periodicity or crystallinity.

Although there are many different spectroscopic methods they all work on the same basic principle. Under some conditions, an incident beam of radiation can be absorbed, transmitted, reflected or scattered by matter, or alternatively, can cause the emission of radiation from the material. The energy differences between ground and excited states cover the entire range of the EM spectrum from radio frequency ($\sim 10^6$ Hz) to x-ray and g-ray frequencies (up to $\sim 10^{20}$ Hz, Fig. 1). For example, in the lowest energy range, nuclei have energy levels associated with their spin with the differences between these energy levels being in the radio frequency range; transitions between spin energy levels of electrons have energy in the microwave region; rotations of molecular groups lie in the far-IR range; molecular vibrations involving stretching and bending of atomic bonds,

have a higher energy, in the mid-IR range; at still higher energies, electronic transitions involving valence electrons are associated with frequencies in the visible range; and those involving inner shell electrons at still higher energies, in the x-ray range. Each of these phenomena in a material can be studied by using incident radiation within a limited frequency range matching the energy of the transitions.

History

Sir William Herschel analyzed in 1800 the distribution of heat in sunlight dispersed through a glass prism. By measuring the temperature of each color he found that the hottest temperature was actually beyond red light. The radiation causing this heating was not visible and Herschel termed this invisible radiation "calorific rays". Today, we know it as infrared. By placing a water-filled container between the prism and the thermometer Herschel discovered, e.g. that water partially absorbs the infrared radiation making his experiments the beginning of **infrared spectroscopy**. On the other hand, **Raman spectroscopy** was "born" more than a century after Herschel's discoveries when the phenomenon of inelastic scattering of light by matter was first observed by Raman and Krishnan (1928). In the original experiment filtered sunlight was focused onto a sample with a second lens collecting the scattered radiation. A system of optical filters was used to show the existence of scattered light with an altered frequency from the incident light – the basic characteristic of Raman spectroscopy.

Basics of Raman and infrared spectroscopy

Vibrational spectroscopy involves the use of light to probe the vibrational behavior of molecular systems, usually via an absorption or a light scattering experiment. Vibrational energies of molecules lie in the approximate energy range 0 – 60 kJ/mol, or 0 – 5000 cm⁻¹. This corresponds to the energy of light in the IR region of the EM spectrum (Fig. 1). As a first approximation, the energy of a molecule can be separated into three additive components associated with (i) the motion of the electrons in the molecule, (ii) the vibrations of the constituent atoms, and (iii) the rotation of the molecule as a whole: $E_{\text{total}} = E_{\text{el}} + E_{\text{vib}} + E_{\text{rot}}$. The basis for this separation lies in the fact

that electronic transitions occur on a much shorter time scale, and rotational transitions occur on a much longer time scale, than vibrational transitions.

The energy changes we detect in vibrational spectroscopy are those required to cause nuclear motion. Vibrational transitions can be observed as IR or Raman spectra. However, the physical origins of these two spectra are markedly different. In IR spectroscopy, IR light covering a broad range of frequencies is directed onto the sample. Absorption occurs where the frequency of the incident radiation matches that of a vibration so that the molecule is promoted from the electronic ground level to a vibrational excited state (Fig. 2). The loss of this frequency of radiation from the beam after it passes through the sample is then detected. From the quantum mechanical point of view a vibration is IR active if the dipole moment of the vibrating molecule is changed. It does not matter whether the molecule has a permanent dipole moment or not, only the change associated with the vibration is important.

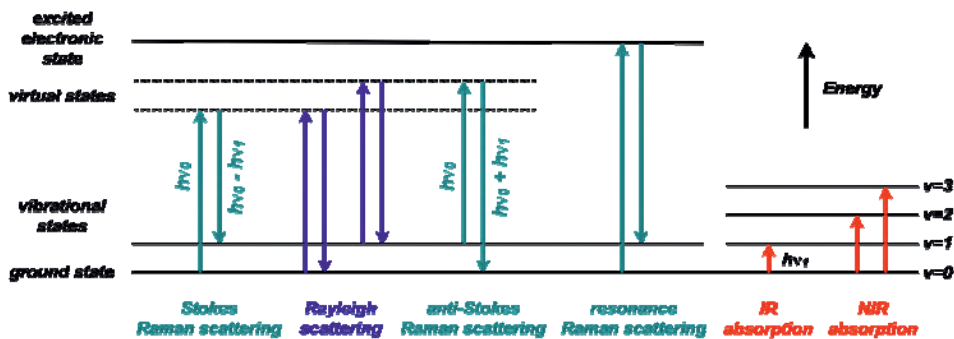


FIGURE 2. Spectroscopic transitions underlying several types of vibrational spectroscopy.

On the other hand, Raman spectra have their origin in the electronic polarization caused by UV, visible or near-IR light. In contrast to IR spectroscopy, Raman spectroscopy uses monochromatic radiation to irradiate the sample and it is the radiation scattered from the molecule, which is detected. Thus, unlike IR absorption, Raman scattering does not require matching of the incident radiation to the energy difference between the ground and excited state. If only electron cloud distortion is involved in scattering, the photons will be scattered with very small frequency changes, as the

electrons are comparatively light. This process is regarded as elastic scattering and is the dominant process (Fig. 2).

For molecules it is called Rayleigh scattering. (Blue light, e.g., is more efficiently scattered than red light, by approx. a factor of n^4 , and Rayleigh scattering is responsible for the blue color of the sky.) However, if nuclear motion is induced during the scattering process, energy will be transferred either from the incident photon to the molecule or from the molecule to the scattered photon (Fig. 2). In these cases the process is inelastic and the energy of the scattered photon is different from that of the incident photon by an amount equal to a vibrational transition, $\pm hn_j$. This is Raman scattering. The oscillating electric field of the light interacts with the molecule and polarizes (distorts) the electron cloud around the nuclei to form a short-lived state called a "virtual state" (Fig. 2). This unstable state is not necessarily a true quantum state of the molecule and the photon is quickly re-radiated. Although it is inherently much weaker process than Rayleigh scattering (by a factor of 10^{-3} to 10^{-6}), it is still possible to observe the Raman scattering by using a strong exciting source.

Energy units

According to its wave nature, EM radiation is characterized by two quantities: the wavelength l and the frequency n . In the IR spectral region the wavelength is usually given in units of [mm]. The frequency is given in units of [s^{-1}] or Hertz [Hz]. The product of l and n is the velocity of light ($c = ln$), which is approx. $3 \cdot 10^{10}$ $cm\ s^{-1}$ in vacuum. Since the vibrational frequencies of molecules are so high, units such as Hz are not convenient. An additional parameter, which is commonly used in Raman and IR spectroscopy instead of the frequency, is the *wavenumber*, $\bar{\nu}$, defined as the reciprocal of the wavelength in cm [cm^{-1}]. In general, the energy of the EM radiation is proportional to its frequency and its wave number, but inverse to the wavelength: $E = hv = hc\bar{\nu} = hc/l$.

The following relation exists between the wavelength l , the frequency n , the wavenumber $\bar{\nu}$ and the velocity of light c : $\bar{\nu}[cm^{-1}] = 10^4 / l[\mu m] = \nu[s^{-1}] / c[cm\ s^{-1}]$. Although the dimensions of n and $\bar{\nu}$ are different, they are often used interchangeably. Thus, an almost slang expression such as "a frequency shift of 5 cm^{-1} " is very common.

Even though Raman spectroscopy probes vibrational transitions indirectly by light scattering, the Raman shift has the same energy range as IR absorption.

Selection rules

Different vibrational modes have different relative intensities in IR and Raman spectra – some modes are active in one and not the other, and some modes are not observed at all. The IR and Raman activities of particular modes are determined by the quantum mechanical selection rules for the vibrational transitions, and by the mode symmetry. In a simple model, the selection rules can be rationalized by considering the interaction between the oscillating electric field vector of the light beam and a changing molecular dipole moment associated with the vibration. In an IR experiment, the light interacts directly with an oscillating molecular dipole, so for a vibrational mode to be IR active, it must be associated with a changing dipole moment. In general, asymmetric vibrations tend to give stronger IR absorption than symmetric species, since they are associated with larger dipole moment changes. Similarly, highly polar (“more ionic”) molecules and crystals have stronger IR spectra than non-polar samples. In Raman scattering, the light beam induces an instantaneous dipole moment in the molecule by deforming its electronic wave function. The atomic nuclei tend to follow the deformed electron positions, and if the nuclear displacement pattern corresponds to that of a molecular vibration, the mode is Raman active. The magnitude of the induced dipole moment is related to the ease with which the electron cloud may be deformed, described by the molecular polarizability α .

The classification of the vibrational quantum states and the description of the spectroscopic interaction are greatly simplified by exploiting the symmetry of the vibrating atomic groups. The mathematical framework of the group theory is the basis of the quantitative description of the symmetry relations possessed by the vibrating groups, finally giving rise to the formulation of the symmetry-based selection rules. As the symmetry of the atomic group increases, the number of different energy levels decreases. The degeneracy, i.e. the number of vibrational states, which have the same energy increases with increasing symmetry. The more symmetric the atomic group, the fewer different energy levels it has, and the greater the degeneracy of those levels. The symmetry must be compatible in order that the molecule may absorb light and the

symmetry-based selection rules tell us which transitions are possible. Thus, the number of allowed transitions in polyatomic molecules is greatly reduced.

Transitions can take place between different vibrational levels (ν). The selection rule allows any transitions corresponding to $D\nu = \pm 1$ if the molecule is assumed to be a harmonic oscillator. Thus, only the *fundamental normal mode vibrations* that originate in the transition from $\nu = 0$ to $\nu = 1$ in the electronic ground state can be observed. *Overtones* (multiples of the fundamental) and *combination bands* (sum or difference of two or more fundamentals) are forbidden. However, they could be observed in the spectra because of the anharmonicity of the vibrations.

The IR portion of the EM spectrum is divided into three regions; near- (NIR), mid- (MIR) and far-IR (FIR), named for their relation to the visible spectrum (Fig. 1). The FIR, $\sim 1\text{--}400\text{ cm}^{-1}$ (2000–25 mm), lying adjacent to the microwave region, has low energy and may be also used for rotational spectroscopy. This range covers the vibrational frequencies of fundamental modes (usually weak) associated with metal-oxygen vibrations as well as complex deformations of polymeric units. The MIR, $\sim 400\text{--}4000\text{ cm}^{-1}$ (25–2.5 mm), may be used to study fundamental vibrations. The higher energy NIR, $\sim 4000\text{--}14000\text{ cm}^{-1}$ (2.5–0.7 mm) can excite overtones or combination vibrations. However, one should keep in mind that such division is somewhat arbitrary.

Light sources

In general, a spectroscopic experiment requires a light source, a means of providing energy resolution of the light before or after interaction with the sample, and a detection system. Since peaks due to Raman scattering are relatively sharp and are measured as a shift from the energy of the excitation source, a monochromatic source is required if quality data is to be obtained. Most Raman spectroscopy is carried out using a laser in the visible region, e.g. 488 nm and 514.5 nm lines of Ar^+ ion laser, 532 nm Nd-YAG solid-state laser, 632.8 nm He-Ne laser, or alternatively using lasers in the UV as well as in the NIR regions, e.g. Kr or Nd-YAG lasers, resp. Various IR sources are used, depending on the wavelength region of interest. Typical light source in laboratory equipment is a ceramic rod "Glo(w)bar" held at high temperature, essentially a "blackbody source". It gives useful intensity between approx. 50 and 10000 cm^{-1} . For FIR studies of silicates, a Globar is usually sufficient, but below $\sim 150\text{ cm}^{-1}$ more

intensity can be obtained from an Hg arc lamp. NIR experiments at wavenumbers greater than $\sim 10000\text{ cm}^{-1}$ require a W filament lamp as source. Synchrotron radiation as a special type of IR source will be briefly introduced in the section *advantages and disadvantages*.

Spectrometers and interferometers

Most modern IR instruments are interferometers, while only a negligible number of grating IR spectrometers and some remainders of prism instruments are still preserved in few laboratories. Fourier transform infrared (FTIR) spectrometers are based on the principle of the Michelson interferometer. Light from the IR source is passed through a 50% reflective beamsplitter, which directs half of the incident intensity to a fixed mirror, and half to a moving mirror. The two beams are recombined at the beamsplitter, so that constructive or destructive interference occurs, depending on the path difference. The result is an interferogram, plotted as light intensity vs. time. For a single frequency source such as laser, the result is a sine wave. This is the Fourier transform (FT) of a delta function at the laser frequency, when intensity is plotted against light energy. In a Fourier transform spectroscopic experiment, light intensity is measured in the time domain, then converted via a FT (using appropriate computer software) to intensity vs. energy (usually expressed in units of wavenumbers, wavelength, or frequency). When the source emits a range of light frequencies, all the resulting sine waves add constructively only when the moving mirror is at the same distance from the beamsplitter as the fixed mirror. Each point of the resulting interferogram contains information over the entire IR region covered by the source. This signal is modified by the particular IR absorbance signature of the sample before reaching the detector. During the FTIR experiment, a reference laser line, usually 632.8 nm He-Ne laser, is also passed through the beamsplitter. The laser signal is monitored by a separate detector, and is used to precisely determine the position of the moving mirror relative to the fixed mirror, and also serves as an internal frequency standard.

To collect Raman scattering effectively it is necessary to remove the much more intense Rayleigh scattering and stray light. The separation of the frequency-shifted Raman scattering and the energy resolution can be done with two or even three monochromators. The purpose of the first monochromator is mainly to separate the

frequency-shifted Raman scattering from the other radiation. The second monochromator increases the dispersion and separates individual Raman peaks. However, filter technology has improved with the development of effective notch and edge filters. The notch filters, in particular, are widely used. They are designed to absorb the light of the frequency of the incident laser light. Usually a filter, which collects most of the light within 200 cm^{-1} of the excitation frequency is regarded as sufficient. Some experiments do require measurements closer to the exciting line and in these cases, the use of monochromators would still be the preferred method for separating the Raman scattering.

FT-Raman was introduced in 1980s. By that time FTIR was developed to a high level of refinement and many components were transferred from FTIR to FT-Raman with minor modifications. Many vendors offer FT-Raman attachments to otherwise conventional FTIR spectrometers, so that both techniques share the same interferometer.

Detectors

There are mainly two classes of IR detectors: thermal and quantum detectors. Thermal detectors detect temperature changes related to the infrared radiation coming from the sample. These detectors have slow response times, but generally have a wide wavelength range of operation. Quantum detectors rely on the interaction of incoming IR photons with the electronic wavefunction of the solid detector material. These detectors have fast response times, but only cover narrow wavelength ranges. Many IR detectors have been developed to operate optimally at liquid-N₂ or liquid-He temperatures, thus reducing the noise from the thermal IR background found even at room temperature. Typical detectors in the MIR range are TGS (triglycin sulphate) or MCT (mercury cadmium telluride). For FIR work TGS is often used despite their low sensitivity. Liquid-He-cooled bolometers with Si or Ge elements cover the FIR with a hundred-fold increase of sensitivity. The main disadvantages of these detectors are their cost and the need of handling liquid-He as coolant. For the NIR liquid-N₂-cooled InAs or InSb detectors are available. Recent developments include two-dimensional arrays of e.g. MCT or bolometer detectors for IR imaging.

In Raman spectroscopy single-channel detectors (photomultipliers and semiconductor photodiodes) are now only employed in scanning, dispersive

spectrometers with special requirements such as access to the very low frequency region as well as in interferometric instruments working in the NIR region. The multichannel solid-state detectors tend now to predominate in micro-Raman systems, either for spectral analysis or Raman imaging. Most of these detectors are based on silicon technology and thus are sensitive to photon energies from the near-UV, ~ 280 nm, to ~ 1 μm in the NIR region. Other devices are based on different semiconductors such as Ge or InGaAs whose response extend further into the NIR region.

Microscopy

Raman and IR microscopes developed independently over the past 30 years. The development of both was motivated by the need for acquiring spectra from microspots. Raman microbeam techniques found applications in the earth sciences already in the 1970s. The spatial resolution is determined by physics based on the wavelength of the light used. For Raman in which the wavelengths of excitation and detection are done in the visible range, typically between 400 and 850 nm, the spatial resolution, which is diffraction limited is observed to be better than 1 μm . In micro-Raman spectroscopy, the incident laser beam is directed into an optical microscope and focused through the objective onto the sample. The scattered light is collected back through the same objective ($\sim 180^\circ$ geometry), and sent into the spectrometer. The focus of the incident beam forms an approximate cylinder, whose dimensions are dictated by the wavelength of the laser light and the optical characteristics of the objective and the sample. The diameter of the cylinder is fixed by the diffraction limit of light in air, and is ~ 0.5 -1 μm for an objective with numerical aperture (NA) ~ 0.9 and laser light in the blue-green region of the spectrum. Corresponding to this is a depth (length) of the scattering cylinder of ~ 3 μm . This shows that micro-Raman spectroscopy has better lateral resolution than depth spatial resolution. The depth resolution is greatly improved in recently widely employed confocal systems, but is still the less resolved direction. Exact optical conjugation onto the sample of the pinhole apertures, employed for both illumination and detection, rejects the stray light background due to the out-of-focus regions of the specimen. Thus the main contribution to the signal comes selectively from a thin layer close to the focal plane.

Modern developments in IR spectroscopy include the application of the IR technique

to microsamples (down to diameters of 20-50 μm) using IR microscopes. Two types of IR microscopes are available: one based on lenses and the other based on reflecting optics. The reflecting mirror objectives (Cassegrain or Schwarzschild optics) have the advantages to work in the whole IR spectral range. Both have intrinsic limits on the area sampled. If the size of the sample approaches the wavelength of the infrared radiation used, the incident beam is diffracted. For the MIR, the wavelengths are typically between 25–2.5 mm (400–4000 cm^{-1}), which puts the spatial resolution at best at $\sim 5 \mu\text{m}$, but more typically at 10–20 μm . To measure FIR spectra, e.g. down to 100 cm^{-1} , sample size must exceed 100 μm . Although IR is still the most widely used vibrational spectroscopy in both research and application labs, in contrast to micro-Raman spectroscopy, micro sampling in the IR is just starting to become popular in the geosciences. While IR microscopes are generally well-suited for mapping purposes using motorized XYZ stages, modern equipment also provide the possibility of area-sensitive detectors that allow for true spectroscopic imaging with high spatial resolution. As for micro-Raman, confocal geometry is employed in modern IR microscopes leading to a significant improvement in the 3D spatial resolution and image contrast.

Advantages and disadvantages

It is obvious even from this brief introduction that the details of every experiment like sample preparation, instrumentation utilized and experimental geometry should be matched to the problem to be solved. Thorough discussion of pros and contras of the different methods is far beyond the scope of this article. Nevertheless, few considerations regarding sources and spectrometers, which could be useful for the choice of instrumentation, will be discussed below.

Light sources: In Raman spectroscopy the choice of laser wavelength usually involves trade-offs among three factors: Raman cross-section, detector sensitivity, and fluorescence. The Raman cross-section decreases with increasing laser wavelength and shorter laser wavelength will yield larger cross-section with a $1/\lambda^4$ dependence. In addition, shorter wavelengths can usually be detected with higher quantum efficiency and less noise, thus improving sensitivity. However, shorter wavelengths are also more likely to excite fluorescence since more electronic transitions occur in the UV and visible than in the IR regions. If a significant number of potentially fluorescent samples

is anticipated, the laser wavelength should be as long as permitted by sensitivity requirements. So, one is trading off the higher sensitivity at shorter laser wavelengths vs. the lower background at longer wavelengths, with the ultimate objective being maximum signal-to-noise ratio.

While modern IR microscopes are designed to work at the diffraction limit, the constraints for the sample size in the case of conventional IR microspectroscopy (> 20 mm) are considerably larger than those for micro-Raman, but even more importantly, larger than the principal limitation by physics. This limit is caused by poor signal-to-noise ratio in IR microscopes with conventional global light sources due to the low brilliance (also called brightness) of the thermal infrared source. The utilization of synchrotron-based radiation (SR) allows for IR measurements at a diffraction-limited micro-focus, which becomes increasingly important for the characterization of complex samples on the micro- and even on the nano-scale level. As an infrared source, synchrotron radiation has five major advantages compared to conventional laboratory sources: (i) *higher brilliance*: as it is almost a point source, one can focus the light to a diffraction limited size (gain up to 1000x); (ii) *broader spectral range*: continuous from FIR to the visible; (iii) *higher photon flux in the FIR*; (iv) *intense coherent emission* in the lower energy part of the FIR: gain up to 10^5 compared to incoherent SR; (v) *pulsed source* in the ns range: the light is emitted from electron bunches which allows fast timing measurements. There are several high brilliance infrared sources, e.g., synchrotrons, lasers, free-electron lasers (FELs), but of these only the synchrotron provides a “white” source spanning the entire infrared range and is compatible with efficient FTIR techniques.

Spectrometers: while in earth sciences IR spectroscopy is nowadays dominated by the use of FT spectrometers and there is currently no better choice, in Raman spectroscopy the question is dispersive or nondispersive (FT) spectrometer. Dispersive/CCD systems are quite sensitive, laser wavelength can be between ~200 – 800 nm (limited by CCD response), and they use lower laser power. Disadvantages could be the spectral coverage/resolution trade-off and fluorescence. FT-Raman has an excellent frequency precision and better fluorescence avoidance (laser wavelength ≥ 1064 nm), but the laser power used is often higher. Since the current separation (wavelength availability) is

technical rather than fundamental, it may change with evolving technology. With today's technology, a spectrometer with a laser wavelength longer than 850 nm will be FT, since suitable multichannel detectors are not available for Raman-shifted wavelengths longer than ~1000 nm. Furthermore, there are good reasons (in general) to avoid laser wavelengths <850 nm with a nondispersive system due to the multiplex disadvantage.

In general, spectrometers differ significantly in their ability to observe IR bands or Raman shifts below ~300 cm⁻¹ due to the difficulties related to accepting, propagating and detecting long FIR wavelengths and due to the methods used to reject stray laser light, respectively.

Applications of Raman and Infrared spectroscopy

Nowadays mineral spectroscopy has become such an exciting field and applications of Raman and IR spectroscopy in mineralogy and geochemistry are so manifold that it is clearly not possible to do justice to all of this research activity in the scope of this brief article. In the following section, specific aspects of different techniques and instrumentation will be highlighted on the basis of few examples of the use of Raman and IR spectroscopy in mineralogy and geochemistry.

As mentioned above, vibrational spectroscopy measures the vibrational frequencies of interatomic bonds. These frequencies depend on the masses of the atoms involved in the vibration (i.e. on their elemental identity), on the strengths of the bonds (force constants), and on the bond lengths and angles - in other words, on all the parameters that constitute the structure of a molecule or crystal. To identify the vibrations that give rise to features in IR and Raman spectra, we can be guided by a number of qualitative considerations. For example, lighter atoms will vibrate at higher frequencies than heavier atoms, if their bonding is of similar strength; higher bond strengths, usually associated with higher valencies or greater covalency lead to higher bond-stretching frequencies; in covalent structures, bond-stretching vibrations lie at frequencies higher than bond-bending deformations. If single crystals are available, the symmetries of IR and Raman active vibrational modes can be deduced from polarized spectroscopic experiments with the help of factor-group analysis. Since the set of vibrational modes is a characteristic *fingerprint* of the chemistry and structure of the molecular groups in a sample, IR (and

increasingly Raman) spectroscopy is widely applied for routine identification of materials, without necessarily knowing the structural origin of the individual spectral peaks. In some cases there are significant advantages over diffraction methods, as the spectra are easy to obtain from solids, liquids and gases, and from materials with low atomic weight. In earth sciences, vibrational spectroscopy is commonly used to identify specific molecular groups (or to monitor their changes in diverse *in-situ* reactions) such as OH, H₂O, CO₂, CO₃, SO₄, NO₃, SiO₄, CrO₄, CH₂, CH₃, CH₄, etc., all of which usually give intense Raman and IR peaks. Structural changes can be monitored in time-resolved experiments, and the distribution of species in heterogeneous samples can be investigated by mapping and imaging.

Fingerprint analysis in fluid inclusions studies

Fluid inclusion (FI) research, for example, is a worth mentioning field of geochemistry, which greatly benefits from these abilities. Studies of FI provide insights into geological processes in the Earth's crust governed by chemical reactions between rocks and natural fluids. Raman and IR microspectroscopy provide qualitative and quantitative information on molecular species. Sometimes H₂O and OH may cause interferences in the IR analysis of aqueous and gas inclusions due to their strong absorption. On the other hand Raman spectra can be completely obscured by fluorescence emission from inclusions, host minerals, or organics present in the sample

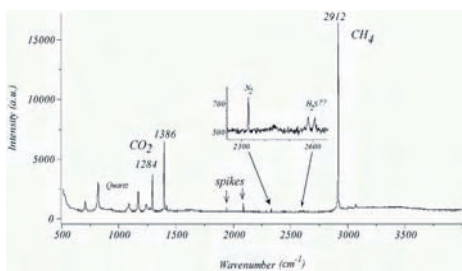


FIGURE 3. Raman spectrum of the vapor phase of aqueous inclusion in quartz (from Samson *et al.*, 2003).

or in the mounting media. Molecular components like N₂ (only Raman active), CO₂, CH₄, H₂O and molecular ions such as OH⁻, HS⁻ or SO₄²⁻ can be routinely analyzed in fluid inclusions by Raman and IR spectroscopy. The spectrum in Fig. 3 contains prominent Raman peaks of CH₄ and CO₂ with a trace of N₂ and possibly of H₂S. Other features are

bands of the quartz host mineral and cosmic ray spikes.

Hydrocarbon (HC) inclusions are common in petroleum reservoirs and may be considered as fossil oils, which have preserved the original oil composition. Diagenetic minerals generally contain small fluid inclusions (often <15µm) or multi-phase inclusions and it is essential that they are studied individually at the microscale. FTIR is inherently very sensitive to HC, H₂O, etc. but conventional IR microscopes have an unfavorable trade-off between the brilliance of the IR source and the size of the analyzed spot. Fig. 4 presents IR spectra from three different phases in HC inclusion in CaF₂. The oil inside the FI was modified by water impact. To resolve the three phases the measurements were taken at 4 µm spot using the high-brilliance synchrotron IR radiation (SR-IR) at the ANKA light source.

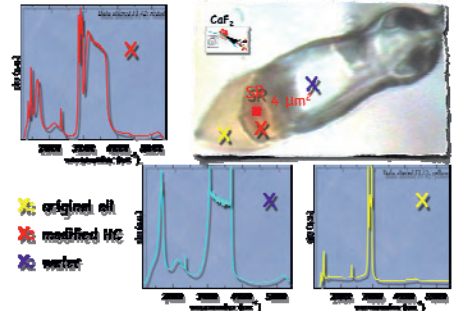


FIGURE 4. IR spectra of the three phases present in HC/aqueous inclusion from Baluchistan.

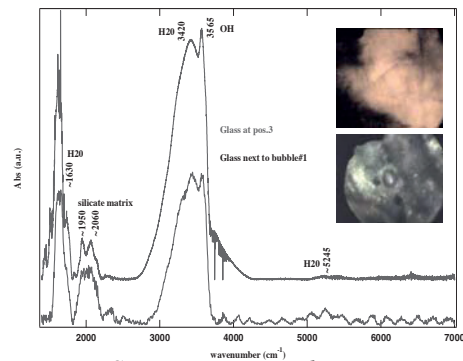


FIGURE 5. SR-IR spectra revealing presence of molecular H₂O as well as OH in two different positions in the silicate matrix of the Bencubbin meteorite.

High-brilliant SR-IR facilitated detection of H₂O inside bubbles in primitive meteorites (Guilhaumou et al., 2005). These meteorites contain high amount of nitrogen, as detected by Raman spectroscopy, which is concentrated mainly as molecular N₂ in relatively large bubbles (20-50 µm) exsolved in some glass phases. SR-IR studies at ANKA have shown that water is also present in detectable quantities inside the bubbles and in some of the glass phases (Fig. 5).

Quantitative analysis, IR mapping and imaging

A further example of use of SR-IR involves the study of water in nominally anhydrous minerals, which in the last two decades has become a “hot topic” in mineralogy, geochemistry and geophysics. Nominally anhydrous minerals (NAMs)

constitute the main reservoir for water in the Earth's mantle. Even traces of water in minerals such as olivine drastically reduce mechanical strength, with major consequences for mantle convection and the formation of minerals as diamonds. The distribution of H₂O around inclusions and cracks in nominally anhydrous mantle minerals such as olivine is studied by IR microspectroscopy mapping (Fig. 6, Sommer et al., 2008).

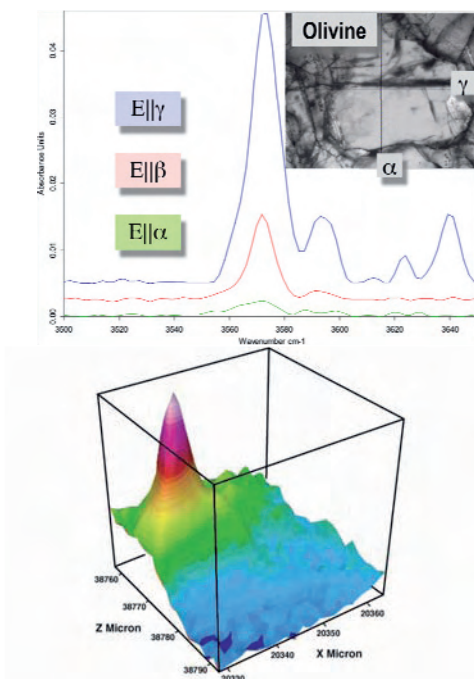


FIGURE 6. *Left:* Synchrotron IR spectra of OH stretching bands of olivine in α , β , γ directions. The quantitative analysis of anisotropic minerals involves summing absorption intensities from polarized spectra. The water content was calculated with the help of the Beer–Lambert law and a calibration after Bell et al. (2003). The absorbance was normalized to 1 cm sample thickness. The water content (normalized in ppm H₂O by weight) is 138 ppm in the clear, inclusion-free olivine matrix. *Right:* 3D graph (40x40 μm^2) showing the increase of water towards a totally embedded Cr-spinel inclusion (5–8 μm in size) in olivine. The H₂O content significantly increases towards the inclusion up to values of about 800 ppm.

Large number of overlapping spots was analyzed in a confocal geometry using apertures of 4 or 6 μm and a step size of 2 μm in a grid pattern accessed by an automated stage. The brilliant synchrotron IR light of ANKA is providing the required high spatial resolution. The results show that for all three types of defects in the olivine matrix, i.e. cracks, grain boundaries and Cr-spinel inclusions, the water content increases systematically by a factor of 5–10 towards the defect. Similarly, the defects are all surrounded by halos of water, which increases towards the defects. The data are used to derive passage of aqueous fluids through the lithosphere thus obtaining more detailed information about the ascent rates of kimberlitic melts and their potential for diamond deposits.

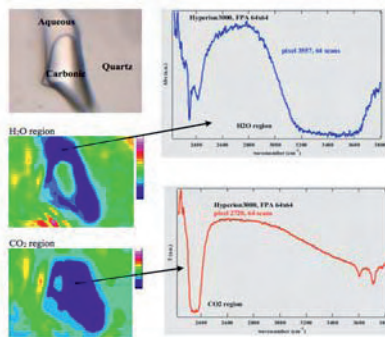


FIGURE 7. IR images of a $\text{CO}_2\text{-H}_2\text{O}$ FI with the corresponding H_2O and CO_2 spectra as extracted from a single pixel of the FPA.

Step-by-step mapping in a confocal arrangement, as shown in the previous example, provides the best spatial resolution and image contrast. The severely reduced flux on the detector at sampling size approaching (or even smaller) than the diffraction limit can be compensated by the high brilliance of the SR-IR. One disadvantage that remains is the long time required to scan the sample (e.g. the sample area shown in the map in Fig. 6, right, was scanned in ~ 10 h). Much faster one-shot

images can be acquired using a multielement focal plane array (FPA) detector. One such study carried out at ANKA involved imaging with a 64×64 pixel FPA detector (Fig. 7, Moss et al., 2008). Each pixel in these images corresponds nominally to $1.15 \mu\text{m}^2$ on the sample. The time for this experiment was less than 5 minutes! ANKA was the first to demonstrate the value of such multielement detectors at synchrotron IR beamlines (Moss et al., 2006), and this work has proved highly influential, leading to many beamlines worldwide acquiring such detectors. One should keep in mind that this is an apertureless technique and the true spatial resolution as well as the image contrast are deteriorated by diffraction and scattering.

Structural studies: biominerals

Structural changes and dehydration of water/OH containing (bio)minerals could be monitored usually very well by vibrational spectroscopy. In a study by Klocke et al. (2006) thick sections of extracted human teeth were irradiated by CO₂-laser to simulate teeth treatment under different laser operational modes. Raman and IR microspectroscopy were the methods of choice, since the aim was to analyze the gradient of structural alteration and molecular exchange across the CO₂-laser irradiated areas in the dental enamel. The IR absorption spectra were measured with an IR microscope equipped with Ge-ATR objective, for the samples were too thick to observe first-order phonons in transmission geometry. The IR spectra in Fig. 8 indicate loss of water (broad stretching band at 3232 cm⁻¹ and the bending band at 1649 cm⁻¹) and OH (sharp peak at 3570 cm⁻¹) as a function of distance from the center of the CO₂-laser spot after irradiation of human dental enamel (outside (curves *a*), at the periphery (curves *b*) and inside (curves *c*) the laser spot. The IR spectra in Fig. 8 show as a function of distance from the center of the CO₂-laser spot a decomposition of CO₃ groups present in the apatite structure (bands around 1400-1550 cm⁻¹), their consequent transformation into CO₂ groups (bands at 2343 cm⁻¹) and their final disappearance in the center of the laser spot. For samples E(1|5|c), those irradiated in a CW laser mode, the CO₃-CO₂ conversion is accompanied by rearrangement of the CO₃ groups in the apatite crystal structure. As the IR absorption at 1412 and 1547 cm⁻¹ is associated with CO₃ groups substituting for PO₄ (so-called B-type CO₃) and for OH (A-type CO₃), resp., the observed change in the relative intensities represents a relative decrease of the amount of B-type and an increase of the amount of A-type CO₃ groups. Comparison between the structural changes in the enamel apatite observed in this study to those in heated samples revealed that under laser treatment the achieved average temperature in the center and near the CO₂-laser crater was about 1100 and 700 K, resp. The most intense Raman peak at ~963 cm⁻¹ arises from the symmetric stretching mode of PO₄ groups. Its broadening and the appearance of many additional shoulders after irradiation indicates, e.g. variations in the P-O bond lengths and it is evident for structural amorphization.

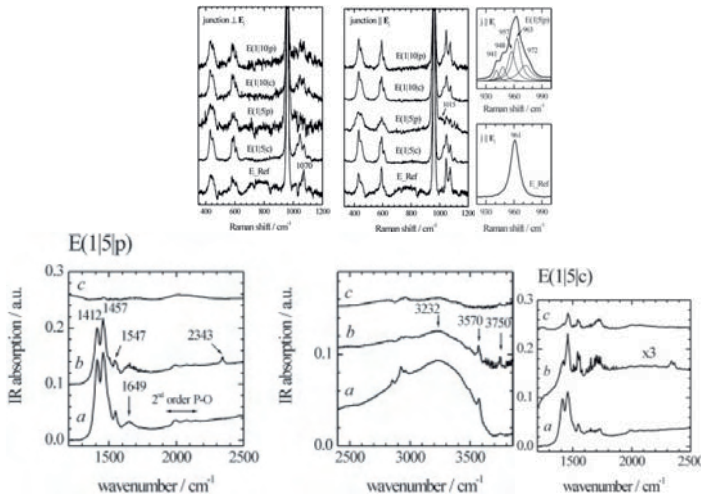


FIGURE 8. Raman scattering and ATR IR spectra of CO₂-laser-treated human dental enamel (consisting mainly of hydroxyapatite, 12% water and 3% organics). After Klocke et al., 2006.

In the IR spectra from inside the laser spot of the samples treated in super pulse laser mode (E(1|5)p, curve c) the second order P-O absorption peaks are poorly resolved, which gives further evidence for a lowering of the degree of crystallinity, confirming the Raman results. The smearing of the C-H stretching bands around 2900 cm⁻¹ (IR) indicates an impact of the laser treatment on the organics. Increased intensity of the IR band at 3750 cm⁻¹ (surface OH groups) is a sign of grain size reduction under irradiation.

Silicates: Silicates are mineralogically and geochemically very important as well crystallographically very exciting class of minerals. In their complex mineral structures, “molecular groups” are not always readily identifiable, especially where the structure is strongly bonded in two or three dimensions. An isolated SiO₄ group (or any tetrahedral XY₄ group) would have nine internal degrees of freedom but only four modes of vibration due to degeneracy (Fig. 9). In structures with isolated SiO₄ tetrahedra it is a

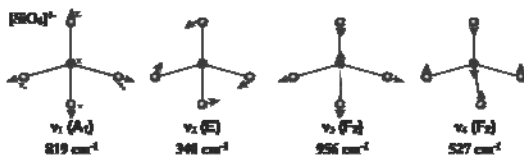


FIGURE 9. Normal modes of vibration of tetrahedral molecules and vibrational frequencies of isolated SiO₄ tetrahedra (Nakamoto, 1997).

very useful starting point to consider the vibrational modes of SiO₄ tetrahedron. The SiO₄ stretching modes are in the high frequency range: n₁ symmetric and n₃ asymmetric stretch ~800-1100

cm^{-1} , while the SiO_4 bending modes have a lower frequency: n_2 symmetric and n_4 antisymmetric bend $\sim 300\text{-}650 \text{ cm}^{-1}$.

The rules $n_3 > n_1$ and $n_4 > n_2$ hold for the majority of the compounds with isolated SiO_4 tetrahedra. It should be noted that n_2 and n_4 are often too close to be observed as separate bands in Raman spectra. The polymerization of SiO_4 groups to form complex chain anions has important effects on the spectra. For example, the degeneracy of the n_2 , n_3 and n_4 modes is lifted, causing the spectrum to become more complex. This is a reflection of the differences of the bonding of the terminal (non-bridging, O_{non}) and bridging (O_{br}) oxygens, which result in different force constants for the Si-O_{non} and Si-O_{br} bonds. Second, a new type of bands attributable to deformation of the Si-O-Si linkage appears in the $550\text{-}750 \text{ cm}^{-1}$ region, at position(s) depending on the Si-O-Si angle(s), e.g. Lajzerowicz (1966). Thus the effect of polymerization into chains is to split into several components those bands, which occur in the spectra of orthosilicates, and to introduce new bands, which reflect variations in Si-O-Si angle. In practice, Si-O_{non} stretching bands appear in the $950\text{-}1200 \text{ cm}^{-1}$ region while Si-O-Si bending bands between 550 and 750 cm^{-1} , on the high- and low-frequency sides of the orthosilicate bands at $800\text{-}950 \text{ cm}^{-1}$. The vibrations of the cations, which link the complex silicate anions occur $\leq 400 \text{ cm}^{-1}$. The low frequency compared with the silicate bands reflects the higher coordination number (usually 6-8), the longer metal-oxygen distances, and the lower formal charge (usually 1-3). Taking the symmetric stretching frequency of an AlO_6 octahedron as $\sim 600 \text{ cm}^{-1}$, comparable frequencies for MgO_6 , CaO_8 , and NaO_8 are calculated as ~ 470 , ~ 380 and $\sim 270 \text{ cm}^{-1}$, respectively.

Structural studies: poorly crystalline phases

The structure of poorly crystalline calcium-silicate-hydrates (C-S-H) is still a controversial issue, although these materials are extremely important in cement mineralogy. One important aspect in C-S-H structural studies is the degree of polymerization of the silicate units. Its study is a challenging issue due to the poor structural ordering of C-S-H. Therefore, methods not dependent upon long-range structural order are well suited. Raman and IR spectra of series of C-S-H samples with different CaO/SiO_2 ratios (Ca/Si) reveal changes in structure dependent upon Ca/Si ratio (Garbev et al., 2007; Gasharova et al., 2006). Because of the low electronegativity of Ca

a minimal coupling between vibrations involving Ca with those arising from the silicate anionic structure is assumed. This allows the identification of the internal vibrations of the silicate anions. Finite silicate chains (Q^2) dominate the structures of the samples at Ca/Si ratios 0.2-1.0, the spectra showing characteristic symmetric stretching (SS) bands between 1010 and 1020 cm^{-1} (Raman, Fig. 10) and antisymmetric stretching (ASS) $\sim 965 \text{ cm}^{-1}$ (IR, Fig. 10). The main characteristic feature of the Raman spectra is the Si-O-Si symmetric bending (SB) vibration at $\sim 670 \text{ cm}^{-1}$. Comparisons with bending frequencies of some known crystalline phases composed of single silicate chains has led to an estimation of the mean Si-O-Si angles in the C-S-H phases to be $\sim 140^\circ$, which is the energetically favored bond angle (Garbev et al., 2007). The shift of the SB vibration to a higher frequency (668-672 cm^{-1} , Raman) indicates narrowing of the Si-O_{br}-Si angle with silicate depolymerization. For Ca/Si > 1, silicate depolymerization occurs and dimeric silicate units are formed witnessed further in the IR spectra by the increasing intensity of the SS vibration of Si-O Q^1 units $\sim 806 \text{ cm}^{-1}$ and the increased splitting of the $n_2/n_4 \text{ SiO}_4$ bending around 470 cm^{-1} with increasing Ca/Si ratio. Considering the frequency, intensity, and width of the Raman stretching vibration bands of Q^1 and Q^2 silicate units it was possible to reconstruct some characteristic structural features, such as the chain length of the silicate species as a function of the Ca/Si ratio. The variation in the frequency of the broad OH stretching bands for the different samples is also Ca/Si ratio specific thus implying that the role of H₂O in the structure is essential. The broad shoulder around 3245 cm^{-1} in the Raman spectra is assigned to collective in-phase stretching motions of OH involved in a network of hydrogen bonds. On the other hand, the appearance of a relatively well defined peak at $\sim 3565 \text{ cm}^{-1}$ in the Raman spectra of Ca/Si 1.33 and 1.5 suggests increasing ordering of Ca-bonded OH groups. Similarly, increased ordering of the Ca environment is seen in the increase and sharpening of the Ca-O bands at 332 cm^{-1} (Raman) and 255 cm^{-1} (IR). The prominent sharp band at 3618 cm^{-1} (Raman) and 3640 cm^{-1} (IR) due to O-H stretching in portlandite, Ca(OH)₂, which first appear in the sample with Ca/Si 1.33 (Raman) and 1.5 (IR) point to excess Ca indicating an upper limit for the incorporation of Ca into the C-S-H structure of less than 1.33 (probably ~ 1.25). Additional OH band at 3740 cm^{-1} in the IR spectra due to surface silanol (Si-)OH groups is indicative for surface charge, which is also Ca/Si dependent.

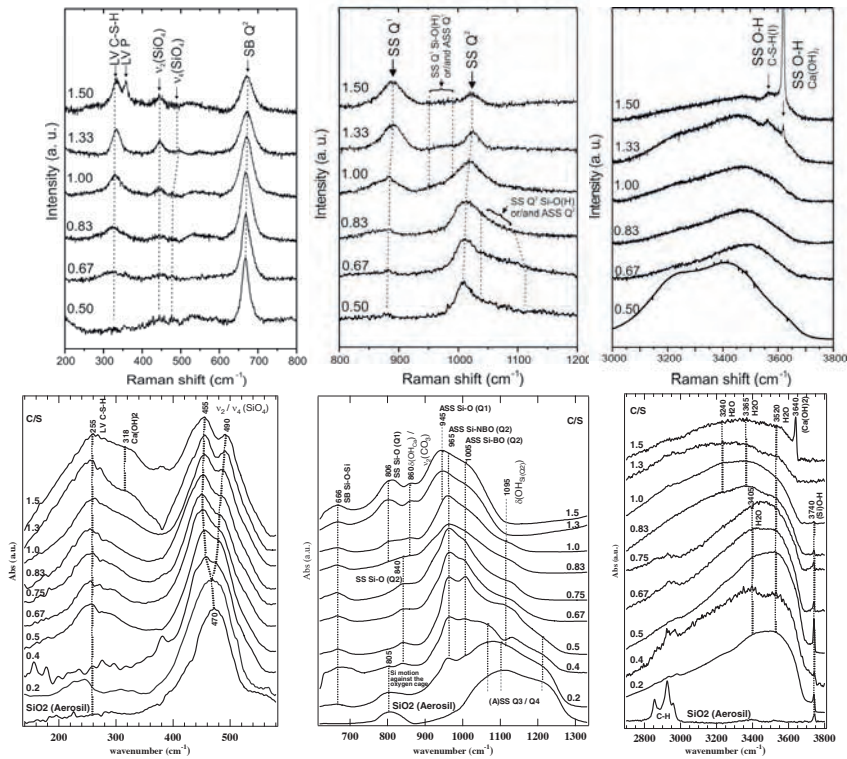


FIGURE 10. The Raman and IR spectra of C-S-H samples of type C-S-H(1) with Ca/Si ratios ranging from 0.2 to 1.5 reveal changes in structure dependent upon Ca/Si ratio.

Surface carbonation of fresh C-S-H samples starts immediately upon exposure to air. The ν_1 CO_3 bands overlap with the silicate Raman scattering around $\sim 1080 \text{ cm}^{-1}$. For unambiguous Raman band assignment of C-S-H phases, it is thus imperative to avoid exposure to CO_2 , which was assured in the above study by analyzing the samples in sealed quartz glass capillaries. A 40x objective with an adjustable cover-slip correction lens helped minimizing the scattering from the capillary. Further, the effect of carbonation of the same C-S-H samples under ambient conditions for up to 6 months have been investigated by Raman spectroscopy (Black et al., 2007). The technique's sensitivity toward the various CaCO_3 polymorphs illuminates the sequence of carbonation and decalcification processes during aging of C-S-H. Amorphous calcium carbonate hydrate is formed within minutes upon exposure to air as indicated by a broad band $\sim 1080 \text{ cm}^{-1}$. It crystallizes, over time, to give primarily vaterite at $\text{Ca/Si} \geq 0.67$ (e.g.

intense n_1 CO_3 doublet at 1076 and 1091 cm^{-1} ; split in-plane n_4 CO_3 bending at 740 and 750 cm^{-1}) and aragonite at $\text{Ca/Si} \leq 0.5$ (e.g. intense n_1 $\text{CO}_3 \sim 1080$ cm^{-1} ; n_4 $\text{CO}_3 \sim 700$ cm^{-1}). Calcite was not observed as a primary carbonation product within the time frame investigated. Thus, the most probable mechanism of C-S-H carbonation appeared to be of dissolution-precipitation character. Carbonation leads to decalcification of the C-S-H resulting in silicate polymerization (the SB mode at 672 cm^{-1} in the fresh samples sharpened and shifted to 668 cm^{-1} due to polymerization of the Q^1 units).

Structural studies: polarized spectra

As IR activity is dependent on a changing dipole moment, the orientation of the dipole moment change of a given vibration and hence the orientation of a particular bond involved in this vibration relative to the crystallographic crystal axes can be determined, which can give information on the crystal structure and the nature of the vibrational

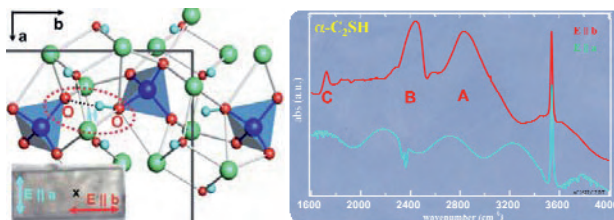


FIGURE 11. OH stretching of OH involved in strong H-bonding in $\alpha\text{-C}_2\text{SH}$. (Garbev et al., in prep.).

modes. This type of analysis has been particularly useful in the analysis of O-H stretching vibrations in minerals (e.g. Hawthorne, 1988). Synchrotron IR microspectroscopy has been used by Garbev et al. (2008)

to study the mechanisms of the phase transformations in the $2\text{CaO-SiO}_2\text{-H}_2\text{O}$ system, which understanding has crucial importance for the development of low-energy belite cement materials. The new materials should substitute the common cement clinker produced at 1450°C, with the goal of lowering both the production costs of cement as well as the CO_2 emissions. Part of these studies focus on the dehydration process of $\alpha\text{-Ca}_2[\text{SiO}_3(\text{OH})](\text{OH})$ ($\alpha\text{-C}_2\text{SH}$) because it transforms into hydraulic Ca_2SiO_4 polymorphs at temperatures much lower than 1450°C. Although often studied the structure of $\alpha\text{-C}_2\text{SH}$ and the mechanism of its dehydration have been not fully resolved. IR studies of $\alpha\text{-C}_2\text{SH}$ single crystals were carried out under the IR microscope at the ANKA-IR beamline. The brilliance of SR-IR allowed the selection of untwined and homogeneous areas. Study of polarized IR spectra of $\alpha\text{-C}_2\text{SH}$ contributes to the refinement of its crystal

structure. For example, when the orientation of the electric field vector (\mathbf{E}) is set to be parallel to the crystallographic b axis ($\mathbf{E} \parallel b$, Fig. 11) three bands are observed between 1600 and 3000 cm^{-1} typical for OH stretching of hydroxyl involved in strong hydrogen bonding. They are denoted C (1715 cm^{-1}), B (2380 cm^{-1} , very broad), and A (2780 cm^{-1} , very broad). Rotating the crystal by 90° ($\mathbf{E} \parallel a$) leads to disappearance of these bands. This observation not only proves the existence of hydroxylated $\text{SiO}_3(\text{OH})$ tetrahedra in the $\alpha\text{-C}_2\text{SH}$ structure, but also suggests that they are interconnected in a chain-like pattern by H-bonds with orientation along the b axis (Fig. 11, right). Studies between 18 and 470 K in a liquid-He cryostat under the IR microscope suggest that the hydrogen bonds are triggering the phase transformation reactions of $\alpha\text{-C}_2\text{SH}$ upon thermal treatment (Garbev et al., in prep.).

RAIR studies of thin films

Vibrational spectroscopy has great advantages over other techniques such as x-ray diffraction (XRD) and even synchrotron XRD in detecting crystalline particles with a size of just a few unit cells. In addition, the vibrational spectra can unambiguously distinguish between amorphous and crystalline features, which are sometimes a problem for other surface-sensitive spectroscopic methods. In a recent experiment at the IR beamline at ANKA it has been shown that RAIR experiments in grazing incidence geometry are very suitable to examine the efficiency of synthesis methods for ultrathin zeolite film growth (Tosheva et al., submitted). The ultrathin films were transferred to Au coated slides and the spectra were collected using p-polarized light. The enhancement of the IR absorption due to the presence of a strongly reflecting noble metal surface allows the detection of even monomolecular layers when grazing-incident RAIR spectroscopy is used. The utilization of the synchrotron IR source ensured the acquisition of highest quality RAIR spectra due to the natural collimation of the beam.

Overcoming the diffraction limit: near-field Raman and IR nanospectroscopy

The possibility to measure samples at a nano-scale spatial resolution with Raman and even with infrared radiation will soon become a further attraction for mineralogists. Near-field Raman and IR spectroscopy (also called tip-enhanced spectroscopy) will be briefly introduced during the oral presentation.

References

- Beran A. and Libowitzky E., Eds. (2004). European Mineralogical Union, Notes in Mineralogy, Eötvös University Press, Budapest.
- Burns R.G. and Greaves C. (1971). *Amer. Mineral.*, 56, 2010-2025.
- Black L., Garbev K., Gasharova B., Breen C., Yarwood C., Stemmermann P. (2007). *J. Am. Ceram. Soc.*, 90, 908-917.
- Chalmers J. and Griffiths P., Eds. (2001). Handbook of vibrational spectroscopy, John Wiley & Sons, Inc.
- Garbev K., Gasharova B., Bernotat-Wulf H. and Stemmermann, P. (2005). *FZKA Nachrichten*, 37, 235-241.
- Garbev K., Gasharova B., Beuchle G., Kreiszi S. and Stemmermann P. (2008). *J. Am. Ceram. Soc.*, 91, 263-271.
- Garbev K., Gasharova B., Black L., Breen C., Yarwood C., Stemmermann P. (2007). *J. Am. Ceram. Soc.*, 90, 900-907.
- Gasharova B., Garbev K., Bornefeld M., Black L. and Stemmermann P. (2006). *Acta Crystallographica*, A62, 208. Leuven, Belgium.
- Guilhaumou N., Gasharova B., Mathis Y.-L., Perron C. and Fieni C. (2005). ANKA annual report.
- Farmer V.C., Ed. (1974). The infrared spectra of minerals. Mineralogical society, monograph, 4.
- Hawthorne F.C., Ed. (1988). Spectroscopic methods in mineralogy and geology. Reviews in mineralogy, Vol. 18.
- Klocke A., Mihailova B., Zhang S., Gasharova B., Stosch R., Güttler B. Kahl-Nieke, B., Henriot P., Ritschel B., Bismayer U. (2006). *Journal of Biomedical Materials Research Part B: Applied Biomaterials*, 81B, 499-507.
- Lajzerowicz J. (1966). *Acta Crystallographica*, 30, 357-363.
- McCreery R.L. (2000). Chemical analysis, Vol. 157. John Wiley & Sons, Inc.
- Mirabella F.M., Jr., Ed. (1992). Practical spectroscopy series, Vol. 15, Marcel Decker, Inc.
- Moss D.A., Gasharova B., Mathis Y.-L. (2008). *Synchrotron Radiation News*, 21, 51-59.
- Moss, D.A., Gasharova, B., and Mathis, Y.-L. (2006). *Infrared Phys. Techn.*, 49, 53-56.
- Nakamoto K. (1997) Infrared and Raman spectra of inorganic and coordination compounds, 5th edition, John Wiley & Sons, Inc.
- Putnis A. (1995) Introduction to mineral sciences. Cambridge University Press.
- Raman C.V. and Krishnan K.S. (1928). *Nature*, 121, 501.
- Samson I., Anderson A., Marshall D., Eds. (2003), Fluid inclusions: analysis and interpretation. Mineralogical association of Canada.
- Sommer, H., Regenauer-Lieb, K., Gasharova, B., Siret, D. (2008). *Miner. Petrol.* DOI 10.1007/s00710-008-0002-9.
- Turell G. and Corset J., Eds. (1996), Raman microscopy: Developments and applications. Elsevier Academic Press.

Alike as two water drops: distinguishing one source of the same substance from another

Clemente Recio Hernández

Departamento de Geología y Laboratorio de Isótopos Estables, Fac. de Ciencias, Univ. de Salamanca. Plaza de la Merced, S/N. 37008 – Salamanca. <http://www.usal.es/isotopos>

Introduction

It is usually possible to identify a substance by using chemical or physical methods. However, when two substances are alike, physicochemical methods are unable to distinguish between different sources of that same substance. When the question is not “how much”, but rather “where from”, stable isotopes may be a helping tool: isotope ratio measurement is a tool useful in a large range of fields, frequently completely unrelated; not a science in itself.

In fact, every process of biogeochemical interest will involve substances that contain one or more of the light elements H, C, N, O and S, in different proportions: they are in the air we breath, the food and drink that we take, the environment that we live in ... And the processes that determine the direction and magnitude of isotopic fractionation are fundamental ones, responding to basic thermodynamic principles that cannot be tampered with.

Definitions: Elements and Isotopes

Isotopes are atoms of the same element that have the same numbers of protons and electrons, but different numbers of neutrons. The difference in the number of neutrons between the various isotopes of an element means that these have similar charges, but different masses. For example, among the hydrogen isotopes, deuterium (denoted as D or ^2H) has one neutron and one proton. This is approximately twice the mass of protium (^1H), whereas tritium (^3H) has two neutrons and is approximately three times the mass of protium.

Isotope Terminology: the "δ" notation

Measuring an absolute isotope ratio or abundance is not a simple task, requiring sophisticated instrumentation. Further, measuring this ratio on a routine basis would lead to problems in comparing data sets from different laboratories. However, we are mainly interested in comparing the variations in stable isotope concentrations rather than actual abundance, and so a simpler approach is used. Rather than measuring a true ratio, an apparent ratio can easily be measured by gas source mass spectrometry. The apparent ratio differs from the true ratio due to operational variations (machine error, or *m*) and will not be constant between machines or laboratories, or even different days for the same machine. However, by measuring a known reference on the same machine at the same time, we can compare our sample to the reference.

$$\delta^{18}O_{Sam} = \frac{m\left(\frac{^{18}O}{^{16}O}\right)_{Sam} - m\left(\frac{^{18}O}{^{16}O}\right)_{Ref}}{m\left(\frac{^{18}O}{^{16}O}\right)_{Ref}}$$

Isotopic concentrations are thus expressed as the difference between the measured ratios of the sample and reference over the measured ratio of the reference.

$$\delta^{18}O_{Sam} = \left(\frac{\left(\frac{^{18}O}{^{16}O}\right)_{Sam}}{\left(\frac{^{18}O}{^{16}O}\right)_{Ref}} - 1 \right) \times 1000$$

Mathematically, the error (*m*) between the apparent and true ratios is cancelled.

This is expressed using the delta (δ) notation (with oxygen as an example, where "*Sam*" stands for the unknown sample, and "*Ref*" for the reference

material). Since fractionation at the natural abundance levels is usually small, δ -values are expressed as the parts per thousand or "per mil" (‰) difference from the reference. This equation then becomes the more familiar form usually employed:

The stable isotopic compositions of low-mass (light) elements such as hydrogen, carbon, nitrogen, oxygen, and sulphur are therefore normally reported as "delta" (δ) values in parts per thousand (denoted as ‰) enrichments or depletions relative to a standard of known composition.

Basic Principles: fractionation

Since the various isotopes of an element have different mass, their chemical and

physical properties are also slightly different. The isotopes of the light elements have mass differences that are large enough for many physical, chemical, and biological processes or reactions to "fractionate" or change the relative proportions of various isotopes. Two different types of processes - equilibrium and kinetic isotope effects - cause isotope fractionation. This fractionation may be indicative of the source of substances involved, or of the processes through which such substances went through.

Equilibrium isotope-exchange reactions involve the redistribution of isotopes of an element among various species or compounds. At equilibrium, the forward and backward reaction rates of any particular isotope are identical. Equilibrium isotope effects derive from the effect of atomic mass on bond energy. The bond energy consumed by molecules incorporating the heavy isotope is higher than bond energy of molecules formed by the light isotope. Bonds involving the light isotope are weaker, and therefore easier to break. Molecules incorporating the light isotopes are thus "more reactive" than molecules of the same substance, but formed by a higher proportion of the corresponding heavy isotope.

Kinetic isotope fractionations occur in systems out of isotopic equilibrium where forward and backward reaction rates are not identical. The reactions may, in fact, be unidirectional if the reaction products become physically isolated from the reactants. Reaction rates depend on the ratios of the masses of the isotopes and their vibrational energies; as a general rule, bonds between the lighter isotopes are broken more easily than the stronger bonds between the heavy isotopes. Hence, the lighter isotopes react more readily and become concentrated in the products, and the residual reactants become enriched in the heavy isotopes.

Biological processes are generally unidirectional and are excellent examples of "kinetic" isotope reactions. Organisms preferentially use the lighter isotopic species because of the lower energy "costs", resulting in significant fractionations between the substrate (heavier) and the biologically mediated product (lighter).

Measurement: Gas Source Mass Spectrometry (Isotope Ratio Mass Spectrometry; IRMS)

Although the first precise measurements of isotope abundance ratios had been done in 1936 by Alfred Nier, it was not until 1947 that he built the first dual inlet, double

collector gas source mass spectrometer. Since then, the IRMS has become the measurement technique of choice for most of the light elements (certainly so for H, C, N, O and S).

Main differences between IRMS currently derive from the inlet method and the on-line preparation systems available. Originally, gases were generated off-line, and admitted into the sample bellows of the dual inlet (DI) system. A second bellow would have the reference gas, and sample and reference would be alternatively admitted into the ion source by means of capillaries and a 4-way change-over valve. The variable bellows allow matching the pressures of sample and reference gases, to prevent fractionation.

Recently, continuous flow (CF) machines have become common. In CF instruments the dual inlet system is replaced by a carrier gas flow, commonly He. This type of design is particularly suitable for the use of on-line preparation systems, such as elemental analyzers, gas chromatographs or equilibrium devices.

Regardless of inlet method (DI or CF), on reaching the ion source, the gas is ionized by electrons emitted by a heated filament, that strip an electron off the molecule, creating positive ions. Ionization efficiency is very variable, commonly in the range 0.01 to 0.1% (850 to 2000 molecules required per ion formed). A high voltage accelerates these ions through a set of exit slits that focus the beam into the mass analyzer, where ions are separated as a function of mass. The resolved ion beam is collected on ion detectors (commonly Faraday Cups), the signal is electronically amplified, and the isotopic ratios are reported by the data system.

Sample gases fed to the DI systems are produced from the sample offline the mass spectrometer, in purpose built extraction lines. This is time consuming, and requires relatively large samples and specialized knowledge, but results in turn in highly precise measurements.

The two most important advantages of the continuous flow systems are the increase in sample throughput and the decrease in the amount of sample required, such that measurements in the nanomol range (10^{-9} M) are routine now.

All CF methods use a He flow to introduce the sample gas into the mass spectrometer. The sample gas is produced in a range of automated preparation systems, that can lead to “bulk” (BSIA) or “compound-specific” (CSIA) isotopic analysis.

Elemental Analyzers

An elemental analyzer coupled to a magnetic sector mass spectrometer (EA-IRMS) gives the bulk isotopic composition of the sample. Depending on the specific set up, it is possible to measure isotopic ratios of H, C, N, O and S in a range of solid and liquid matrices.

In combustion mode, C-, N- and S-containing materials are loaded into Sn capsules, which are dropped into a reactor packed with suitable catalysts. O₂ is admitted into the reactor, resulting in flash combustion of the sample to a mixture of N₂, NO, CO₂, O₂, SO₂ and H₂O, depending on the nature of the substances combusted. This gas mix is carried by the He flow to a reduction reactor, where NO_x are reduced to N₂, and excess O₂ is eliminated. Water is eliminated in a chemical trap, and the gases of interest separated on a suitable chromatography column.

The pyrolysis mode is employed for the analysis of O and/or H. For oxygen, samples are loaded into Ag capsules and dropped into a ceramic reactor lined by a glassy carbon tube in the inside, and packed with nickelized carbon, where the sample is pyrolyzed to CO. As before, water is chemically trapped, and contaminant gases separated by chromatography. H from water samples is obtained by injecting 0.2-0.4 μl via a liquid autosampler onto a reactor packed with Cr.

GC-C-IRMS

CSIA is possible by coupling a GC to the mass spectrometer via a combustion interface. Initially, only C could be determined. Later on, however, modifications were made that allow measurement of N, O, and H isotope ratios.

In its simplest form, the interface is an oven packed with an oxidant (CuO, NiO, Pt, ... depending on manufacturer). The compounds eluted from the chromatography column are carried by the He flow; combusted in the interface, and carried into the source of the mass spectrometer. H₂O generated during combustion is physically eliminated by membrane diffusion. If N is to be determined, an additional reduction oven is required. Precise δ¹⁵N measurements depend on quantitative exclusion of CO₂ (since this fragments in the source into CO⁺, which isobarically interferes with N₂ at masses 28 and 29). To this end, a cryogenic trap is placed before the inlet of the mass spectrometer. This requirement prevents C and N being determined on the same sample.

Something similar happens for H and O, which require different reactors, and that cannot, therefore, be measured from the same aliquot.

LC-IRMS

The main problem associated to GC-C-IRMS is that samples need to be soluble in a suitable volatile solvent. If they are not, they need to be derivatized to a suitable form. But derivatization can affect the isotopic results. Fractionation can occur either by kinetic effects or incomplete conversion, and the derivatizing agent adds extraneous C, and maybe other elements as well.

Coupling a liquid chromatograph to the IRMS may overcome some of these problems. However, LC-IRMS requires that the liquid phase be prevented from reaching the mass spectrometer, eliminating it either before or after oxidation of the sample of interest. Several solutions have been proposed to this end, such as nebulizing the LC effluent and reacting the sample in a plasma; placing the effluent in a moving wire or belt, evaporating the solvent and combusting the dry sample, or else oxidizing the sample to CO₂ while still dissolved, and separating the CO₂ afterwards.

Whatever the approach, the technique is useful to analyze high molecular weight compounds not well suited for GC-IRMS, such as sugars, aminoacids or active components of pharmaceuticals and drugs.

Applications and uses

Food and food fraud

Food and food-related products represent a large percentage of GDP. They also are a major component to be considered within the average family's domestic economy. Additionally, certain products are perceived as of higher quality on grounds such as provenance (“Denominación de Origen” –DO-; “Appellation d’Origine Contrôlée et Garantie” –AOCG-, ...), growing and/or breeding method (“Organically Grown Product”) or health benefits, and as such reach substantially higher market prices, warranting the need for objective quality and provenance control methods.

Since the physical, chemical or biochemical reasons underpinning isotope fractionation can be affected by factors such as geography (climate, altitude, latitude,...), species and variety, culture method, ... etc., each product to be considered requires

establishing a suitable database to be used as reference. In Europe, this is done through the European Commission's Joint Research Centre (JRC), who establishes validated methods, analytical standards, and mutually recognized approaches to analytical quality assurance (Table 1).

TABLE 1. Official EU analytical methods employing isotope data, and current projects (Calderone et al., 2003).

Product	Official method / Research Project	Application
Wine	UE # 2676/90, 822/97, 440/2003, OIV ré. ENO 2/96, ENO 17/2001, Wine-DB, GLYCEROL	Chaptalization, Geographical provenance, Watering.
Alcohol	OIV, BEVABS	Botanical origin, Ethanol
Spirits	OIV, BEVABS	Botanical origin
Sugar	SUGAR ¹⁸ O	Botanical origin
Honey	AOAC method 999.41	Addition of sugars
Perfumeand Fragance	GCC-IRMS	Botanical origin, anethol, vainillin
Dairy and cheese	MILK	Geographical provenance
Fruit juice	CEN/TC #s. 108, 109, 110, AOAC method 995.17, SUGAR ¹⁸ O	Addition of sugars, Dilution
Oil and fat	MEDEO	Origin
Fish	COFAWS	Geographical provenance; Wild / Cultured
Vinager	OIV	Botanical origin

The term "food" normally includes a complex and highly variable set of products, both natural and at various stages of processing, making it extremely difficult to define detailed chemical compositions that are common to a range of products. Stable isotope distribution, however, responds to fundamental processes, that are fixed at primary production, thus providing a suitable method to test for the authenticity of the items of interest.

As it is not commercially viable to circumvent isotopic detection, stable isotopes have provided a way to detect fraud in products as diverse as, among many others, honey, fruit juices, wine, milk and dairy, Iberian ham, vegetable oil, mineral waters, beverages, food additives and even animal feed (i.e., Rossmann, 2001).

An actual example of how stable isotopes can be used is that of Fig. 1, where the $\delta^{13}\text{C}$ and $\delta^{15}\text{N}$ of the solid extract of locally purchased beer has been plotted according to the ingredients declared in the label. All beers brewed according to the "Bavarian Purity Law" of 1516 have $\delta^{13}\text{C} < -25\%$, as do the wheat and most pure barley malt

beers. Some brands claiming to be “pure barley malt”, however, are suspicious of mislabelling.

Other recent examples have to do with characterizing pork products. Traditional breeding of the Iberian pig depends on the “*Dehesa*”, a distinctive ecosystem where the animals are free ranging, feeding on natural resources all year long, with a major contribution by acorns in the winter months. It is acorns that impart special characteristics, both in terms of taste and health benefits, to this class of pork, with quantity and quality of the product mirroring the resources available. But modern market demands are decoupled from natural cycles, which results in a modification of traditional practices in order to satisfy demand, leading to an ever increasing number of animals being reared on non-natural resources; mostly on formulated feed.

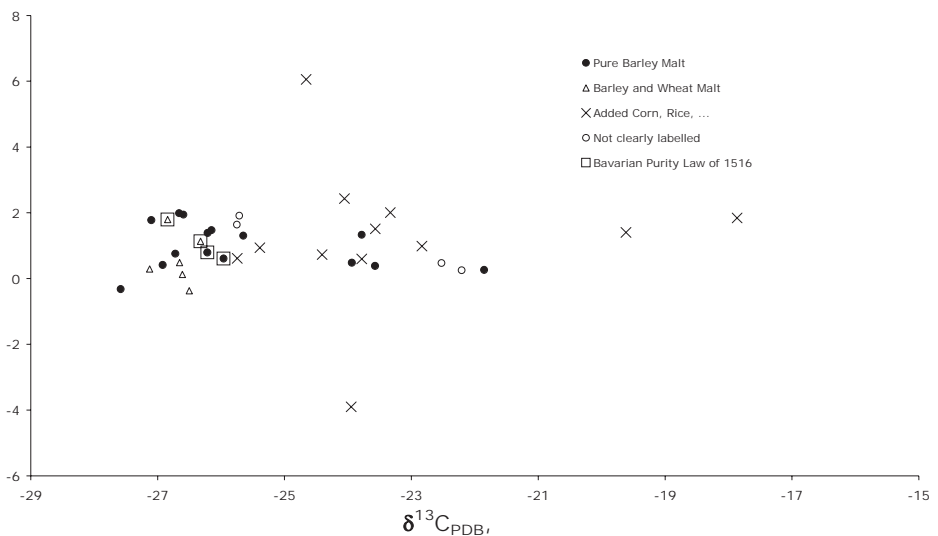


FIGURE 1. Binary plot of $\delta^{13}C$ vs $\delta^{15}N$ measured on the dry extract of beer. Note two well-separated groupings, mostly determined by C isotopic values. Some samples gave values that, a priori, do not correspond with the declared ingredients. Data from Cubides Castillo et al. (2007).

The high quality of Iberian pork products -and subsequent consumer appreciation and willingness to pay a corresponding high price- derives, however, from the traditional breeding and feeding system, so a method to test for substantial acorn consumption is

required. Fig. 2 shows that $\delta^{13}\text{C}$ of oleic fatty acid is a useful index to differentiate animals raised on grass + acorns from those fed formulated feed.

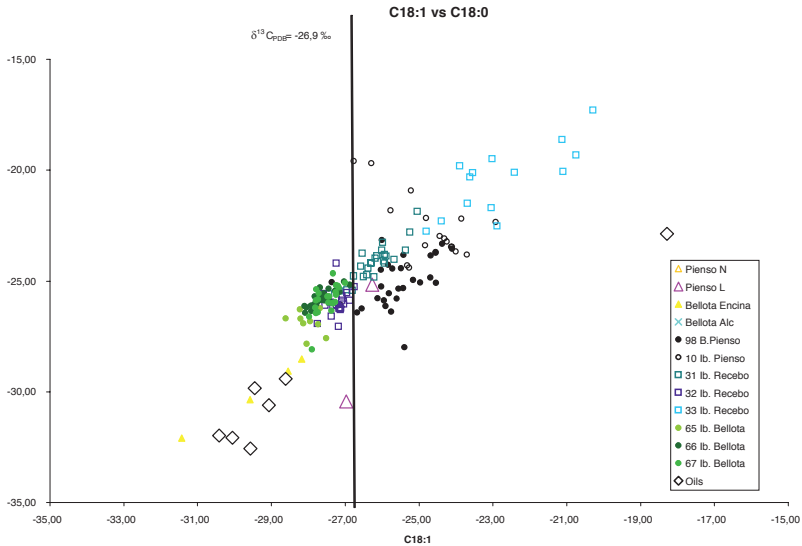


FIGURE 2. $\delta^{13}\text{C}_{\text{VPDB}}$ obtained for the methyl ester of Oleic Acid (C18:1) versus those of Stearic Acid (C18:0). No single sample classed as Bellota has $\delta^{13}\text{C}_{\text{C18:1}} > -26,88\%$. Values of different formulated feeds, acorns and several vegetable oils have been included for reference. From Recio (2007).

Forensics

The analytical techniques commonly available to forensic scientists allow identification of the substances present, but cannot tell one source of the same substance from another. Stable isotope variation, however, responds to fundamental physical, chemical and biological processes, and can thus be used to differentiate among otherwise chemically identical substances. Stable isotopes can corroborate and confirm many evidential leads in the investigation of serious crime (Benson et al., 2006). One potential use is in geo-location, that is, the relationship between stable isotopes and location. Stable isotope ratios can also be used to provide information about the origin of counterfeit money by measuring the hydrogen and oxygen isotope ratios in the paper.

The source of the cellulose can be determined. Other fields of use include the investigation of drug-related crime, where it can assist in distinguishing between different countries of manufacture or different manufacturers of pharmaceutical drugs, and can be employed to determine the precedence of drugs such as heroin: differences in the growing regions of the drug plant will result in differences in the N, C and O isotopic ratios.

Explosives and Fire

All commonly used explosives (gunpowder: a mixture of sulphur, charcoal, and saltpeter -potassium nitrate, KNO_3 ; Trinitrotoluene (TNT): $\text{C}_6\text{H}_2(\text{NO}_2)_3\text{CH}_3$; Nitroglycerine: $\text{CH}_2(\text{ONO}_2)\text{-CH}(\text{ONO}_2)\text{-CH}_2(\text{ONO}_2)$; RDX: $(\text{CH}_2\text{-N-NO}_2)_3$; PETN: $\text{C}(\text{CH}_2\text{ONO}_2)_4$, and the mixtures known as Plastic Explosives) have at least C and N into their formulation, and some also H, O and S; all of which have stable isotopes, whose isotopic ratios are amenable to determination by mass spectrometry..

TABLE 2.- Range of $\delta^{15}\text{N}$ and $\delta^{13}\text{C}$ observed for different explosives (Belanger, 2002).

Material	$\delta^{15}\text{N}$	$\delta^{13}\text{C}$	No. of samples
Ammonium Nitrate	Range = 5.4 ‰	-	7
Gunpowder	Range = 30.4 ‰	Range = 2.5 ‰	7
TNT	Range = 19.8 ‰	Range = 3.1 ‰	3
Plastic Explosive	Range = 14.0 ‰	Range = 10.1 ‰	4

Studies with PETN have shown that batches produced by the same manufacturer fall within a tight cluster of stable isotope ratio values, distinguishable from other manufacturers. Therefore, information can be obtained as to whether a suspect sample is consistent with being produced by a certain manufacturer. The analysis of samples of ammonium nitrate, gunpowder, TNT and plastic explosive confirmed that there was indeed a range of values for carbon and nitrogen isotope ratios and that the technique had the potential for the forensic analysis of explosives (Table 2; Fig.3).

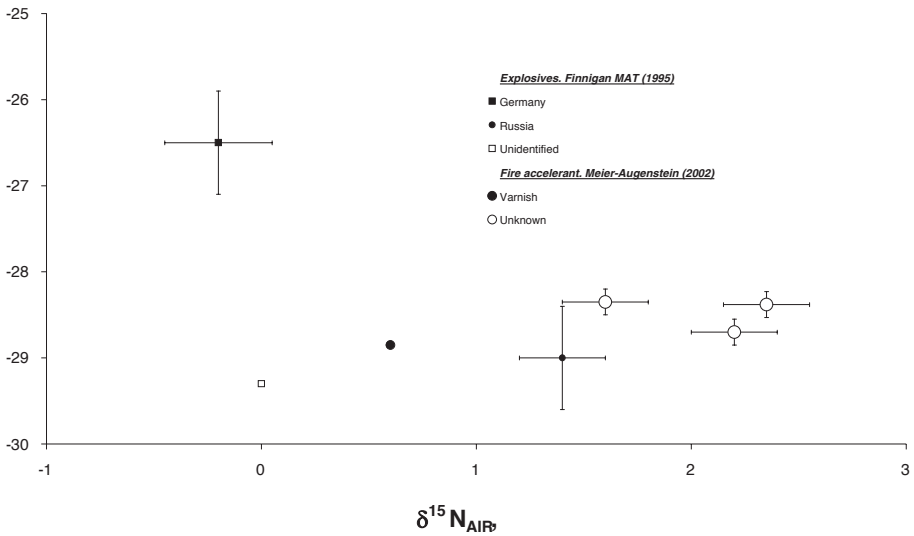


FIGURE 3. Values of $\delta^{15}N$ vs $\delta^{13}C$ measured for actual explosives (Finnigan MAT, 1995) and fire accelerants (Meier-Augenstein, 2002).

When investigating an intentional fire, its origin and how it propagated can frequently be established by physical means. But gathering unequivocal evidence that can be sustained on Court is not always an easy task (Jasper et al., 2002). Traditionally, arson residues are characterized by GC-MS that gives a "fingerprint" of the organic compounds of the accelerants employed. This fingerprint can then be used to identify specific classes of petroleum products by forensic chemists. But this just identifies the accelerant, not the individual that used it.

By using GC-C-IRMS, it is possible not only to identify the individual hydrocarbons composing the accelerant, but also the individual $\delta^{13}\text{C}$ of each of them. Commonly, accelerants may be formed by a mixture of up to 50-100 individual hydrocarbons that can be chromatographically separated. Obviously, after a fire, most of them will have degraded, but if we can recover say 4 useful compounds, our chances of unequivocally characterizing the accelerant used are high. GC-C-IRMS techniques can link together accelerant residues from the scene with partially evaporated residues on the arsonist or its environment, and with the remaining pristine accelerant in the container used (Jasper et al., 2002).

Drugs of Abuse and Pharmaceuticals

When fighting trafficking of drugs, an extremely useful piece of information for Authorities is to determine both the area of production and the possible routes followed by dealers. When a batch of heroin, cocaine or other drugs is seized, the drug itself and the impurities it contain keep a record of its origins and its distribution circuit.

Drugs such as heroin or cocaine derive from plant materials. The photosynthetic pathway of the plant (C_3 vs C_4), the soil nitrogen the plant had available for growth, and environmental factors, such as climate and water availability, all impart an specific isotope signature to the final product (Desage et al., 1991; Ehleringer et al., 1999, 2000; Galimov et al., 2005). If adulterants used to "cut" the drug are also considered, the final result is that every batch is almost unique on its combined $\delta^{13}\text{C}$ and $\delta^{15}\text{N}$ signature (Fig. 4).

But not only batches can be characterized. Heroin is a highly addictive drug that is processed from morphine, a naturally occurring substance extracted from the seedpod of the Asian opium poppy *Papaver somniferum*. Once inside the body it is rapidly metabolised to morphine, which is then excreted in the urine. The presence of morphine in urine cannot alone be used as a marker for illicit heroin abuse since morphine and codeine (which is also metabolised to morphine) can be found in prescriptive medicines (treatments for pain, coughs and diarrhoea) and foods (pastries containing poppy seeds have also been shown to lead to the presence of morphine and codeine in the urine). However, the intermediate metabolite of heroin, 6-monoacetylmorphine (6-MAM), can

be used as a specific marker for heroin as it does not result from the metabolism of either morphine or codeine. In addition, acetylcodeine is a known impurity of illicit heroin synthesis and may be used to distinguish between the pharmacologically pure heroin that is used in heroin maintenance programs and illicit ‘street’ heroin. Stable isotopic analysis of such components, extracted from body fluids, can aid in distinguishing between prescribed and illicit drugs.

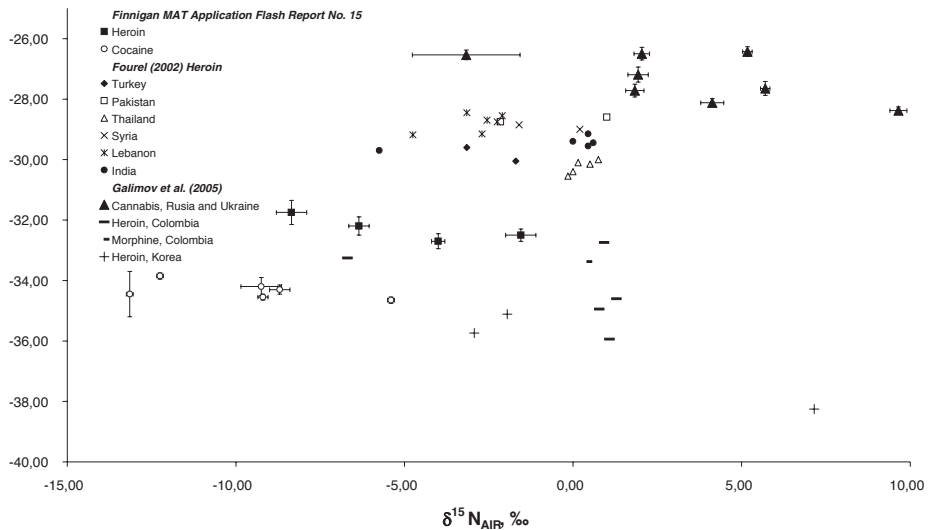


FIGURE 4. C and N isotopic values in four different seizures of heroin and and six shipments of cocaine. Variation of $\delta^{13}C$ is relatively small, but $\delta^{15}N$ clearly individualizes each batch (Finnigan MAT, 1995). Additional data on Heroin and Cannabis samples of known origin have been included for comparison (from Fourrel, 2002; Galimov et al., 2005).

In contrast with heroin and cocaine, ecstasy is a synthetic drug, not derived from plant extracts. Ecstasy (3,4-methylenedioxyethylamphetamine; MDMA) is typically prepared from a number of cheap and readily available natural products, via conversion to 3,4-methylenedioxyphenylacetone (MDA) and reductive amination to form an N-substituted amine (Palhol et al., 2003, 2004; Carter, 2002).

According to the UK's Home Office statistics for 1999, 29% of 16-29 year olds have experienced hallucinogenic drugs. Police and HM Customs seized approximately 6.5 million ecstasy tablets, for an estimated supply of 26 million tablets. In France, with

about 25% of total ecstasy seizures of Europe, the number of tablets analyzed by Customs authorities increased 400% in 5 years (Carter et al., 2002).

Tablets sold as ecstasy are notorious for containing, in addition to MDMA, other drugs e.g. MDA, MDEA, amphetamine and caffeine. Target analysis of these and other amphetamines in biological samples is of great importance for clinical and forensic toxicologists alike. Plasma is traditionally one of the most commonly investigated specimens for the confirmation of illicit drug use.

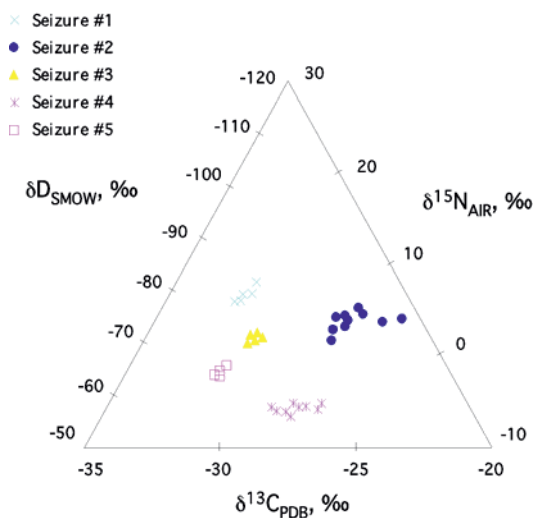


FIGURE 5. Combined use of H, C and N isotopic values allows characterisation of individual ecstasy seizures. From Carter et al. (2002).

provide information on geographical precedence. Results to date indicate that $\delta^{15}\text{N}$ is a major discriminating factor, while δD and $\delta^{13}\text{C}$ are minor factors. The combined use of $\delta^{13}\text{C}$ and $\delta^{15}\text{N}$ reflects reductive amination, and δD reflects origin and solvent history.

Geolocation

Stable isotopes can be used to track the recent history not only of substances, but also that of people. C and N isotopes record diet (De Niro and Epstein, 1978, 1981; Bold and Pflieger, 2002; O'Connell and Hedges, 1999), and O and H isotopes track drinking habits (water, but also other usual drinks, such as beer) (Cerling et al, 2003; O'Brien and

"Isotopic fingerprinting" can be used to distinguishing from batch to batch (Fig. 5); linking "trace" and "bulk" evidence; to trace drugs to a common source of manufacture or supply, and to determine synthetic method. $\delta^{13}\text{C}$ and $\delta^{15}\text{N}$ on ecstasy directly depend on the physicochemical environment from which they are derived, marking both precursors and method of synthesis, although cannot

Wooller, 2007; Ehleringer et al., 2008). These techniques are widely used to study animal migration, but it is only recently that they have been applied to forensic issues (O'Brien and Wooller, 2007). Several substrates are suitable for seeking evidence: human blood records both local drinking water and diet (Ehleringer, 2002). Breath CO₂ can also inform about recent locations. Bone and teeth keep a longer, sometimes lifelong record, but the implications of obtaining such samples should be obvious. Non-invasive samples, such as hair, nails or even urine, have been proven useful to track medium-term travel (from a few days to a few months; Fraser and Meier-Augenstein, 2007; Bol and Pflieger, 2002; O'Connell and Hedges, 1999; Bowen et al., 2005; Fraser et al., 2008).

Interpreting δD and $\delta^{18}O$ values in terms of geographical location requires an understanding of the multiple sources of oxygen and hydrogen, and of the factors that can contribute to isotopic fractionation. Isotopic values of human hair keratin should be the result of the various contributions from drinking water, food water, dietary protein and atmospheric sources (Ehleringer et al., 2008). However, these various contributions can be successfully modelled (Ehleringer et al., 2008; O'Brien and Wooller, 2007; Fraser and Meier-Augenstein, 2007). Also, different target samples record different information and time periods. According to O'Brien and Wooller (2007), 90% turn over of body water, as recorded by urine, requires some 24 days. Hair and nails, on the other hand, are only "alive" at the root. From there on, no isotopic modification occurs (if properly cared for; see Bowen et al., 2005; Fraser et al., 2008), such that hair, for example, keeps a linear record into the past, whose duration depends on hair length: on average, hair grows at an average rate of 1 cm per month. Bleaching, dying, or coloring has only minor effects on the isotopic composition of hair (Cerling et al., 2003).

Doping in Sport

The analysis of performance enhancing doping agents in sport has become an important area of analytical toxicology. Specific methods of analysis are necessary to meet international regulatory thresholds in a variety of matrices, most commonly urine and blood, but also other biological matrices such as hair and sweat. In addition, new strategies are required to distinguish between exogenously administered hormones and their natural analogues. Quantitative measurement of doping agents in complex matrices

such as blood and urine to regulatory levels requires the high selectivity and sensitivity offered by GC/MS and LC/MS/MS. Gas Chromatography-Isotope Ratio Mass Spectrometry (GC-IRMS), on the other hand, is proving a powerful tool for the detection of drug abuse in both humans and animals, potentially applicable to the analysis of any organic metabolites. IRMS is now widely accepted as the only technique that can unambiguously distinguish between endogenously produced and synthetic, self-administered performance enhancing drugs. The measurement of deuterium isotopes provides additional evidence for sourcing drug metabolites.

This technique has been accepted by the IOC Medical Commission (1997) as a viable technique for distinguishing between exogenous and endogenous steroid metabolites. The World Anti-Doping Agency (WADA, 2004) requests that any T/E ratio above 4 be confirmed by means of stable C isotope analysis.

Testosterone

There is an increasing need in sport for new methodologies in proving testosterone misuse. Up to recently, GC-MS was employed to determine the excreted Testosterone / Epitestosterone ratio from urine. A value of greater than 4:1 was considered as confirmation of drug administration (WADA, 2004). This ratio was accepted because the distribution of world

Study day	V ₁	V ₂	V ₃	V ₄	V ₅
1	0.26	1.28	4.69	0.10	0.12
2	0.33	1.48	5.26	0.11	0.11
3	0.65	8.77	29.30	0.26	0.70
4	1.95	24.20	36.90	1.77	6.69
5	2.81	45.80	41.80	2.01	5.91
6	2.79	33.20	61.80	1.96	3.71
7	3.03	15.40	54.90	1.91	4.24
8	4.13	36.40	57.70	1.48	5.95
9	5.30	30.30	39.70	1.51	5.78
11	3.20	26.50	33.00	0.58	3.69
13	0.77	2.63	3.42	0.68	3.41
15	0.22	0.99	4.37	0.19	2.27
17	0.26	2.02	4.80	0.13	0.21

population fell below this figure. However, there are minorities whose ratio can be naturally higher (Table 3; see Sottas et al., 2008). Also, this ratio can be manipulated downwards by simultaneous administration of epitestosterone. The GC-MS test is therefore fallible, potentially giving both false positives and false negatives (Sottas et al.,

2008). There are methods for overcoming this; the administration of a drug called ketoconazole to an athlete with a naturally high T/E ratio results in a decrease of such ratio, but in athletes who have received exogenous testosterone it causes the ratio to increase.

This test could be used to determine innocence or guilt after a positive T/E test, but it involves administering a drug to detect a drug. Additionally, the athlete needs to be supervised for up to 8 hours for the drug to take affect, therefore being invasive and inconvenient for both the sampling officer and the athlete.

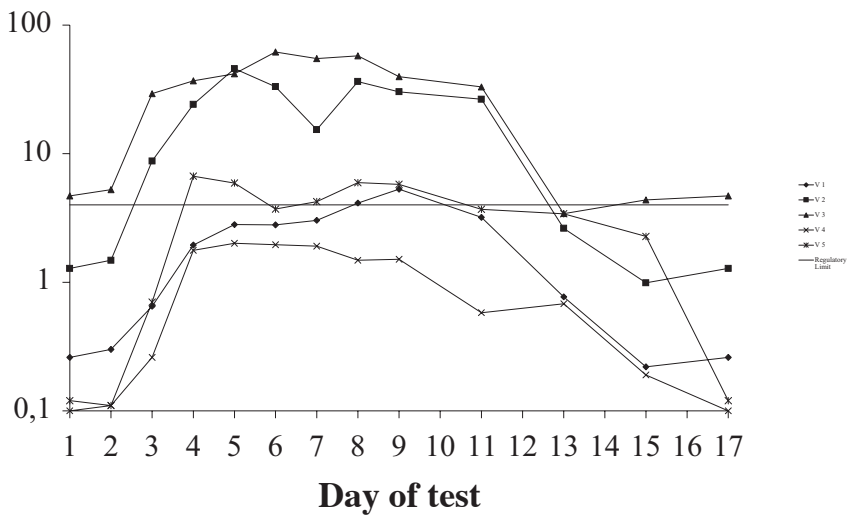


FIGURE 6. Evolution of the $\delta^{13}C$ values of Table 3. All but one volunteer test positive.

The use of Stable Isotope Ratio Mass Spectrometry, however, has shown that synthetic testosterone (derived from plants) has a lower $\delta^{13}C$ than the endogenous hormone (for example, Shackleton et al., 1997). The quantity of urine collectable from an athlete in events is minimum (50-100ml), and this has to be split to perform several analyses. Targeting the metabolites of testosterone, especially the androstanediols, which are naturally abundant and are at a higher concentration than testosterone, would make it easier to detect and monitor isotopically. The technique, therefore, uses a multistep, but

relatively simple procedure, consisting in separating two or three functional groups by LC; removing the pregnane metabolites by oxidation, and derivatising the steroids by acetylation. Only one chromatographic separation removes up to 75% of the unwanted steroids from the urine. The oxidation removes the majority of the complex side chains from the 17-hydroxypregnane steroid resulting in a cleaner sample for a simpler chromatogram. The derivatised samples are dissolved on cyclohexane and injected into the GC-C-IRMS, where they are analysed for their isotopic ratios.

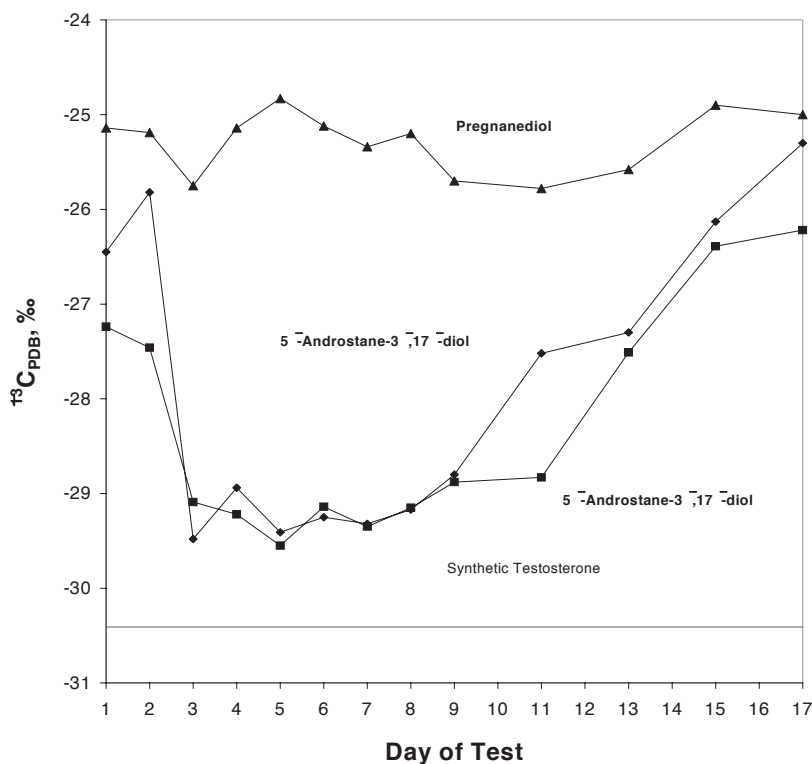


FIGURE 7. Evolution of the $\delta^{13}\text{C}$ value of 5α - and 5β -androstane- $3\alpha,17\beta$ diols and pregnanediol after administration of testosterone at the end of day 2. Data from Shackleton et al. (1997) and Phillips (1999).

Experimental results (Fig. 7) show that $\delta^{13}\text{C}$ of pregnanediol does not change dramatically by administration of testosterone, while $\delta^{13}\text{C}$ of the 5α - and 5β -androstane- $3\alpha,17\beta$ diols become lighter after the administration, and only starts to recover after 6-7

days. The pregnanediol could be monitored as an internal reference to relate to diet, or can possibly be used to develop an indication ratio for abuse. Metabolites that are unaffected by testosterone could be used as the individual's baseline, and therefore regulatory values could be agreed upon for future doping tests.

This technique could also be applied to the testing of other anabolic reagents, such as DHT, DHEA and epitestosterone. Cawley et al. (2004) found that $3\alpha,5\text{-cyclo-}5\alpha\text{-androstane-6}\beta\text{-ol-17-one}$ (“ $3\alpha,5\text{-cyclo}$ ”) is a natural byproduct of metabolism of dehydroepiandrosterone (DHEA), but whose concentrations are elevated (5-15 times) following DHEA administration. By considering average values from available databases, it was proposed that any sample with $3\alpha,5\text{-cyclo} \geq 140$ ng/ml be tested by IRMS for significant ^{13}C depletion, since it was confirmed experimentally that $\delta^{13}\text{C}$ of $3\alpha,5\text{-cyclo}$ change from -24.3‰ to -31.1‰ 9 hrs after administration of a single dose of DHEA, returning to baseline after 48 hrs. In case of continued administration of DHEA, $\delta^{13}\text{C}_{3\alpha,5\text{-cyclo}}$ reached even lower values at -33.9‰ .

Nandrolone

Evidence is emerging that exercise and legal supplements may raise endogenous 19-norandrosterone (19Na) above 2 ng per ml of urine, the current IOC threshold for reporting a doping offence. As a result, a preliminary study was undertaken by Phillips et al. (2000) to establish the feasibility of using stable isotope ratio mass spectrometry (IRMS) to distinguish between high endogenous urinary excretion and high excretion due to administration of a nandrolone doping agent.

Six volunteers (3 male and 3 female) provided a single urine sample prior to steroid administration. The $^{13}\text{C}/^{12}\text{C}$ isotopic ratio of urinary pregnanediol (PD) and 19-norandrosterone (19Na) were then determined in a similar analytical manner to that described in Shackleton *et al.* (1997.a, b). The volunteers then self-administered 100 mg of 19-norandrostenedione, a legal “over the counter” food supplement. A second urine sample was taken 48 hours following administration and the $^{13}\text{C}/^{12}\text{C}$ isotopic ratio of urinary PD and 19Na was determined.

Prior to steroid administration the $\delta^{13}\text{C}$ value of PD (a nandrolone precursor) and 19Na (a nandrolone metabolite) were approximately equal (Fig. 8, top). 48 hours

following administration of 19-norandrostenedione the $\delta^{13}\text{C}$ value of urinary 19Na decreased relative to PD (Fig. 8, bottom). IRMS analysis of the doping agent returned a lower abundance of ^{13}C ($\delta^{13}\text{C}_{\text{PDB}}$ of 19-norandrostenedione equalled $-32.8 \pm 0.3\%$) than endogenous 19Na. As a result, it appears that oral administration of the doping agent altered the isotopic value of the steroid's metabolites, yet left the steroid precursors unchanged.

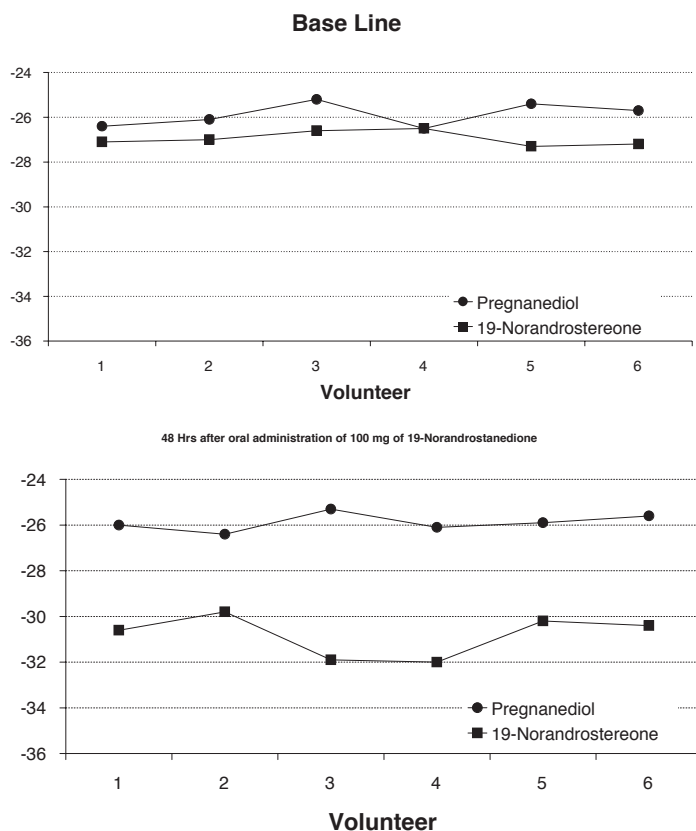


FIGURE 8. Evolution of the $\delta^{13}\text{C}$ value of urinary steroids before and 48 hrs. after administration of 19-norandrostenedione. Data from Phillips et al. (2000).

Urine from pregnant women in their third trimester were also analysed and the ^{13}C values were very much the same as those of the volunteers prior to nandrolone administration, yet it is known that at this stage in their pregnancy, women can show large increases in concentration of urinary 19Na. The data shows that the IRMS analysis

of nandrolone metabolites and nandrolone precursors could provide a feasible method for detecting nandrolone abuse. This is however a preliminary study and requires considerable work before a valid test can be applied to doping control.

Pollution / Environmental

Compound-specific isotope analysis (CSIA) is facilitating the application of isotopic tools at much finer spatial and temporal scales than was possible ever before, and opening up for detailed isotopic investigation of a whole new range of organic compounds typically present at ppm to ppb levels in the subsurface. CSIA has made a major impact in biogeochemical and environmental research. Basic and applied questions pertaining to pollutant fate and transport in near-surface environments can be addressed employing isotopic techniques, resulting in the ability to trace the sources and pathways of a wide variety of natural and anthropogenic organic compounds.

As with any tool applied to environmental research, there should always be recognition by practitioners of isotope geochemistry that, at best, we may hold a small piece to a grand environmental puzzle. Isotopic measurements are most useful when used in tandem with careful field observations and other geochemical, geophysical and geological constraints.

Non Point-Source Pollution

Preventing the pollution of soil and water requires characterising the contaminants, and elucidating their provenance. Among the many possible contaminants, the nitrates present in soil and water are of major concern. Conventional chemical methods suffer from multiple interferences that render them of only limited use at best. Nitrates can originate from a point source –industrial and urban sources: liquid waste and leachate of MSW landfill sites-, or from a non-point source –agricultural activities, for example-.

Agriculture –crop fertilizers and watering- represents a non-point source, and is the most important contributor to nitrates in continental waters, although point sources can be locally important (Perlmutter and Koch, 1972, Kreitler, 1975; Kreitler and Jones, 1975; Kreitler et al., 1978; Porter, 1980; Flipse et al., 1984; Flipse and Bonner, 1985). Natural fixation of nitrogen by the biosphere will only exceptionally result in anomalously high nitrate contents in soil and, eventually, water (Böhlke et al., 1997; Kreitler and Jones, 1975). High N and P contents result in water mass eutrophication,

and high N in drinking water has been linked to diseases such as methemoglobinemia and cancer (Vigil et al., 1965). The issue is widely acknowledged by international organizations. In Europe, the “Nitrates Directive”, 91/676/EEC, establishes mandatory maximum limits of 50 mg/l NO_3^- (11,3 mg/l N, although it recommends not to exceed 25 mg/l NO_3^- or its equivalent 5,6 mg/l N, as established in the “Drinking Water Directive”, 80/778/EEC). These are very similar values to those recommended by the WHO¹, and the ones currently adopted by the US's EPA.

Process	Reaction	α , fractionation factor
N_2 fixation	$\text{N}_2 \rightarrow \text{NH}_4^+ \rightarrow \text{organic N}$	0.991 to 1.0041
N_2O reduction	$\text{N}_2\text{O} \rightarrow \text{NH}_4^+ \rightarrow \text{organic N}$	1.00343
Denitrification	$\text{NO}_3^- \rightarrow \text{N}_2\text{O}$	1.028; 1.033
NO_3^- assimilation	$\text{NO}_3^- \rightarrow \text{NH}_4^+ \rightarrow \text{organic N}$	1.0027 to 1.03
NH_4^+ assimilation	$\text{NH}_4^+ \rightarrow \text{organic N}$	1.0091 to 1.02
NO_2^- assimilation	$\text{NO}_2^- \rightarrow \text{NH}_4^+ \rightarrow \text{organic N}$	1.007
Nitrification	$\text{NH}_4^+ \rightarrow \text{NO}_2^-$	1.025 to 1.035
Diffusion	NH_4^+ , NH_3 , or NO_3^- in solution	~ 1.00
	NH_3 diffusion in gas phase	1.018

Table 4.- Nitrogen isotope fractionations during biologically-related reactions. From Handley and Raven (1992). Fractionation factors are composites from a variety of organisms cultured in laboratory or field experiments.

Transcription of the European Directive to Spanish national legislation (R.D. 261/1996, 16 February; B.O.E. # 61, 11/3/1996), keeps the concentration of nitrate mentioned, and includes the publication of the so called “Código de Buenas Prácticas Agrarias” (Good Agricultural Practice Code), that, among other things, regulates fertilizer application (quantity and season) and density of livestock per surface area, such that the nitrogen load is always lower than $170 \text{ KgHa}^{-1}\text{yr}^{-1}$. This represents between 367

¹ The WHO set an upper limit of 10 mg/l of N derived from NO_3^- , and 1 mg/l N derived from NO_2^- (equivalent to 44,3 and 3,3 mg/l of the respective ion in drinking water; World Health Organization, 1984, Guidelines for Drinking-Water Quality; WHO, Geneva)

and 2125 Kg/Ha/year of chemical fertilizer (depending on its nature; Orús et al., 2000), or a livestock density that varies between 580 hens and 2 cows per Ha and year (Regulation CEE 2092/91).

It is therefore evident from the above that control instruments must be sought in the search for possible links between source and sink. But cause-effect relationships are not enough; it is necessary to search for parameters that allow a firm association between source and pollutant, as well as quantifying relative contributions in the case of multiple sources.

Classical chemical methods can easily determine nitrate in water; however, they are not suited to identify the source of pollution. Whatever its origin, the different forms of soil N are subject to transformations that mask its origin. The stable isotopic ratios D/H, $^{13}\text{C}/^{12}\text{C}$, $^{15}\text{N}/^{14}\text{N}$, $^{18}\text{O}/^{16}\text{O}$ and $^{34}\text{S}/^{32}\text{S}$, however, can fulfil the requirements. Different substances have characteristic isotopic ratios, that allow not only identification, but also quantification of individual pollutants (Kendall and McDonnell, 1998). Natural soil N derives ultimately from the atmosphere via biological fixation. Except in very particular locations, the geological materials are not a significant source of N. Anthropogenic nitrate or ammonium, however, can locally or regionally represent a noticeable contribution.

Atmospheric N_2 is also used to produce NH_3 by the Haber method, and this is the base to synthesise chemical fertilizers. It is estimated that by the year 2000, the amount of fertilizer-N already equalled the amount of N fixed in organic matter by natural processes. Once incorporated into the soil, organic matter is employed as substrate by multiple microbial reactions. Nitrates are highly soluble; they are not as reactive with organic complexes as ammonia, and can be easily transported by water percolating through the soil.

Each of the steps described has the potential for fractionating N isotopes. Except fixation and assimilation as a nutrient, other processes can result in fractionations between 10 to 30‰ (Table 4), or even larger (the product depleted in ^{15}N with respect to the reagent), as observed after fertilizer application.

Nitrate $\delta^{15}\text{N}$ is useful in tracing its provenance (for example, Aravena et al., 1993, Durka et al., 1994; Wassenaar, 1995; Ging et al., 1996; Kendall et al., 1997). However,

although $\delta^{15}\text{N}$ depends directly on the N source, exchange with soil-N can affect its isotopic signature (Komor and Anderson, 1993). An even larger effect is associated to ammonium volatilization (Mariotti et al., 1988; Böttcher et al., 1990). It is therefore necessary to establish the isotopic relationships within the context of the local conditions of the area under investigation. A multielement / multisotopic study will help in this regard. For example, the additional determination of $\delta^{18}\text{O}$ allows characterisation of possible processes that might potentially modify the concentration and the isotopic ratios of N in nitrates, such as denitrification (Amberger and Schmidt, 1987; Böttcher et al., 1990).

The few remaining uncertainties after N and O isotopic analysis can be clarified by the use of additional isotopic systems (S and O in sulphates; O in phosphates, ... etc) and chemical data (for example, Böhlke and Denver, 1995). Typical $\delta^{15}\text{N}$ values are between -5 to $+3,5\text{‰}$ in soils where chemical fertilizers have been applied; natural soil organic matter has $\delta^{15}\text{N} \approx +3,5$ to $+7,5\text{‰}$; animal manure is between $+10$ to $+20\text{‰}$, and downstream of septic tanks values around $\delta^{15}\text{N} \approx +10\text{‰}$ (Aravena et al., 1993) to $\delta^{15}\text{N} \approx +8\text{‰}$ (Kreitler et al., 1978) have been measured.

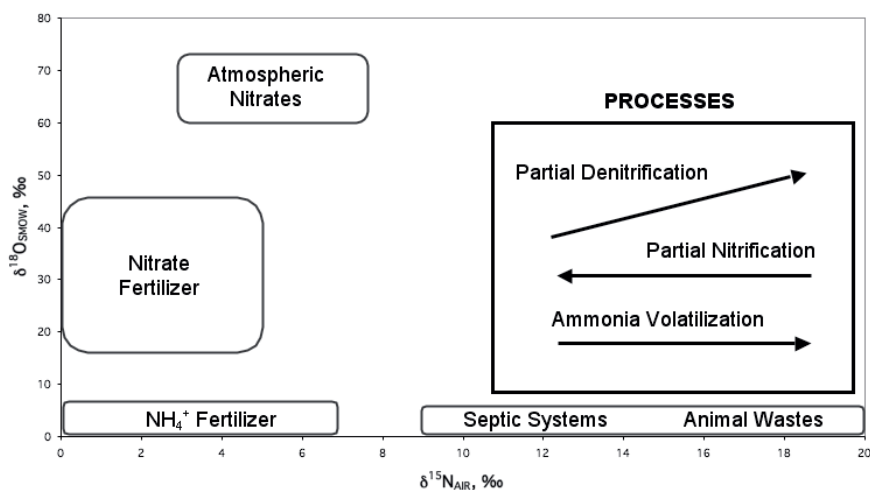


FIGURE 9. O and N isotope characterisation of various sources and processes that can contribute nitrate pollution to soil and water. From Bleifuss et al. (2001).

The combined use of $\delta^{15}\text{N}$ and $\delta^{18}\text{O}$ is useful for differentiating nitrates of varied provenance (see Fig. 9). O isotopes are particularly suited to identify atmospheric N, particularly in contrast with that derived from bacterial nitrification that occurs naturally in the soil. It is thus relatively easy to tell nitrate derived from chemical fertilizers from soil nitrate, or that derived from manure. Bacterially fixed nitrate varies regionally, since only one oxygen derives from gaseous O_2 , while the remaining $2/3$ are derived from ambient water (Amberger and Schmidt, 1987; Durka et al., 1994; Kendall et al., 1997; Anderson and Hooper, 1983; Hollocher, 1984), whose $\delta^{18}\text{O}$ follows the meteoric water line (MWL).

Concluding Remarks

In former pages, we have taken a very quick tour around some of the multiple applications of stable isotopes, in fields as different as Food Science, Environmental Pollution, Forensic Science.... It never was my intention to do an exhaustive review of possible applications -an impossible task, anyway, for any single scientist in a reasonable time- but to provide a quick overview of the fundamentals underpinning the analysis and interpretation of stable isotopic ratios, and how "scientific common sense" can make use of such a tool to get answers to intricate scientific subjects, but also to down-to-Earth everyday problems.

Many fundamental fields of research have been left intentionally and unavoidably out. No mention has been made of the use of stable isotopes in Earth Sciences, the mother science from which stable isotope analysis was born. Biological Sciences at large -and particularly Ecology- have also been left aside, together with natural derivations such as Agricultural Sciences. The reason behind is that these fields have, in the course of time, created a body of science able to stand alone as important disciplines in their respective fields, and the interested reader should be able to find plenty of treatises and research articles which will address the use of stable isotopes in due depth. Other sectors of active research employing stable isotopes, such as climate change, oil exploration, medical and clinical applications, ... to mention but a few, are subdisciplines of broader scientific areas, and normally of interest to the specialists only.

As mass spectrometry evolves, new technological developments, both in the mass

spectrometers themselves and in the preparation systems coupled to them, open up new perspectives for the use of stable isotopic ratios, but the fundamental principles remain unchanged. Current technology allows the analysis of isotopic ratios on specific molecules, and on samples on the nanogram size.

In terms of the traditional physicochemical techniques, to substances can be “*alike as two water drops*”. Stable isotopes, however, are a useful tool when in hands of a skilled researcher, able to *tell one source of the same substance from another*. It is only the imagination of the researcher that can place limits on the application of stable isotope techniques to the solution of an increasingly wider range of challenges.

References

- Amberger, A. and Schmidt, H.-L. (1987). *Geochim. Cosmochim. Acta*, 51, 2699-2705.
- Anderson, K. K. and Hooper, B. E. (1983). *FEBS Lett*, 164, 236-240.
- Aravena, R., Evans, M. L. and Cherry, J. A. (1993). *Ground Water*, 31, 180-186.
- Belanger, C. (2002). "Network Developing Forensic Applications of Stable Isotope Ratio Mass Spectrometry Conference 2002". DSTL Fort Halstead, Kent, 8.
- Benson, C., Lennard, C., Maynard, P. and Roux, C. (2006). *Forensic Sci. Int.*, 157, 1-22.
- Bleifuss, P.S., Hanson, G.N. and Schoonen, M.A.A. (2001) "Tracing Sources of Nitrate in the Long Island Aquifer System". " Long Island Geology Research Papers on the Web". SUNY. <http://pbisotopes.ess.sunysb.edu/reports/bleifuss/>
- Böhlke, J. K. and Denver, J. M. (1995). *Water Resour. Res.* 31, 2319-2339.
- Böhlke, J. K., Ericksen, G. E. and Revesz, K. (1997). *Chem. Geol* 136, 135-152.
- Bol, R. and Pflieger, C. (2002). *Rapid Comm. Mass Spec.*, 16, 2195-2200.
- Böttcher, J., Strebel, O. Voerkelius, S. and Schmidt, H.-L. (1990). *J. Hydrol.*, 114, 413-424.
- Bowen, G.J., Chesson, L., Nielson, K., Cerling, T.E. and Ehleringer, J.R. (2005). *Rapid Comm. Mass Spec.*, 19, 2371-2378.
- Calderone, G., Guillou, C. & Naulet, N. (2003). *L'Actualité Chimique*, 8-9, 2003, 22-24.
- Carter, J. (2002). "Network Developing Forensic Applications of Stable Isotope Ratio Mass Spectrometry Conference 2002". DSTL Fort Halstead, Kent, 12-13.
- Carter, J., Titterton, E., Murray, M. and Sleeman, R. (2002). "Network Developing Forensic Applications of Stable Isotope Ratio Mass Spectrometry Conference 2002". DSTL Fort Halstead, Kent, 12-13.
- Cawley, A.T., Hine, E.R., Trout, G.J., George, A.V. and Kazlauskas, R. (2004). *Forensic Sci. Int.*, 143, 103-114.
- Cerling, T.E.; Ehleringer, J.R., West, A.G., Stange, E. and Dorigan, J. (2003). *Forensic Sci. Int.* 136: 172.
- Cubides Castillo, M.A., García Vicente, M., Gómez Gallego, J., Gómez Sánchez, M.J., González Neira, I. y Recio, C. (2007) “Isotopic characterization of beer: a quality control tool”. Unpublished.
- De Niro, M. J. and Epstein, S. (1978) *Geochim. Cosmochim. Acta* v.42 pp.495-506.

- De Niro, M. J. and Epstein, S. (1981) *Geochim. Cosmochim. Acta* v.45 pp.341-351.
- Desage, M., Guilly, R., Brazier, J.L., Chaudron, H., Girard, J., Cherpin, H. and Jameau, J. (1991). *Analytica Chimica Acta* 247, 249-254.
- Durka, W., Schulze, E.-D., Gebauer, G. and Voerkelius, S. (1994). *Nature* 372, 765-767.
- Ehleringer, J.R., Casale, J.F., Lott, M.J. and Ford, V.L. (2000). *Nature*, 408, 311-312.
- Ehleringer, J.R., Bowen, G.J., Chesson, L.A., West, A.G., Podlesak, D.W. and Cerling, T. E. (2008). *PNAS*, 105, 2788-2793.
- Ehleringer, J. (2002). "Network Developing Forensic Applications of Stable Isotope Ratio Mass Spectrometry Conference 2002". DSTL Fort Halstead, Kent, 10-11.
- Ehleringer, J.R., Cooper, D.A., Lott, M.J. and Cook, C.S. (1999). *Forensic Sci. Int.*, 106, 27-35.
- Finnigan MAT (1995) "¹⁵N/¹⁴N and ¹³C/¹²C by EA-IRMS. Forensic studies using the ConFlo II interface". Application Flash Report No. 15.
- Flipse, W. J. and Bonner, F. T. (1985). *Ground Water*, 23, 59-67.
- Flipse, W. J., Katz, B. G., Lindner, J. B. and Markel, R. (1984). *Ground Water* 22, 418-426.
- Fourrel, F. (2002). "Network Developing Forensic Applications of Stable Isotope Ratio Mass Spectrometry Conference 2002". DSTL Fort Halstead, Kent, 18-19.
- Fraser, I. and Meier-Augenstein, W. (2007). *Rapid Comm. Mass Spec.*, 21, 3279-3285.
- Fraser, I. Meier-Augenstein, W. and Kalin, R.M. (2008). *J. Forensic Sci.*, 53, 95-99.
- Galimov, E.M., Sebestyanov, V.S., Kulbachevskaya, E.V. and Golyavin, A.A. (2005). *Rapid Comm. Mass Spec.*, 19, 1213-1216.
- Ging, P. B., Lee, R. W. and Silva, S. R. (1996) "Water chemistry of Shoal Creek and Waller Creek, Austin, Texas, and potential sources of nitrate". *U. S. Geol. Surv. Water Resour. Invest. Rep.* 96-4167.
- Handley, L.L. and Raven, J.A. (1992). *Plant Cell Environ.*, 15, 965-985.
- Hollocher, T. C. (1984). *Arch. Biochem. Biophys.*, 233, 721-727.
- Jasper, J. P., Edwards, J. S., Ford, L. C. and Corry R. A. (2002). *Fire and Arson Inv.* 51(2):30-34.
- Kendall, C. and McDonnell, J.J. (1998; Eds.) "Isotope Tracers in Catchment Hydrology". Elsevier Science B.V., Amsterdam.
- Kendall, C., Campbell, D. H., Burns, D. A. and Shanley, J. B. (1997). *EOS Trans. AGU*, 78(17), 169, Spring Meeting, Baltimore, 1997.
- Komor, S. C. and Anderson, H. W. Jr. (1993). *Ground Water*, 31, 260-270.
- Kreitler, C. W. (1975) "Determining the source of nitrate in ground water by nitrogen isotope studies". Bureau of Econ. Geol., Univ. of Texas at Austin, Rep. of Invest., 83.
- Kreitler, C. W. and Jones, D. C. (1975). *Ground Water*, 13, 53-61.
- Kreitler, C. W., Ragone, S. E. and Katz, B. G. (1978). *Ground Water*, 16, 404-409.
- Mariotti, A., Landreau, A. and Simon, B. (1988). *Geochim. Cosmochim. Acta*, 52, 1869-1878.
- Mas, F., Beemsterboer, B., Veltkamp, A.C. and Verweij A.M.A. (1995). *Forensic Sci. Internat.* 71, 225-231.
- Meier-Augenstein, W. (2002). "Network Developing Forensic Applications of Stable Isotope Ratio Mass Spectrometry Conference 2002". DSTL Fort Halstead, Kent, 20-21.

- O'Brien, D.M. and Wooller, M.J. (2007). *Rapid Comm. Mass Spec.*, 21, 2422-2430.
- O'Connell, T.C. and Hedges, R.E.M. (1999). *Am. J. Phys. Anth.*, 108, 409-425.
- Orús, F., Quílez, D. and Beltrán, J. (2000). *Informaciones Técnicas*, 93. Departamento de Agricultura, Gobierno de Aragón.
- Palhol, F., Lamoreux, C. and Naulet, N. (2003). *Anal. Bioanal. Chem.*, 376, 486-490.
- Palhol, F., Lamoreux, C., Chabrilat, M. and Naulet, N. (2004). *Analytica Chimica Acta*, 510, 1-8.
- Perlmutter, N. M. and Koch, E. (1972). *U.S. Geol. Surv. Prof. Pap.* 800-B, pp. 225-235.
- Phillips, A. (1999). *Micromass Application Note* 501.
- Phillips, A. and Shackleton, C.H.L. (1999). *SIMSUG '99. Poster*.
- Phillips, A., Davies, S. and Mounier, L. (2000). *IMSC 2000. Poster*.
- Porter, K. S. (1980). *Ground Water* 6, 617-625.
- Recio, C. (2007). Ponencias, comunicaciones y pósteres IV Congreso Mundial del Jamón. Salamanca 2007, 59-63.
- Rossmann, A. (2001). *Food Rev. Int.*, 17, 347-381.
- Shackleton, C. H. L., Phillips, A., Chang, T. and Li, Y. (1997.a). *Steroids*, 62, 379-387.
- Shackleton, C.H.L., Roitman, E., Phillips, A. and Chang, T. (1997.b). *Steroids*, 62, 665-673.
- Sottas, P-E., Saudan, C., Schwizer, C., Baume, N., Mangin, P. and Saugy, M. (2008). *Forensic Sci. Int.*, 174, 166-172.
- Vigil, J., Warburton, S., Haynes, W.S. and Kaiser, L. (1965). *Public Health Reports*, 80, 1119-1121.
- WADA (2004) Reporting and Evaluation Guidance for testosterone, epitestosterone, T/E ratio and other endogenous steroids. WADA Technical Document TD2004EAAS. http://www.wada-ama.org/rtecontent/document/end_steroids_aug_04.pdf
- Wassenaar, L. I. (1995). *Appl. Geochem.*, 10, 391-405.

Radiogenic isotopes and their applications within a range of scientific fields

Kjell Billström

Swedish Museum of Natural History, Laboratory for isotope geology
Box 50 007, SE-104 05 Stockholm, Sweden

Introduction

Isotopic methods have become a very important tool in the study of natural processes, and numerous applications have proved valuable in a diversity of research areas. Most of the early developed methods were devoted to solve problems in bedrock geology and other geological disciplines, and the ability to obtain absolute ages provided a break-through in the understanding of the Earth's history. More recently, novel applications have been tested successfully within e.g. forensics and environmental studies. As a result, a wealth of information has grown over the last few decades through studies involving both stable and radiogenic isotopes. This contribution focuses on the application of radiogenic isotopes, whilst the approach using stable isotopes is further developed by Recio (2008, this volume). To a large extent, the tremendous increase in using isotope geochemical tools in new research areas has been driven by the technical development and introduction of new generations of very sensitive instrumentation. Besides, the chemical separation methods have developed to a point where extremely small samples (down to nanogram levels) can be handled and effects of interferences and contamination can be kept at a minimum.

Contrary to stable isotopes whose abundances are unchanged by radioactive processes, a radioactive/radiogenic isotope is either unstable and decay to another nuclide, or is the result of a decay series. Radiogenic isotopes may be divided into long-lived and short-lived isotopes, and their different half-lives ($T_{1/2}$; the time during which 50 % of the radiogenic (parent) isotope decay to produce a daughter isotope) have implications for their usage in science. For instance, long-lived isotopes, e.g. ^{238}U (which decays to ^{206}Pb with a half-life of 4468 million years, Ma), are well suited for measuring

time in old geological systems which may have developed billion of years ago. By contrast, a short-lived nuclide, like ^{210}Pb (half-life is around 22 years), may be relevant for dating processes having a duration of a few years.

The aim of the present over-view is to illustrate how radiogenic isotopes can be applied in science, and examples will be presented with relevance for bedrock geology, archeology, forensics, food industry and environmental sciences. The theory of radiogenic isotopes are described in several text-books (see e.g. Faure & Mensing, 2005 for an excellent review), and only a few relevant issues will be recalled here in order to ease further reading.

Some theoretical concepts of radiogenic isotopes

Basically, radiogenic isotopes are applied in two different ways; (1) to provide an absolute age of a sample, and (2) to trace the origin of a component. The decay of ^{87}Rb to ^{87}Sr taken place in biotite can be used to illustrate the age concept. Biotite has a tendency to incorporate a significant amount of rubidium, and to exclude Sr, in its lattice during crystallisation. Rubidium has two naturally occurring isotopes; ^{87}Rb and ^{85}Rb , and the former decays to ^{87}Sr with a half-life of 48.8 billion years. This decay process, following an exponential law, is similar to the principle of an hour-glass; the sand in the upper part (cf. the “parent ^{87}Rb isotope”) is passing down to the lower part (“decays to ^{87}Sr ”) at a controlled rate described by a linear relationship. The time that has passed since the moment when the hour-glass was over-turned can be approximated by comparing the proportions of the remaining upper sand fraction with that of the lower fraction. Similarly, the ratio between radiogenically formed ^{87}Sr and the remaining ^{87}Rb in the biotite at the time of analyses, a ratio determined by means of mass spectrometry, is proportional to the time elapsed since biotite crystallisation. Using a mathematical notation, the time (t) is defined as follows;

$t = 1/\lambda \times \ln (^{87}\text{Sr}/^{87}\text{Rb} + 1)$, where λ is the decay constant for the $^{87}\text{Rb} \rightarrow ^{87}\text{Sr}$ decay process.

Thus, the daughter/parent isotope ratio ($^{87}\text{Sr}/^{87}\text{Rb}$) becomes bigger with time, which is the same as saying that the age of the biotite is increasing. Similarly, there are other isotopic clocks or geochronometers that can be used, and some of the most widely used

in geochronological applications are the U-Pb, Pb-Pb, K-Ar, Ar-Ar, Sm-Nd, Re-Os and Lu-Hf isotope systems for which some data are given in Table 1.

Method	Decay system	Decay constant	Initial ratio of interest	Common application
U-Pb	^{238}U to ^{206}Pb	1.55125×10^{-10}		age dating
Pb-Pb	^{238}U to ^{206}Pb		$^{206}\text{Pb}/^{204}\text{Pb}$, etc.	tracer and model age
K-Ar	^{40}K to ^{40}Ar	5.81×10^{-11}		age dating
Ar-Ar	^{40}K to ^{40}Ar			cooling ages
Sm-Nd	^{147}Sm to ^{143}Nd	6.54×10^{-12}	$^{143}\text{Nd}/^{144}\text{Nd}$	age dating, tracer
Re-Os	^{187}Os to ^{187}Re	1.612×10^{-11}	$^{187}\text{Os}/^{188}\text{Os}$	dating ores, tracer
Lu-Hf	^{176}Lu to ^{176}Hf	1.93×10^{-11}	$^{176}\text{Hf}/^{177}\text{Hf}$	tracer

TABLE 1. Some relevant parameters for a few selected radioactive isotope system (the half-life is related to the decay constant through the expression; $T_{1/2} = \ln 2 / \lambda$)

The principle behind tracing the source for an element, e.g. Sr, can be explained by looking at an event whereby a crustal component separates from the mantle. In this case, the ratio between ^{87}Sr (radiogenically produced isotope) and ^{86}Sr (a stable Sr isotope - not affected by any kind of radioactive process) is of interest and the latter is used as a reference isotope whose abundance remains unchanged with time. Typically, a Rb/Sr fractionation process is related to this kind of event, and the produced crust will have an elevated Rb/Sr ratio compared to that of the residual mantle. As a result of differing Rb/Sr ratios, the post-event accumulation of radiogenic ^{87}Sr in the mantle will be lower than that in the crust, cf. Figure 1. This in turn means that the $^{87}\text{Sr}/^{86}\text{Sr}$ ratio will differ between these two geological domains, and the difference will be more pronounced with time and as a consequence the provenance of a sample (mantle- or crustal-derived) can be constrained using its Sr isotopic signature. Similarly, other isotopic systems evolve in an analogous way, and the Sr, Nd and Os isotopic signature for a rock can thus be used to model its origin. Another tracer system of interest in this context is the so called common Pb method which is built on the slow decays of U and Th isotopes to stable Pb isotopes. For instance, in ore geological studies, where the origin of galena often is of interest, the $^{206}\text{Pb}/^{204}\text{Pb}$, $^{207}\text{Pb}/^{204}\text{Pb}$ and $^{208}\text{Pb}/^{204}\text{Pb}$ isotope

ratios (^{204}Pb is unradiogenic and is used as a reference isotope) are typically determined. These ratios increase with geological time and with increasing levels of U and Th in a studied system, but in opposite to the behaviour of Sr in the crust/mantle, the obtained Pb isotope ratios of galena (with a U/Pb ratio virtually being zero) do not change with time once Pb has been incorporated into its lattice. Hence, galena-bearing ores formed at different times (and in different geological environments) are characterized by different sets of Pb isotope ratios, and occasionally the Pb isotopic signature of a specific ore is unique providing a direct link between a specimen and a known ore. The way the Pb isotope ratios evolve with time in different environments (e.g. upper crust, lower crust and mantle) has been modelled by different authors, and one of the most widely used model is known as the plumbotectonics model (Doe & Zartman, 1979). Figure 2 displays galena data from the Gangdese copper belt in Tibet (Qu et al., 2004) forming a linear array in consistency with a mixing process involving lead from different environments.

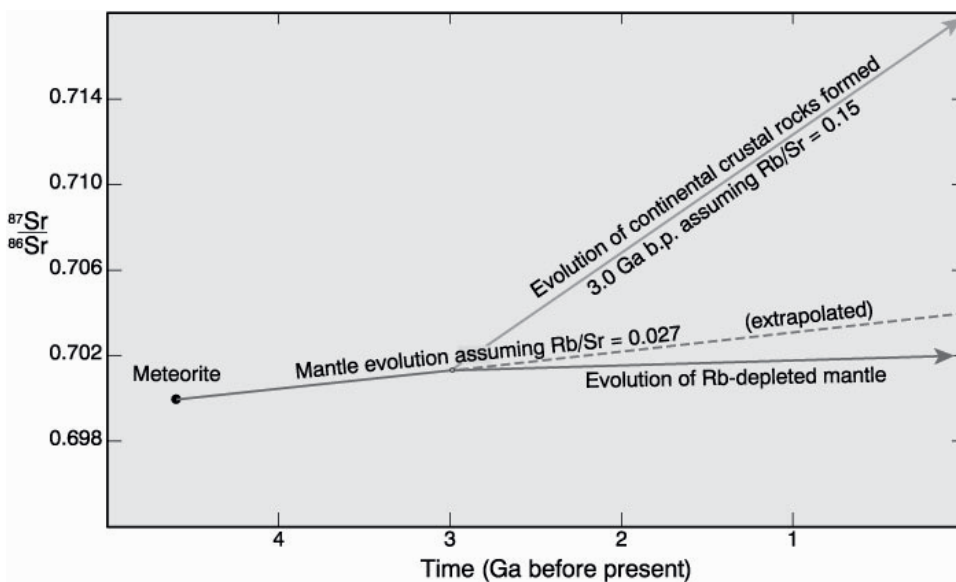


FIGURE 1. Principal sketch-map showing the differences in Sr isotope ratios that develop once a crustal segment is separated from the mantle at some 3 billion years ago (after Wilson, 1989).

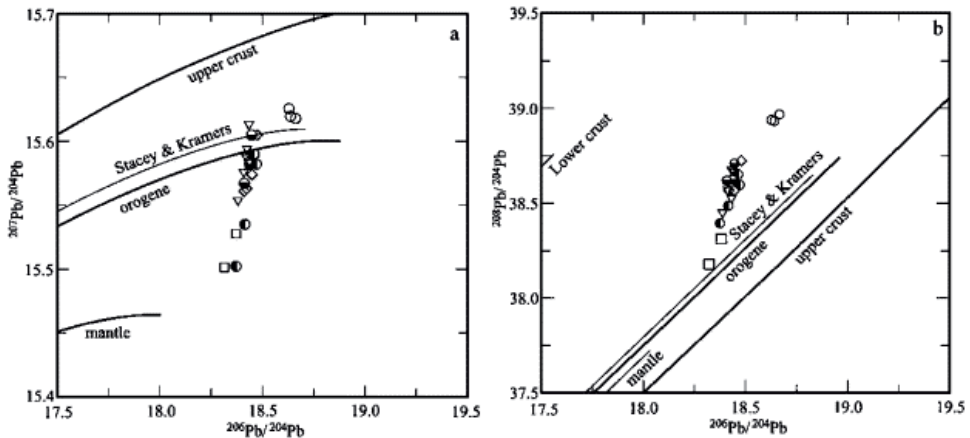


FIGURE 2. Plumbotectonics diagram showing data of galena from the Gangdes copper belt, Tibet along with the evolution curves for the upper crust, lower crust, mantle and orogene (Qu *et al.*, 2004). Also shown is the two-stage model of crustal lead of Stacey and Kramers (1975).

A wide range of applications

Applications where radiogenic isotopes are used will here be demonstrated within the fields of bedrock geology, archaeology, forensics, food and beverage industry, and environmental sciences. Given the space limitation, only a few, illustrative case studies can be presented. Essentially, many isotope studies make use of the fact that isotope ratios could act as finger-prints that constrain the origin of the studied object. Sr and Pb isotopes are two isotopic systems which were developed for geological applications, but which are also useful in other disciplines. Compared to many lighter elements which are presently explored (e.g. Si, Sn, Mo, Fe, etc.), Sr and Pb have some advantages. Their isotope systematics is well characterized, their isotopic variations are quite large and easily analyzed, and proven methods for their chemical isolation before analysis exist. In addition, there are several sample types (e.g. carbonates) exhibiting very low Rb/Sr element ratios which make them particularly relevant to analyze. Remembering that carbonates are rich in Ca, and that Sr is geochemically similar to Ca, there will also be substantial amounts of Sr present in carbonates, but basically no Rb. From this follows, that the Sr isotopic ratios in carbonates do not change with time as a result of radioactive decay, and such data have been used to monitor the temporal changes in Sr isotope ratios of the oceans (see e.g. Faure and Mensing, 2005).

Certain samples, like galena and K-feldspar, are characterized by essentially U/Th free systems which suggest that their post-crystallisation Pb isotope ratios stay the same. It deserves mentioning that lead is widely used in many materials, to e.g. improve the quality of glass, and it is found in significant amounts in lead-acid batteries, piping, solder, cable sheathing, radiation shielding, paint and ammunition. Obviously all these categories of objects mimic essentially U/Th free systems that can be fingerprinted by lead isotopes. Considering other heavy elements; such as Nd and Hf, there are only rare Nd or Hf-bearing samples which may be free of the parent elements (Sm and Lu). This means that in applications involving Nd and Hf, sample isotopic ratios actually will evolve slowly with time which is a clear draw-back in tracing sources for old systems often encountered in geological applications. However, in e.g. an archaeological case study where the important question may be to pin-point a nearby source (finger-printing) which delivered Nd/Hf to a young object (man-made in recent time), this limitation may not be serious.

Bedrock geology

Most of the non-geological applications rely on the isotope tracer, or provenance concept, and therefore it seems natural to concentrate on isotope age dating techniques in this section. However, it must be remembered that tracer studies are extremely important in for example petrological work. For instance, both Nd and Hf isotopes are used to provide information about the crustal history of a zircon's host rock. Examples will be given here with relevance for age dating of ore formation and rock crystallisation.

Dating ores by means of the Rb-Sr and the Re-Os methods

A major task in ore geological research is to date ore formation, but as a rule this is often difficult as minerals suitable for dating typically are not part of the ore assemblage itself. This means that dating normally needs to be accomplished on non-ore minerals whose genetic relationship to the main pulse of ore formation is questionable. There are, however, two relatively recent findings, which form an exception to this rule; Rb-Sr dating using sphalerite and Re-Os dating using molybdenite (and other sulphides) have been demonstrated to give reliable ages.

Successful sphalerite datings have been reported on e.g. Mississippi Valley type (MVT) deposits (see e.g. Nakai et al., 1990). This approach requires that a series of sphalerites are analyzed, defining a certain range in Rb/Sr ratios, which makes it possible to fit a line (this line is called an isochron having the feature that its slope is proportional to the age of the system) in a diagram where $^{87}\text{Rb}/^{86}\text{Sr}$ is plotted versus $^{87}\text{Sr}/^{86}\text{Sr}$. As sphalerite contains only very minor amounts of Sr and Rb, the crucial step is to avoid the contamination of hypothetically present fluid inclusions. If such inclusions occur, these could carry small amounts of Rb and Sr that may disrupt the isotope systematics related to the proper ore-forming episode. The way to deal with this is to carefully grind the sphalerites using a boron carbide mortar with a very hard surface, thereby removing fluid inclusion waters prior to analysis. The data displayed in Figure 3 represent one of the pioneering studies (Nakai et al., 1990), and in addition to an isochron age it also shows the initial Sr isotope ratio. The latter reflects the type of Sr originally entering sphalerite at the time of ore formation, and the value of ca. 0.7105 is relatively high suggesting a significant input of crustal Sr.

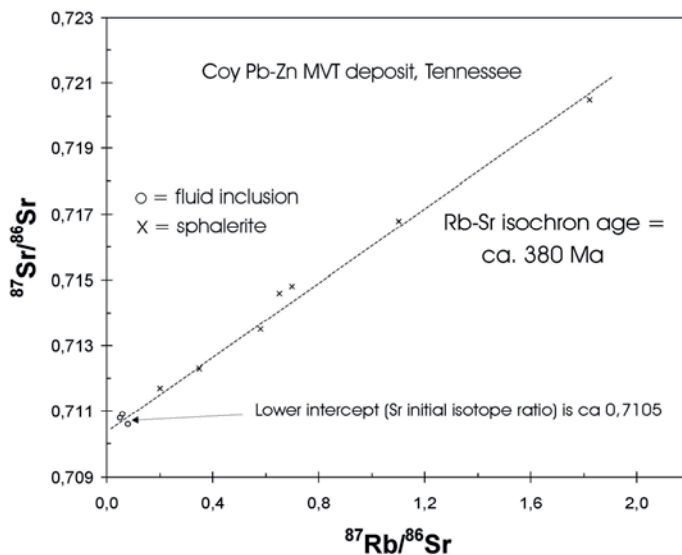


FIGURE 3. A Rb-Sr isochron diagram showing data for sphalerites sampled from the Coy mine in Tennessee (after Nakai et al., 1990).

Molybdenite is a phase, which is not uncommon in ore-forming environments and which has the unique feature of concentrating significant amounts of Re (and to exclude Os) during crystallisation. As a consequence, the amount of radiogenic ^{187}Os present at the time of analysis (due to the decay of ^{187}Re to ^{187}Os) is a monitor of the time elapsed since molybdenite formed, and this time period obviously equals the age of the mineral. A case study from the Harnäs gold deposit in Sweden has also shown promising results when applied to sulphides, like pyrite and arsenopyrite, which are ubiquitous in many ore-forming environments (Stein et al., 2000).

Geochronological dating - U-Pb method on zircon (laser and ion microprobe approaches)

Zircon is an accessory mineral, containing trace levels of uranium but basically negligible amounts of unradiogenic lead that crystallises in small amounts from most intermediate to felsic magmas. It is also a very robust mineral that often withstands alteration and metamorphic processes, and as a result it has been the most commonly U-Pb dated mineral in geochronological applications. In more recent time, the classical way of zircon analysis (by means of thermal ionization mass spectrometric analyses of separate Pb and U aliquots available after wet chemistry separation) has been partly replaced by ion microprobe (SIMS; secondary ion mass spectrometry) and laser ICP-MS (inductively coupled plasma - mass spectrometry) techniques. Two obvious advantages with the latter in-situ techniques are (i) point analyses of individual parts of a zircon crystal could be undertaken, (ii) an ability to derive many point-analyses within a short time. As zircon grains commonly are composite, this means that in-situ techniques can help to unravel a complex, igneous and metamorphic history of a rock. The high-speed of ion microprobe (and laser ICP-MS) analysis has opened up a kind of provenance application, where a large number of zircon grains from sediments are analyzed.

This approach is often used to target potential regions showing age population records that match that of the investigated sample, enabling the reconstruction of the nature of past erosional areas. Imaging techniques using BSE (back-scattered electrons) or CL (cathodoluminescence) are helpful tools guiding the selection of suitable zones for dating (cf. Figure 4).

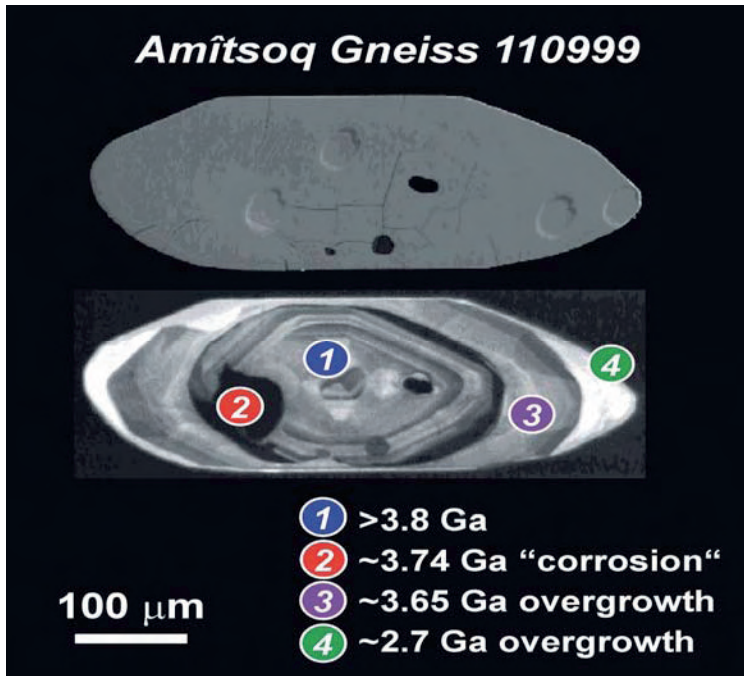


FIGURE 4. Obtained ion microprobe ages (in billion years, Ga) from a zircon of the Amitsoq gneiss, Greenland (upper part shows a SEM image with traces of the craters produced by the incident primary ion beam, whilst the lower is a CL image showing oscillatory zoning and overgrowths).

This is obviously important when for instance a zircon contains inclusions (crystallized prior to the main zircon-forming event) that may contain non-negligible amounts of either U or Pb, or secondary over-growths. If such zircons are analyzed in a conventional manner using a small number of crystals, a geologically meaningless, mixed age would result. The quality of ion probe data (ca. $\pm 1\%$ uncertainty in individual U-Pb ages) is comparable with that of laser results, but the latter is a destructive method creating ablation craters with a depth penetration of some 10-20 micrometers compared to only a few micrometer deep pits induced by the ion microprobe. Lasers produce very short light pulses, with a uniform wavelength, that can be focused onto the surface of a sample (see Kosler & Sylvester, 2003 for applications in geochronology). When the sample is hit, material sputters away (ablates) and can be transported by a carrier gas to a ICP-MS system where small, solid sample particles are ionized and subsequently

analyzed with respect to its isotope ratios. Possibly, laser ICP-MS applications will be even more used in the future as this a versatile tool allowing trace element analyses, Hf and U-Pb analyses to mention a few, and besides this instrumentation is much cheaper than ion microprobes. The presently introduced new generation of femtosecond laser systems appears to yield almost negligible fractionation effects which otherwise may be an obstacle in deriving reliable data. Moreover, this laser type is not heating its immediate neighbourhood, and in medicine such lasers are investigated for the usage of killing individual cancer cells.

Archeology

Provenance studies using stable and radiogenic isotopes have in a way revolutionised the last decades of work in archaeology. In non-geological applications, such as archaeology, it may not be required to interpret the ultimate origin of an object and to constrain the nature of the geological process(es) involved in the formation of the raw material used in the manufacturing process. Instead, the main concern may be to relate an object to a specific environment (e.g. a stone axe to a specific rock quarry, a skeleton to a certain inhabited area). This is to say, that finger-printing is typically of main concern in many archaeological studies, and a limiting factor may occasionally be that appropriate isotope reference data are lacking. Obviously, distinct mineralogical features may also be essential when it comes to constrain the origin of e.g. a stone axe exhibiting some specific banding or intergrown textures. The subjects brought up in the present context include age dating of organic carbon-containing objects, tracing the origin of artifacts, and the migration patterns of animals and humans.

Age dating using the C-14 (radiocarbon) method

^{14}C is produced in the atmosphere by a nuclear reaction where ^{14}N is transformed to ^{14}C (Libby, 1946). Once ^{14}C forms it starts decaying to stable ^{14}N by beta-emission (the half-life is around 5730 years), and its presence in the atmosphere is principally balanced by its production rate and its removal rate through precipitation. When a living plant is growing it absorbs CO_2 from the atmosphere that contains a small proportion of ^{14}C . This small amount is in steady-state equilibrium with ^{14}C in the atmosphere, but when the plant dies the incorporation of CO_2 stops. As a consequence, no further

addition of external ^{14}C to the plant takes place, and the activity of ^{14}C declines at a rate, which is controlled by its half-life. Plants, or organisms which eat plants (including animals and ultimately humans), can be dated by using a beta-counting system. The relatively short half-time and limitations in the detection systems restrict material much older than ca 50.000 years to be dated. Numerous successful ^{14}C dates have been published during the last half-century, and one of the latest was carried out to establish the age of Ötzi, the iceman who died when crossing the Alps some 3330 years B.C. (Fowler, 2000).

Origin of artifacts

The origin of archaeological artifacts has been successfully established at many excavation sites all over the world. The trace amounts of strontium and lead in many archaeological objects have made it possible to apply Sr and Pb isotopes in investigations, giving e.g. insights into past trade routes. A basic foundation for their usefulness in provenance studies, is that these isotopes do not fractionate neither during natural reactions, nor due to treatment by local craftsmen. What may be a serious drawback, and particularly relevant for Pb, is that isotope populations of known ore districts may overlap considerably. Three examples with relevance to archaeology will be given here.

Batavia, a ship of the Dutch East India Company, was shipwrecked on her maiden voyage in 1628, and made famous by the subsequent mutiny and massacre that took place among the survivors. The remains of this ship is now at a museum in Perth, Australia and some of the items found (copper tacks and nails with traces of lead) have been used in a lead isotope study to provenance their origin (Van Duivenvoorde, 2008). These results demonstrate that the copper metal was derived from more than one source. Lead isotope ratios plotted in Figure 5 prove the existence of a low-radiogenic Pb isotope signature which matches very well the relatively unique signature of ores from the mining district of Bergslagen in southern Sweden. Trading with Sweden at this time is well documented, but it is also clear from the way data plot in the diagram that another, more radiogenic source of lead (exhibiting higher lead isotope ratios), characterize the majority of the samples. This source is more difficult to pin-point as lead from several ore districts in different countries would be consistent with the Batavia

radiogenic signature. On the basis of independent evidence, it is likely that in addition to Swedish Bergslagen copper ore, either ores mined in Japan or Morocco were transported by Batavia.

The plumbing system in Pompeii during the Roman empire exemplifies another case where Pb isotopes were applied (Boni et al., 2000). By analyzing lead pipes belonging to the water supply system, the authors could identify a quite complex data pattern involving three, or more, lead sources. The isotope patterns also suggest that lead in the pipes have been melted and re-circulated to be used in new constructions as part of a major reconstruction programme involving the entire town. The ultimate sources of lead cannot easily be identified, but the suggested end-members include one specific ore at Sardinia. The other sources remain unidentified as the appropriate isotopic compositions can be matched with several ore districts in the Mediterranean region.

At Sagalassos in SW Turkey, archeological excavation works have lately included isotope methods. The main approach has been to use a multi-isotope, and trace element approach in order to constrain the possible sources of raw materials used in manufacturing iron and glass artifacts (Degryse et al., 2006). Three local glass types are known from the area (green glass, blue glass and HIMT = High Iron Manganese Titanium glass), and Sr and Pb data support a theory where the latter two were recycled to produce green glass. On the basis of Sr isotope signatures and absolute Sr contents in the glasses, suggestions have also been put forward with relevance for the ultimate origin of the glass types. Locally found iron artifacts and their origins constitutes another source of discussion at Sagalassos. Limestone-hosted hematite and magnetite ores and hematite placer deposits are known from the area, and their potential association with the iron artefacts is clearly of interest. It turned out that Sr isotope signatures were most useful to provenance the iron-containing objects, whilst Pb data often show a more scattered or overlapping character. Combined with trace element analyses the cited isotope work at Sagalassos provide a good basis for interpreting the origin of raw materials.

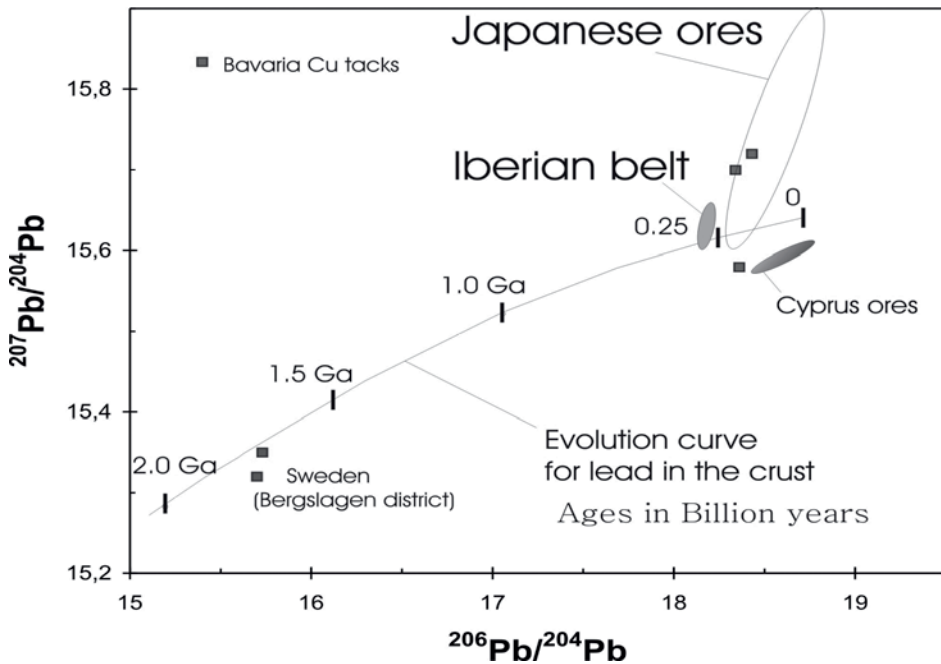


FIGURE 5. Lead isotope data of Cu-tacks from the Bavaria wreckage and some reference fields (after Van Duiwenvoorde, 2008).

Mints and coins form another group of objects which have been successfully provenanced by lead isotopes. Silver coins often carry a substantial amount of lead which follows from the circumstance that argentiferous lead ores often are used for silver production. Laser ablation ICP-MS analyses of Roman silver coins were reported to have been used for assessing the trade and exchange of metals and ores (Pointing et al., 2003).

Tracing the life story of humans ("you are what you eat")

Archaeologists, interested in how people have moved between inhabited regions, may benefit from applying Sr isotopes in their work. The reason is that different regions, characterized by different geology, tend to have quite distinct Sr isotopic signatures or finger-prints. Taken Sr isotopes as an example, there is principally a 1:1 relationship between bedrock, soil, plants and other organisms higher up in the food chain which can be explained as follows. The strontium isotope signature of the bedrock is controlled by geological factors – the soil inherits the isotopic signature of the weathered bedrock – the

plants inherits that of the soil (although added fertilizers may complicate the picture) – animals inherit the signature of the plants, and ultimately this may be reflected in humans which mainly feeds on special animals. An illustrative example of a big isotopic contrast between food, is given by fish from a marine environment (showing a marine, relatively unradiogenic Sr signature) and crops growing on soil derived from an old basement being characterized by a highly radiogenic signature). As the primary isotope signatures are preserved (i.e. not fractionated) as Sr is processed through the food chain, the body skeleton retains a Sr isotope memory of the diet taken in by an individual. As noted before, the usefulness of Sr isotopes is related to the fact that Sr is geochemically similar to Ca which is a major element in the human body. As a result, Sr occurs in amounts (ppm levels) high enough to be analyzed in e.g. teeth and skeleton remains. The Sr isotope systematics in teeth and bones, however, are different. The enamel of teeth becomes mineralized to apatite which hinders teeth-Sr to interact with strontium stored in other parts of the body, and in this way the Sr isotope compositions of teeth reflect a fossil isotope signature that is related to the child-hood. For other parts of the body, there is continuous exchange of Sr between the skeleton and the new Sr ingested through the diet, and it takes like 7-10 years for the isotopic signature of Sr in bone to become fully re-setted once a completely new kind of diet pattern has been in place. Therefore, on the basis of Sr isotope data from teeth and bones, one could in theory identify both the geographical region associated to the child-hood, and the region related to the last ten year period before death (Beard et al., 2000). Beard et al. (2000) used this approach to investigate the migration history of people the remains of which were found in an archaeological site in south-western U.S.

Forensic sciences

An isotope analysis is one of several analytical techniques used in the field of forensics. Here a novel technique will briefly be discussed where short-lived isotopes are used for constraining the time elapsed since the death of a person. Besides, it will be shown how the Pb isotope ratios in bullets and ammunition can be used to discuss their sources(s). It may also be mentioned that smuggling of nuclear materials is posing an increasing threat to society. In the field of nuclear forensics, isotope methods are important in the work of characterizing suspicious material.

Dating post-mortem intervals

A common problem for forensic pathologists is to estimate the post-mortem interval, and several methods involving e.g. growth of insects and application of isotopes (short-lived radionuclides) have been investigated. Diagenetic effects, and related mobilisation of radionuclides, may complicate the interpretation of some results related to certain isotopes, like ^{90}Sr produced by aboveground nuclear weapons testing, not naturally occurring in human bones. Carbon-14 is commonly used in life sciences but its relatively long half-life of 5730 Ma prohibits its use for accurately dating very young objects. Recent investigations have shown a potential of using ^{210}Pb (half-life of 22.3 years) and ^{210}Po (138 days) as a tool for pathologists (Swift et al., 2001). These nuclides, which are intermediate, beta-emitting radioactive members of the ^{238}U decay series, enter the human body either directly through the food, or as an effect of decay of ^{226}Ra which is retained in the body after inhalation. As for C-14 there is a steady-state equilibrium situation, with the levels of ^{210}Pb and ^{210}Po staying approximately constant as long as a human being is alive. These levels are low and require a beta-counting system capable of precise measurements of radioactivity. Although more work is required to explore the full applicability of this approach, the differing half-lives of the mentioned nuclides suggest that the post-mortem interval, being relevant for forensics (i.e. ranging from days to a few decades), could be constrained with a precision superior to previously used methods.

Bullets and their origin

Ballistic determinations are perhaps the most important method in investigations involving shooting incidents. On the other hand, there are situations where ballistic investigations are inconclusive due to deformation of bullets, and sometimes bullets could not even be found at the crime scene. Bullet residues may remain in the victims body and since bullets typically are made of lead alloys, Pb isotope analyses of such fragments could be a useful tool. A number of studies have been devoted to test the usefulness of Pb isotopes in forensic work (e.g. Ulrich et al., 2004), and considerable differences among Pb isotope signatures of ammunition do indeed exist (Zeichner et al., 2006). One conclusion is that the combination of lead isotope data and trace element analyses usually give the best result. Antimony seems to be a relevant indicator of origin

in some cases as Sb is intentionally added to ammunition to give it desirable properties. It is favourable if reference ammunition could be tested, and ideally a very clear match is found with a bullet used in a crime. In February of 1986 Sweden suffered a national trauma when Olof Palme, the present prime minister, was shot to death. Lead isotope analytical data of bullets form part of the vast investigation material, but so far no perpetrator has been possible to link to the crime. Certain factors must always be considered when provenancing ammunition. One is that isotopic variations could occur even for the same lot of ammunition if the manufacturer mixes different raw materials representing different sources. Another thing to keep in mind is that Pb isotope data normally only make it possible to either demonstrate a similarity, or lack of similarity, between a bullet and some reference material. That is, one has to be careful not to exclude an alternative interpretation of available isotope data.

Food and beverage industry

In particular, N, C, S and other stable isotopes are nowadays widely used to detect frauds in the food industry. The stable isotopes of the light elements may provide information about altitude/latitude and reflect a climate control, whilst e.g. Sr isotopes may add lithological source information important for an authenticity documentation. The usefulness of Sr isotope data is very much dependent on the presence of clear isotopic contrast in a study area which would govern the development of distinct isotopic differences among the samples investigated. For instance, two extreme end-members would be constituted by young basaltic rocks having quite unradiogenic Sr isotope compositions, and old crustal felsic rocks whose elevated Rb/Sr ratios would lead to increasingly radiogenic Sr isotope ratios with time.

Provenancing juice, waters and coffee

Several hundreds of fruit juices have been systematically analyzed from all over the world in a study reported by Rummel et al. (2006). These authors found that Sr isotopes provided useful information pertinent to the origin of juices. This was due to the fact that the geological conditions are quite homogeneous (bringing Sr isotope signatures to be relatively characteristic) in many juice-producing areas within countries such as Spain and countries from Middle and South America. Moreover, occasionally

Besides, mineralogical and trace element studies may give additional information. The isotope approach has the advantage of providing a direct comparison between collected dust and its potential source area(s).

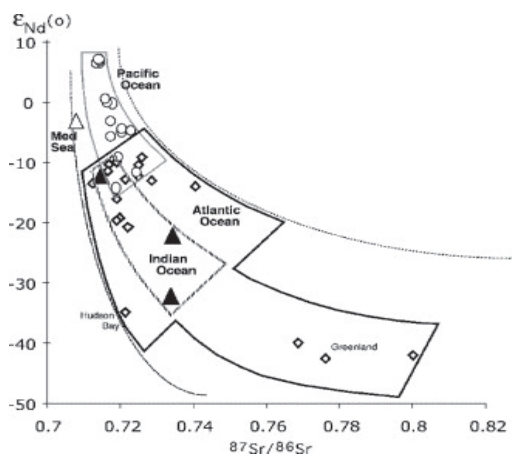


FIGURE 7. Sr-Nd isotopic composition of suspended matter from rivers entering the main world oceans (after Goldstein and Jacobsen, 1988).

This opens up the possibility for modelling dust transport in the past which have important implications for climate reconstructions and historical atmospheric circulation patterns. For example, aeolian dust in the atmosphere can either reflect or absorb solar energy as a function of e.g. mineralogy and grain size. Moreover, continental dust settling in the oceans may affect the marine productivity, and pollutants are also easily carried by dust particles (Grousset and Biscaye, 2005). As for other finger-printing applications, the ability of provenancing dust makes use of the fact that the Nd, Sr and Pb isotope ratios are different in mantle- versus crustal-derived rocks. The example presented here is taken from Greenland's ice-sheet which was found to have quite variable lead contents. One peak coincided with the period between ca. 150 B.C. and A.D. 50 during the Roman era (Rosman, 1998). The lead isotope composition actually measured in that interval of the ice core demonstrated a good match with lead mined at Rio Tinto in Spain. As this mine is known to have been processed by the Romans it can be concluded that air-borne lead was transported north-wards from Spain and finally

reaching Greenland. Another peak in the lead concentration record, representing about 25-50 times higher Pb concentrations, characterizes the period between ca. 1930 and 1980 and is readily interpreted as a contamination effect of leaded petrol.

Anthropogenic Pb in petroleum and other pollutants

The ALAS model is an important tool for estimating the age of hydrocarbon release (Hurst, 2000). It is based on systematic increases in lead isotope ratios in petrol caused by shifts in sources of lead ores used by the petroleum industry in North America. The ALAS calibration curve relies on isotope measurements of soils and water of known age, affected by petroleum products, and isotope data of the hydrocarbon products themselves. Due to an increasing usage of radiogenic MVT type of ores in leaded petrol, age uncertainties are as low as a few years. An application of this model is to correlate environmental releases of e.g. diesel and motor oil to their sources, and anthropogenic gasoline-derived lead has been mapped for many areas in the U.S.

Numerous studies have been devoted to metal dispersions from mine sites. Pb isotopes is an ideal tool as lead occurs in detectable amounts in most ore-forming environments, whilst the parent elements U and Th typically occur in amounts that is negligible in most provenance studies. Even if the U and Th contents are relatively high in a studied system, the slow decay of these elements to form stable lead isotopes means that for young systems, like those affected by anthropogenic processes, this is not a problem. MacKenzie and Pulford (2002) investigated to what degree former activities at a mine site at Tyndrum, Scotland, could be detected in the environment. Samples of mining wastes, river sediments and peat cores were analyzed. Pb concentrations were high in e.g. river sediments near the mine, but the concentrations decreased markedly downriver from the mining site. Based on obtained Pb isotope data, the main source of lead in the studied samples could be coupled with the mining operations, although a certain influence of local bedrock geology and of leaded petrol could also be detected.

References

- Beard, B.L. and Johnson, C.M. (2000). *J. Forensic Sci.* 45, 1049-1061.
- Boni, M., Dima, G., Frei, R. And Villa, I.M. (2000). *Archeometry* 42, 201-208.
- Degryse, P., Schneider, J., Haack, U., Lauwers, V., Poblome, J., Walkens, M. and Muchez, Ph. (2006). *J. of Arch. Science*, 33, 494-501.
- Doe, B.R. and Zartman, R.E. (1979). Plumbotectonics. In: "Geochemistry of hydrothermal ore deposits". H.L.Barnes. ed. Wiley, 22-70.
- Faure, G. and Mensing, T.M. (2005). *Isotopes: Principles and Applications*. John Wiley & Sons. 897 pp.
- Fowler, B. (2000). *Ice man: Uncovering the life and times of a Prehistoric man found in an Alpine glacier*. New York, N.Y. Random House, 138 pp.
- Goldstein, S.J. and Jacobsen, S.B. (1988). Nd and Sr isotopic systematics of river suspended material: implications for crustal evolution. *Earth Planet. Sci. Lett.* 87, 249-265.
- Grousset, F.E. and Biscaye, P.E. (2005). Tracing dust sources and transport patterns using Sr, Nd and Pb isotopes. *Chemical Geol.* 222, 149-167.
- Hurst, R.W. (2000). Applications of anthropogenic lead archaeostratigraphy (ALAS model) to hydrocarbon remediation. *Environ. For.* 1, 11-23.
- Kelly, S., Heaton, K. and Hoogewerff, J. (2005). Tracing the geographical origin of food: The application of multi-element and multi-isotope analysis. *Trends in food science and technology*, 16, 555-567.
- Kosler, J. and Sylvester, P.J. (2003). Present trends and the future of zircon in geochronology: laser ablation ICP-MS. In: "Zircon", J.M. Hanchar and P.W.O Hoskin, eds. *Reviews in Mineralogy and Geochemistry* 53, 243-275.
- Libby, W.F. (1946). Atmospheric helium-three and radiocarbon from cosmic radiation. *Phys. Rev.*, 69, 671-672.
- MacKenzie, A.B. and Pulford, I.D. (2002). Investigations of contaminant metal dispersal from a disused mine site at Tyndrum, Scotland, using concentration gradients and stable Pb isotope ratios. *Applied Geochem.*, 17, 1093-1103.
- Montgomery, J., Evans, J.A. and Wildman, G. (2006). ⁸⁷Sr/⁸⁶Sr isotope compositions of bottled British mineral waters for environmental and forensic purposes. *Applied Geochemistry* 21, 1626-1634.
- Nakai, S., Halliday, A.N., Kesler, S.E. and Jones, H.D. (1990). Rb-Sr dating of sphalerites from Tennessee and the genesis of Mississippi Valley type ore deposits. *Nature* 346, 354-357.
- Pointing, M., Evans, J.A. and Pashley, V. (2003). Fingerprinting of Roman mints using laser ablation MC-ICP-MS lead isotope analysis. *Archeometry*, 45, 591-597.
- Qu, X., Zenqian, H., Li, Y. (2004). Melt components derived from a subducted slab in late orogenic ore-bearing porphyries in the Gangdese copper belt, southern Tibetan plateau. *Lithos*, 74, 131-148.
- Recio, C. (2008). Alike as two water drops: distinguishing one source of the same substance from another.
- Rummel, S., Rossmann, A., Hölzl, S. and Horn, P. (2006). Determination of fruit juices origin by using multi-element stable isotopes. *Geophysical Res. Abstr.* 8, 08094.

- Stacey, J.S. and Kramers, J.D. (1975) Approximation of terrestrial lead isotope evolution by a two-stage model. *Earth Plan..Sci. Lett.* 26, 207-221.
- Stein, H.J., Morgan, J.W. and Scherstén, A. (2000). Re-Os dating of low-level highly radiogenic (LLHR) sulfides: The Harnäs gold deposit, south-west Sweden, records continental-scale tectonic events. *Econ. Geol.* 95, 1657-1671.
- Van Duivenvoorde, W. (2008). The Batavia shipwreck: an archaeological study of an Early seventeenth-century Dutch east Indiaman. Ph.D. thesis. Texas A&M University, 246 pp.
- Wilson, M. (1989). *Igneous Petrogenesis*. Chapman & Hall, pp .466.
- Zeichner, A., Ehrlich, S., Shoshani, E. and Halicz, L. (2006). Application of lead isotope analysis in shooting incident investigations. *Forensic Science International* 158, 52-64.

Analytical techniques applied to fluid inclusion studies: basics and applications

Salvador Morales Ruano

Departamento de Mineralogía y Petrología, e Instituto Andaluz de Ciencias de la Tierra. Universidad de Granada-CSIC. Facultad de Ciencias. Avenida Fuentenueva, s/n. Granada, 18002. España.

Introduction¹

Fluid inclusions are small amounts of fluid trapped inside minerals. This fluid is "custodian" of the physicochemical properties of the mother fluid and, therefore, it can be seen that this fluid "bottled" inside the crystal is a relic which preserves a faithful record of the physical and chemical conditions of the fluid that was in the environment at the time of the fluid inclusion's formation. Unlike other geothermometric/geobarometric methods, that require indirect calculations (for example, phase equilibriums between minerals, etc.), the study of fluid inclusions allows direct estimates of the original fluid's characteristics to be made, in such a way that characterization of the physical-chemical properties of fluids trapped in the fluid inclusions shows us the characteristics of the mineralizing fluids, in terms of temperature, pressure, composition, density, etc.

Fluid inclusions can be found in any mineral that was formed from a fluid. Because in practice most minerals are formed from processes involving fluids, the study of these tiny remnants of fluid, trapped in the minerals, could be applied to almost any field of geology. Therefore, although in practice fluid inclusions are used mainly in studies related to the metallogeny of mineral deposits due to its applied character, this type of study is becoming increasingly frequent in different areas of geology and in some related

¹ This text is only a summary of the talk that will be given at this workshop. The text does not aim to be a review of the state of the art or a new text about the world of fluid inclusions. For this purpose readers can consult a wide-ranging, interesting bibliography that covers these topics (i.e., Barnes, 1979; Hollister and Crawford, 1981; Roedder, 1984; Shepherd et al., 1985; de Vivo and Frezzotti, 1994; Goldstein and Reynolds 1994; Samson et al., 2003; etc.).

sciences. Solely by way of an example, we can say that these studies have been implemented in:

- * ore deposits
- * hydrothermal environments
- * sedimentary environment and diagenetic processes
- * metamorphic terranes with different metamorphic grades
- * volcanic areas
- * mantle environments
- * petroleum exploration
- * tectonic history of deformed areas
- * gemology
- * paleoclimatology
- * paleohydrogeology
- * extraterrestrial environments
- * weathering of historical monuments
- * analysis of air-inclusions in ice cores
- * ambar
- * etc.!

The reasons why studies of fluid inclusions are becoming increasingly common must be sought at the confluence of a number of factors:

* Microthermometry is a cheap technique: for the price of a small quantity of nitrogen, a high number of results can be obtained (though it is a very subjective estimation, we calculate that with 5-10 euro of liquid nitrogen, determinations corresponding to 10-20 fluid inclusions can be carried out).

* The equipment is relatively cheap in comparison with other analytical techniques: a heating and freezing stage should not cost more than about €30,000 (aprox.). This means that the majority of geology departments at research centres (and many companies) have a fluid inclusion laboratory.

* Sample preparation laboratories do not require special equipment: any laboratory in a university geology department or company that deals with the preparation of common

thin sections can prepare the doubly polished thin sections that are required for the study of fluid inclusions.

* The interpretation of results is done with relative “ease”.

* Any determination "only" requires an observer (... with plenty of patience!).

These factors explain why fluid inclusion studies are currently being applied in an ever more routine fashion in numerous studies related to Mineralogy and other Earth Sciences. As a sign of this boom, the indicators can be analyzed:

(1) At present there are three conferences dedicated specifically to the world of fluid inclusions: PANCROFI (“Pan-American Current Research on Fluid Inclusions Conference”), which held its 9th edition in June 2008; ECROFI (“European Current Research on Fluid Inclusions”), which will be celebrating its 20th edition in 2009, and ACROFI (“Asian Current Research on Fluid Inclusions”) that celebrates its 2nd edition in November, 2008. Likewise, numerous international congresses dedicate monographic sessions to presenting the most recent advances related to geofluids and the world of fluid inclusions.

(2) An abundance of literature is generated in this regard. Not only are there many monographic books devoted to study of fluid inclusion, but the majority of recent textbooks include detailed chapters on fluid inclusions and their application in different fields of science. Likewise, the majority of the scientific magazines on geosciences include numerous papers featuring fluid inclusions. In the same sense, Internet also provides numerous websites on the subject (see examples in Table 1) and there is even a fluid inclusion listserver (fluid-inclusions@lists.wisc.edu, see <http://www.geology.wisc.edu/flincs/fi.html> for details) with more than 350 users dedicated to this subject matter.

(3) There are an enormous number of research groups worldwide, dedicated to the study of fluid inclusions.

(4) Most geology departments offer courses that, to one degree or another, include matters related with fluid inclusions.

Description	Website Address
Fluid inclusion database project	http://www.ga.gov.au/minerals/research/methodology/geofluids/flincs_about.jsp
Fluid inclusion laboratory Leoben	http://fluids.unileoben.ac.at/Home.html
Fluid inclusion laboratory Leoben	http://institute.unileoben.ac.at/mineralogie/Fluid_Inc_Lab/Flinc_Lab.html
Fluid inclusion research at National University of Ireland	http://www.nuigalway.ie/nanoscale/fluid_inclusion.html
Fluid inclusion section of the Duan Group	http://www.geochem-model.org/research/fluidinc/
Geowissenschaftliches Zentrum (Prof. Van den Kerkhof)	http://www.uni-goettingen.de/en/11113.html
Links for mineralogist (fluid inclusions)	http://www.mineralogie.uni-wuerzburg.de/links/petrology/fluid.html
Personal web site Ronald J. Bakker	http://institute.unileoben.ac.at/mineralogie/Bakker/Ronald.html
Petroleum & aqueous inclusion research	http://www.petroleuminclusion.uhp-nancy.fr/
Siena geofluids lab home page	http://www.dst.unisi.it/geofluids-lab/
The world of fluid inclusions	http://www.geology.wisc.edu/flincs/fi.html
University of Bern (Fluid Inclusion group)	http://www.geo.unibe.ch/diamond/diamond.php
Virginia Tech Geosciences/ Fluids Research Group	http://www.geochem.geos.vt.edu/fluids/
Working group on inclusions in minerals (WGIM)	http://www.ima-mineralogy.org//com-wg/WGIM/WGIM.html

TABLE 1. Description and addresses of some websites related to fluid inclusions.

General topics on fluid inclusions²

Fluid inclusions are small cavities inside crystals. These cavities capture remains of fluid from which minerals are formed, or fluids that have circulated through the same

² Many topics of this chapter are summarized from general books on fluid inclusions (see references at footnote 1).

ones after its formation. They are typically smaller than 30-50 microns and can contain different combinations of liquid, solid or gaseous phases. The *liquid phase* is usually constituted by water with different ions in solution (Ca(II), Na(I), K(I), Mg(II), etc.), mostly as chlorides. The *gaseous phase* is constituted by water vapour and, occasionally, varying amounts of CO₂ and, to a lesser extent, N₂, CH₄ or H₂S. The *solid phase* can be divided into two types: phases formed by saturation of salts in the liquid phase (halite, sylvite...) or trapped phases from the environment at the time of formation of fluid inclusions that remain in equilibrium with the phases present in the cavities (generally oxides, sulphides or silicates).

Fluid inclusions are expected in all those minerals which are formed in environments that involve fluids, i.e. they are expected in a large number of minerals formed in nature. The problem for this study is its observation. To this end, we use minerals with sufficient transparency for internal observation. Among transparent minerals, quartz, calcite, dolomite, fluorite and sphalerite are the most common. In the case of opaque minerals, fluid inclusions are also present but their observation is practically impossible, at least in a routine manner. Occasionally, in areas of weakness (fractures, foliations...) of some opaque crystals or in areas of slimmed edges, it is possible to see the presence of fluid inclusions intuitively. In the case of opaque ores, some attempts have been made with infrared microscopy (see details below), although positive results are limited to a few cases.

The criteria used to classify fluid inclusions are very varied (morphology, number of phases at room temperature, chronology with respect to host mineral...).

The first one of them classifies fluid inclusions according to their shape (polyhedral, irregular, oblate...) and does not contribute a lot of genetic information.

Classification based on the number of phases (one-phase, two-phase, three-phase, multiphase) gives rise to a more informative classification about the genesis of fluid inclusions. In a first approximation, single-phase fluid inclusions could be indicative of low temperature processes, coexistence of fluid inclusions with varying degrees of filling (filling degree = ratio of liquid volume vs. gas volume in the cavity) could suggest boiling processes or presence of immiscible fluids, while the abundance of three-phase inclusions including precipitated minerals (halite, sylvite...) indicates saturation in salts, etc.

As for chronological classification, this classifies fluid inclusions as primary (trapped at the same time as the formation of host mineral), secondary (trapped after the formation of the host crystal) and pseudosecondary (fluid inclusions caught in intermediate situations between the primary and secondary ones).

In practice, such rigid classifications are not always useful for daily work in the laboratory. They really impose the criterion of *population*, which groups fluid inclusions of the same characteristics according to a combination of the above criteria (size, shape, number of phases and proportions between them, "age" with regard to host crystals...). Populations must be related with regard to geological context and inside the paragenetic sequence (in terms of mineralization stages, fracturation or folding events, etc.), so that they are representative of the geological process, object of study.

Petrographic study of fluid inclusions

Any study of fluid inclusions must begin with careful petrographic study of the different populations of fluid inclusions, in such way that the fluid inclusions analyzed truly represent the characteristic fluid of the process that we want to characterize. It is frequent that a mineral has been formed in a specific environment (and, as a consequence, caught part of the fluid from which it is formed) and, subsequently, being subjected to various processes, not only traps fluids from these later processes, but even fluid trapped originally can be affected and modified with regard to the conditions of trapping (for example, Roedder, 1984; Shepherd et al., 1985; Goldstein and Reynolds, 1994). This means that the fluid inclusions that can be observed in a crystal can be the result of different fluids with which the crystal has interacted throughout its history. Therefore, to ensure the representativeness of the study in question, we must conduct a proper petrographic study that selects the representative inclusions and avoids the temptation of focusing solely on the more aesthetically beautiful, best-formed or larger fluid inclusions.

The petrographic study usually takes place with a petrographic microscope that, according to the case in question, can be equipped with a camera for microphotographs or a video recorder that allows an adequate documentation of the results of the study. Nevertheless, the use of the cathodoluminescence (see for example Van den Kerkhof and Hein, 2001) equipment is becoming ever more frequent (mounted on optical

microscopes or placed in scanning electron microscopes), which "reveal" the internal structure of crystals, a structure that is not always appreciated with the polarized light microscope. Cathodoluminescence is an effect that occurs as result of electron bombardment on a solid. Amongst other effects, this can produce the emission of light in the focused area. This effect can be determined by chemical factors or as consequence of aspects related with the structure of the mineral. In transparent minerals, this effect can be used to study their internal structure. Specifically in terms of the petrography of fluid inclusions' host crystals, this technique may be useful to reveal zoned growths, dissolution/recrystallization processes, interruptions or discontinuities in the growth of the crystal, etc. The use of cathodoluminescence has, amongst other advantages, low cost, ease of use, use of the same slides used for optical petrography, the possibility of studying with the same microscope used for the polarized light study, and the chance to change the mode of observation without moving the same motive in the same sample (allows instantaneous correlation of the image of transmitted light with the image of cathodoluminescence).

Certain minerals that behave as opaque in observation using transmitted light microscopy become transparent once observed by means of a microscope equipped with an infrared emission source. In accordance with Wilkinson (2001) and references therein, with infrared microscopy and in favourable circumstances it is possible to observe the internal structure (zoning, maclas, etc.) of the host mineral, or it can even be possible to carry out the microthermometric study of fluid inclusions hosted in some opaque minerals (for example, wolframite, stibnite, molybdenite, hematite, pyrrargyrite, cinnabar, chalcocite, enargite, tetrahedrite-tennantite, pyrite, etc.).

As a result of the petrographic study of fluid inclusions using these different techniques, the petrographic study must provide information about populations of fluid inclusions (number, types, relative chronology -between them, with regard to geological events-, etc.). In short, the importance of the petrographic study is that it should be the basis for proper decision-making about the type of fluid inclusions on which the later job is done.

Analytical techniques applied to the study of fluid inclusions

The purpose of fluid inclusion studies is the characterization of the physicochemical properties of fluids trapped in the cavities under study. This characterization usually tries to discover the conditions of temperature, pressure and composition of the original fluids (the latter can involve different aspects: total salinity of the inclusion, proportion among major cations, kind of volatiles –if present-, presence of organic liquids, etc.).

In any case, to obtain this information it is necessary to use a combination of techniques, which can vary from simple petrographic observation to the use of more complex and sophisticated analytical techniques. However, given the small size of fluid inclusions (usually smaller than 30-50 microns), the most common technique is microthermometry. The information obtained from the microthermometric characterization of fluid inclusions is usually the basis for deciding to utilize, where appropriate, other more sophisticated analytical techniques.

Microthermometry^{3,4}

The microthermometric study of fluid inclusions is done using a heating and cooling stage, a device that allows us to increase or diminish temperature over a wide range, between -200°C and $+600^{\circ}\text{C}$ approximately. This stage is placed on a microscope, so that the phase changes occurring can be observed as well as the temperature at which these changes take place. For this purpose, thin sections used in fluid inclusions studies are polished on both sides and are thicker ($\approx 100\text{-}200$ microns) than the thin sections used in conventional petrographic studies (≈ 30 microns).

As a normal working protocol, the fluid inclusions are cooled to the lowest temperature that the stage can achieve and, subsequently, the phase changes taking place are observed while the temperature rises towards room temperature again. The first change of phase that should be observed in the liquid phase is the appearance of the first

³ This technique is very common and is widely described in any of the general books that are included in the section of bibliographical references (for example, Roedder, 1984; Shepherd et al. 1985; De Vivo & Frezzotti, 1994; Goldstein & Reynolds, 1994, etc.). To avoid being repetitive, this section is only a brief summary and readers interested in more information are submitted to any of the above mentioned books.

⁴ See also exercise included in appendix 1 about microthermometric data treatment, especially useful for beginners.

liquid in the cavity (eutectic temperature). This temperature is characteristic of each system and, therefore, allows us to associate the composition of the fluid inclusion with a chemical system. Table 2 summarizes some of the most common chemical systems found in natural fluids as well as their eutectic temperatures. In regard to the gaseous phase, the first change that should be observed during heating is the melting of CO₂ -or other gases that could be present in the cavity-. Table 3 includes some microthermometric characteristics of the most frequently occurring volatiles in nature. Later, other phase transitions may be observed in the liquid phase, in the vapour phase or at the interphase region (melting of the last crystal of ice, melting of hydrohalite or other salt hydrates, melting of clathrates, homogenization of CO₂, etc.). Using the temperatures observed for these phase transitions, and with adequate diagrams, we can estimate the salinity, types and contents of the volatiles, etc.

Later, the inclusions are heated from room temperature to the temperature at which homogenization of the cavities occurs. This temperature is known as the homogenization temperature and represents the minimum trapping temperature for the fluid inclusion. To determine the P-T trapping conditions, it is necessary to calculate the isochore corresponding to the fluid inclusion. In a space P-T, this isochore determines a straight line, for which it can be said that: (1) its slope is a function of the density of the fluid inclusion; (2) the homogenization temperature is the minimum value of the aforementioned straight line; (3) the line contains the trapping P-T, although with unknown coordinates until the present time. To determine the trapping P-T, it is necessary to use an independent geothermometer/geobarometer or any of the procedures described in the relevant literature (see for example chapter 7.6 of Shepherd et al., 1985).

Using different data input (microthermometric data, micro raman data, cation ratios, volume fraction estimations, etc.), several computer packages make extensive calculations related with fluid inclusions (isochores, bulk density, molar volume, salinity, composition of fluid inclusion, etc.). In this sense, the most popular could be FLINCOR (Brown, 1989), MacFlinCor (Brown & Hagemann, 1994), CLATHRATES (Bakker, 1997) or FLUIDS (Bakker, 2003). See also Bakker & Brown (2003) for more details about these software packages, and the website <http://institute.unileoben.ac.at/mineralogie/Bakker/Programs/Computer.html> for latest updates.

Chemical system	Eutectic temperature
H ₂ O-NaCl-CaCl ₂	-52.0°C
H ₂ O-CaCl ₂	-49.5°C
H ₂ O-NaCl-FeCl ₂	-37.0°C
H ₂ O-FeCl ₂	-35.0°C
H ₂ O-NaCl-MgCl ₂	-35.0°C
H ₂ O-MgCl ₂	-33.6°C
H ₂ O-NaCl-KCl	-22.9°C
H ₂ O-NaCl	-20.8°C
H ₂ O-KCl	-10.6°C

TABLE 2. Eutectic temperature for the most frequent naturally occurring salt system (simplified from Shepherd et al., 1985).

Species	T _{triple} (°C)	T _{critical} (°C)	Raman frequency (cm ⁻¹)
N ₂	-210.0	-147.0	2331
CO ₂	-56.6	31.1	1285
CO ₂	-56.6	31.1	1388
CH ₄	-182.5	-82.1	2917
H ₂ S	-85.5	100.4	2580 (liquid)
H ₂ S	-85.5	100.4	2590 (in water)
H ₂ S	-85.5	100.4	2611

TABLE 3. Temperature of the triple point, critical temperature and Raman frequency for common volatiles in fluid inclusions (summarized from Shepherd et al., 1985; Burke, 2001 and Diamond, 2003).

Use of other study techniques

In the majority of fluid inclusion studies, a microthermometric characterization is sufficient to identify the fluids that could have intervened in the genesis of the fluid inclusions and to characterize their conditions of formation, which is the usual aim of this type of studies.

Based on the results from microthermometric analysis, the decision to use other study techniques will be conditioned by several factors. The most important thing is to decide whether additional information about the characteristics of certain phases is needed (characterization of volatile, solute contents, etc.). Depending on economic availability, technical means or instruments available and, above all, depending on the interest in carrying out additional characterization of certain phases, we can use different analytical techniques. In this sense, any analytical technique might be appropriate. However, we must bear in mind that the main limitation of any chemical study of fluid inclusions is the small size of the cavities to analyze. The list of techniques that have been used for this purpose is very large, although some of them have only been used occasionally or with little success. Table 4 summarizes some of these techniques. Later are described some of them.

Raman microprobe

According to Burke (2001) and Burruss (2003), the Raman scattering is a consequence of inelastic collisions of a beam of light with vibrating polyatomic molecules or molecular groups (for example, fluid in an inclusion). These collisions cause energy changes to specific energy states of the molecule, which, in turn, correspond to the mode of vibration of each type of bond in a molecule. Selection rules explain whether a vibrational mode is infrared and/or Raman active (Raman and infrared adsorption spectroscopy are complementary analytical techniques ideal for the study of molecular species in fluid inclusions). Raman scattering is a weak effect (only about 10^{-8} of the incident photons). Thus, an intense light source is needed to illuminate the sample. A monochromatic laser beam is normally used. Using a monochromator and adequate filters to separate and measure the Raman scatter from the elastically scattered light, we can obtain a Raman spectrum. With this spectrum we can study the position and the intensity corresponding to the energies of the vibrational modes of the different species in the sample.

In the case of fluid inclusions, Raman analysis can be quantitative or qualitative. Identification of the phases is based on the position of the peaks of the spectra obtained by the Raman microprobe and quantification is done according to their relative intensity.

Study of fluid inclusions with a Raman microprobe is carried out with three main purposes:

(1) Study of the gaseous phases present in the gas bubble. Of the gaseous phases, the most common are the presence of carbon dioxide, nitrogen, methane or dihydrogen sulphide, with typical bands ($\Delta\nu$ in cm^{-1}) at 1285 and 1388 $-\text{CO}_2-$; 2331 $-\text{N}_2-$; 2917 $-\text{CH}_4-$ and 2580 and 2611 $-\text{H}_2\text{S}-$ (Burke, 2001). From the peak areas it is possible to establish the relative proportion between the volatile phases. If the equipment is properly calibrated, from this information the corresponding molar fractions of every gas can be calculated.

(2) Identification of the solid phases that are trapped as minerals or precipitated minerals. Among them the most frequent are sulphates and carbonates, and less frequent, silicate, native sulphur, or hematite. They are usually identified using databases with spectra of reference. Nevertheless, the databases are not fully developed for a range of reasons (Burke, 2001): (A) Many minerals (e.g., NaCl and KCl, very important for fluid inclusions) have only weak Raman spectra, or no spectra at all – due to type of bonds. (B) The laser beam causes important differences in the spectra (in peak intensities - and also position) and with the orientation of the crystal. (C) In solid solutions, the peak position depends on the chemical composition of the mineral.

(3) On occasions, using cryogenic equipment attached to a Raman microprobe, it is also possible to use Raman for analyzing the solid phase that originates on freezing the liquid phase of the fluid inclusion. In this case, the aim is usually to identify salt hydrates that are formed by subjecting the fluid inclusions to freezing. The Raman microprobe is a powerful tool for identifying the stoichiometric hydrates that crystallize upon cooling, being able to obtain Raman spectra for hydrates of geological interest (for example, $\text{NaCl}\cdot 2\text{H}_2\text{O}$; $\text{CaCl}_2\cdot 6\text{H}_2\text{O}$; $\text{MgCl}_2\cdot 6\text{H}_2\text{O}$;

NONDESTRUCTIVE ANALYSIS*Qualitative and semiquantitative*

- | | |
|--|----|
| - Visible light microscopy | |
| - Cathodoluminescence microscopy | CL |
| - Ultraviolet microscopy (Ultraviolet fluorescence microscopy) | UV |
| - Infrared microscopy | IR |
| - IR absorption spectrometry (Fourier transform IR microspectrometry) FTIR/FTIRM | |
| - Microthermometry (sometime, with infra-red microthermometry) | |

Semiquantitative and quantitative

- | | |
|---|---------|
| - Laser Raman microprobe (or Laser Raman spectroscopy) | LRM/LRS |
| - Electron probes: | |
| Scanning electron microscopy and energy dispersive spectrometer | SEM-EDS |
| Electron microprobe | EPMA |
| Transmission electron microscopy | TEM |
| - Nuclear/ionic probes: | |
| Proton-induced X-ray emission (+/-Rutherford backscattering spectrometry) | |
| PIXE (RBS) | |
| Proton-induced gamma rays | PIGE |
| Elastic recoil detection analysis | ERDA |
| - X-ray probes: | |
| Synchrotron X-ray fluorescence | SXRF |
| Extended X-ray absorption fine structure | EXAFS |
| - Nuclear magnetic resonance/Proton magnetic resonance | NMR/PMR |

TABLE 4. Different techniques used for analysis of fluid inclusions (from Roedder, 1990, and modified with data from Samsom et al. 2003 and from this summary).

DESTRUCTIVE ANALYSIS

Analysis of the gas phase

- Gas chromatography (sometime, combined with mass spectrometry) GC (or GC-MS)
- Laser microprobe mass analyzer or laser induced mass analyzer LAMMA/LIMA
- Mass spectrometry (Quadrupole mass spectrometry) MS (QMS)

Analysis of the solutes in the liquid phase

- Atomic absorption spectrometry AAS
 - Flame-atomic emission spectroscopy FAES
 - Ion chromatography IC
 - Atomic-emission spectroscopy AES
 - (Laser ablation) inductively-coupled plasma mass spectrometry (LA-)ICP-MS
 - (Laser ablation) inductively-coupled plasma optical emission spectroscopy (LA-)ICP-OES
 - Instrumental neutron activation analysis INAA or NAA
 - SEM and cryogenic SEM (with energy dispersive analysis) (Cryo) SEM-EDS
 - Ion probe (secondary ion mass spectrometry) SIMS
- Also reported: thin-film anodic stripping voltammetry, coulometry, radiometry, emission spectroscopy, spectrophotometry, potentiometry -with ion-specific electrodes-, fluorimetry ...

Analysis of inclusion solids

- Scanning electron microscopy and energy-dispersive spectrometry SEM-EDS
- Electron diffraction ED
- X-ray diffraction (+/- using the Gandolfi camera technique) XRD

TABLE 4 (cont.). Different techniques used for analysis of fluid inclusions (from Roedder, 1990, and modified with data from Samsom et al. 2003 and from this summary).

MgCl₂·12H₂O; FeCl₃·6H₂O; KCl·MgCl₂·6H₂O) with sufficient quality in order to determine them in natural fluid inclusions (Dubessy et al., 1982). The salt hydrates can be used to determine the salinity of the solutions. Ni et al. (2006) demonstrates that hydrohalite has a positive correlation to salinity (i.e. the mass of hydrohalite increases with increasing salinities and decreasing mass of ice), being another effective way to

obtain the salinity of fluid inclusions. Thus, both the height and area ratios of hydrohalite 3423 cm^{-1} and 3405 cm^{-1} peaks against the ice 3098 cm^{-1} peak, and the total area ratios of hydrohalite peaks against ice 3098 cm^{-1} peak can be used to estimate the salinity of fluid inclusions.

Analysis of individual fluid inclusions

As has been shown above, fluid inclusions could contain fluids that have been trapped at different moments in the "life" of the host crystal. This gives rise to the existence of different populations of fluid inclusions. It is very common for a crystal not to contain a unique type of fluid. Instead it will reflect, to varying degrees, the different fluids characterizing the various processes that the fluid inclusion host crystal has undergone, from its formation up to the moment of observation. In addition, fluid inclusions may have suffered processes of re-equilibration during the evolution after their trapping. As a consequence, it becomes more and more frequent that, depending on the precision level decided according to the aims of the study proposed, characterization of the composition of fluid inclusions to bulk sample scale is not sufficient and the properties of individual fluid inclusions must be determined.

For this proposal, a number of specific techniques, capable of analyzing individual fluid inclusions in a "point" form, can be found in specialized literature. Among these techniques, we can nowadays emphasize the laser ablation (LA) group (destructive techniques), and the microprobes group (non-destructive techniques).

In relation to the first group, Fabre et al. (1999) explain that LA can be based on ICP-MS (inductively coupled plasma mass spectrometry) or on optical emission spectroscopy (OES). Both techniques are coupled with LA at microscopic scale to extract the liquid to be analyzed within the fluid inclusions. According to the same authors, LA-ICP-MS could be more adequate for determination of trace elements and LA-ICP-OES gives better detection limits results for major elements, especially Na and Ca. The limitations of LA-ICP-AES⁵ arise from the lack of sensitivity of AES for some elements and the difficulty in determining absolute concentrations of components in the fluid inclusions

⁵ LA-ICP-AES and LA-ICP-OES (AES: atomic emission spectroscopy; OES: optical emission spectroscopy) could be considered the same technique.

(Wilkinson et al. 1994). Also, detection limits (Günter et al., 1998) are higher for LA-ICP-AES (in the $\mu\text{g g}^{-1}$ to mg g^{-1} range) than for LA-ICP-MS (in the ng g^{-1} to $\mu\text{g g}^{-1}$ range). As a consequence, LA-ICP-MS is more frequently used today.

Gagnon et al. (2003) indicate different advantages for LA-ICP-MS techniques: low capital cost, ease of use, ability to obtain data from depth fluid inclusions, etc. In addition, these authors point out the minimal sample preparation, the possibility of obtaining quantitative analysis of individual fluid inclusions, the high spatial resolution (down to $2\mu\text{m}$), the high sensitivity (less than $\mu\text{g/g}$), moderate/high precision (5-30%), and the possibility of obtaining rapid multielement analysis over wide mass (6-240 amu) and dynamic (up to 11 order of magnitude) ranges, etc. In contrast, Gagnon et al (2003) indicate some weaknesses to overcome in the future: internal standardization, correction of host mineral contribution to the fluid inclusion signal, elimination of spectral interferences, etc.

Günter et al. (1998) explained a stepwise opening procedure for a controlled ablation (a small hole is drilled for the partial release of liquid and vapour, followed by complete drilling using a pit covering the entire inclusion) in order to avoid the explosion and splashing of material, with the consequent loss of solid internal precipitates. Gagnon et al. (2003) propose an alternative strategy for ablation, consisting in a traversed opening. The method consists of traversing the sample surface until the laser beam is over the top of the fluid inclusion and then allowing the laser beam to drill into the inclusion. In practice, the most adequate procedure for ablation depends on each sample and some preliminary essays must be done prior to analyzing fluid inclusions.

Günter et al. (1998) also explained the procedure for quantification of element concentrations. Element ratios calculated from integrated intensity are calculated from the elements ratios via an internal standard element, whose concentration was determined prior to ablation (in this case, concentration of Na determined using microthermometric measures). A complete description for quantification of element concentration can be found at Gagnon et al. (2003). These authors analyze several alternatives for calibration standard (including NIST and USGS synthetic glasses, synthetic fluid inclusions, desolvated solution standards, microcapillaries, microwells or fluid inclusion analogues) and for measurement of internal standards.

Gagnon et al. (2003) also include an example in which concentration units are obtained from raw data using readily available commercial spreadsheets and spectral analysis software.

Regarding the microprobes group, Anderson & Mayanovic (2003) made an extended review of electron, nuclear and X-ray microprobes. In this review, the techniques using an electron microbeam for analysis of fluid inclusions are divided into three types:

(1) Scanning electron microscopy: used for identification or semiquantitative analysis of daughter minerals (in combination with energy dispersive analysis), for analysis of decrepitated mounds, or for analysis of frozen fluid inclusions (in combination with a cryogenic stage).

(2) Electron microprobe: used for semiquantitative analysis of unopened fluid inclusions, limited by the electron beam's shallow level of penetration.

(3) Transmission electron microscopy: used mainly for morphological studies.

According to Ryan (1999), nuclear microprobe techniques can be divided into PIXE (Particle-Induced X-ray Emission), PIGE (Proton-Induced Gamma-ray Emission) and ERDA (Elastic Recoil Detection Analysis) for the purpose of analyzing fluid inclusions. PIXE provides detection limits around 40 ppm for different elements and is useful for elements ranging from Cl to U (with the exception of rare earth elements). PIGE is particularly used for lighter elements (Li, B, F, Na, Mg and Al) and ERDA for H analysis. In addition, RBS (Rutherford Backscattering Spectrometry) coupled with PIXE provides the geometrical information needed for quantitative elemental analysis (Strivay et al., 2008).

With respect to x-ray probes, synchrotron X-ray fluorescence (SXRF) and x-ray absorption fine structure (XAFS) have been used to analyse fluid inclusions (for example, Anderson & Mayanovic, 2003; Cauzid et al. 2006) providing minimum detection limits of a few ppm for many metals.

As Anderson & Mayanovic (2003) indicate, electron microprobe analyses are semiquantitative but these techniques are accessible to many researchers. In contrast, nuclear and X-ray microprobe analyses are quantitative, but laboratories equipped with these techniques and suitable for fluid inclusion analyses are very limited at present.

Conclusions

The study of fluid inclusions is a highly useful tool for analysing the physicochemical properties of the fluids involved, not only in mineralising processes but also in many geological processes involving fluids. Their detailed study requires an approximation to the problems using different analytical techniques, but this is often sufficient only with a suitable microthermometric characterization. For other investigations with more ambitious objectives, the portfolio of analytical techniques that are available nowadays is quite extensive, ranging from simple techniques commonly used within the majority of research laboratories to complex techniques that are difficult to access. Likewise, advances in the development of new analytical techniques and their application to the study of fluid inclusions, especially in the quantitative study of individual fluid inclusions, is taking place at a frantic pace, so that "barriers" are quickly broken and "borders" take less and less time to be crossed. The use of these techniques depends, therefore, on both the requirements of each specific study and on the economic resources or the facilities for access to instrumentation available to each researcher. However, the future is coming: what will it have to offer us?.

Acknowledgements

This work arise from the knowledge and experience acquired over years of field and laboratory work. This experience arises from numerous contacts with colleagues from different research institutions as well as from the extensive literature that exists in this regard. For the training received I am grateful, both to the people with whom I have conversed directly, and to those with whom I have "only" communicated through their written texts. I have also learned a great deal from peoples that I teach, specially my students, and from the colleagues with I share my research, both geologist and chemists. To all of them, my sincere thanks and my apologies for any mistakes. Financial help from different research projects also contribute this experience (for example, CGL2006-02594BTE, Ministry of Education and Science and FEDER, and "Proyecto de Excelencia" RNM-736, Junta de Andalucía, both nowadays in force). Their contributions are greatly appreciated. I am very grateful to Jim Daniell for reviewing the English version.

References

- Anderson, A.J. and Mayanovic, R.A. (2003). Electron, nuclear and x-ray probe analysis of fluid inclusions. In: "Fluid inclusions: analysis and interpretation", I. Samson, A. Anderson and D. Marshall, eds. Mineralogical Association of Canada, short course series, vol. 32, 323-351.
- Bakker, R.J. (1997). *Computers & Geosciences*, 23, 1-18.
- Bakker, R.J. (2003). *Chem. Geol.*, 194, 3-23.
- Bakker, R.J. and Brown, P.R. (2003). Computer modeling in fluid inclusions research. In: "Fluid inclusions: analysis and interpretation", I. Samson, A. Anderson and D. Marshall, eds. Mineralogical Association of Canada, short course series, vol. 32, 175-212.
- Barnes, H.L. (1979). *Geochemistry of Hydrothermal Mineral Deposits*. 2nd edition., John Willey & Sons.
- Bodnar, R.J. (1993). *Geochim. Cosmochim. Acta*, 57, 683-684.
- Borisenko, A.S. (1977). *Soviet. Geol. Geophys*, 18, 11-19.
- Brown, P.R. (1989). *Amer. Mineralogist.*, 74, 1390-1393.
- Brown, P.E. and Hagemann, S.G. (1994). MacFlinCor: A computer program for fluid inclusion data reduction and manipulation. In: "Fluid inclusions in minerals: methods and applications", B. de Vivo and M.L. Frezzotti, eds. Virginia Polytechnic Inst. State University, Blacksburg VA, 231-250.
- Burke, E.A.J. (2001). *Lithos* 55, 139-158.
- Burruss, R.C. (2003). Raman spectroscopy of fluid inclusions, In: "Fluid inclusions: analysis and interpretation", I. Samson, A. Anderson and D. Marshall, eds. Mineralogical Association of Canada, short course series, vol. 32, 279-289.
- Cauzid, J., Philippot, P., Somogyi, A., Ménez, B., Simionovici, A. and Bleuet, P. (2006). *Chem. Geol.*, 227, 165-183.
- De Vivo, B. and Frezzotti, M.L. (1994). *Fluid Inclusions in Minerals: Methods and Applications*. Short Course of the working group (IMA), *Inclusions in Minerals*. 377 pp.
- Diamond, L.W. (2003). Introduction to gas-bearing, aqueous fluid inclusions. In: "Fluid inclusions: analysis and interpretation", I. Samson, A. Anderson and D. Marshall, eds. Mineralogical Association of Canada, short course series, vol. 32, 101-158.
- Dubessy, J., Audeoud, J., Wilkins, R. and Kosztolanyi, C. (1982). *Chem. Geol.*, 37, 137-150.
- Fabre, C., Boiron, M-C., Dubessy, J. and Moissette, A. (1999). *J. Anal. At. Spectrom.*, 14, 913-922.
- Gagnon, J.E., Samson, I.M. and Fryer, B.J. (2003). LA-ICP-MS analysis of fluid inclusions. In: "Fluid inclusions: analysis and interpretation", I. Samson, A. Anderson and D. Marshall, eds. Mineralogical Association of Canada, short course series, vol. 32, 291-322.
- Goldstein, R.H. and Reynolds, T.J. (1994). Systematics of fluid inclusions in diagenetic minerals. *SEPM short course*, 31.
- Günter, D., Audétat, A., Frischknecht, R. and Heinrich, A. (1998). *J. Anal. At. Spectrom.*, 13, 263-270.

- Hollister, L.S. and Crawford, M.L. (1981). Fluid Inclusions: Applications to Petrology. Mineralogical Association of Canada, Ontario, Short Course Handbook, v. 6, 304 pp.
- Morales, S. (1995). Inclusions fluides appliquées a la prospection et modélisation de gisements hydrothermaux de métaux base, In: "Expert training in applied geology and environment (med-campus project)", P. Fenoll ed. Seminario Permanente Universidad Euro-Arabe, 1115-1135.
- Ni, P., Ding, J. and Rao, B. (2006). Chinese Sci. Bull., 51, 108-114.
- Potter, R.W., Clynne, M.A. and Brown, D.L. (1978). Econ. Geol., 73, 284-285.
- Roedder, E. (1984). Fluid inclusions. Reviews in Mineralogy, Mineralogical Society of America, vol. 12, 644 p.
- Roedder, E. (1990). Geochimica Cosmochimica Acta, 54, 495-508.
- Ryan, C. (1999). Nucl. Instrum. and Methods Phys. Res., B Beam Interact. Mater. Atoms, 158, 523-532.
- Samson, I., Anderson, A. and Marshall, D. (2003). Fluid inclusions: analysis and interpretation. Mineralogical Association of Canada, short course series, vol. 32, 374 pp.
- Shepherd, T.J., Rankin, A.H. and Alderton, D.H.M. (1985). A practical guide to fluid inclusion studies. Blackie & Son Ltd., Glasgow & London, 240 pp.
- Strivay, D., Ramboz, C., Gallien, J.-P., Grambole, D., Sauvage., T. and Kouzmanov, K. (2008). Nucl. Instrum. and Methods Phys. Res., B Beam Interact. Mater. Atoms, 266, 2375-2378.
- Van den Kerkhof, A.M. and Hein, U.F. (2001). Lithos 55, 27-47.
- Wilkinson, J.J. (2001). Lithos, 55, 229-272.
- Wilkinson, J.J., Rankin, A.H., Mulshaw, S.C., Nolan, J. and Ramsey, M.H. (1994). Geochim. Cosmochim. Acta, 58-3, 113-1146.
- Zhang, Y. and Franz, J.D. (1987). Chem. Geol. 64, 335-350.

Appendix 1⁶

This exercise (based on Morales, 1995) is focused on beginners working with the microthermometry of fluid inclusions. The aim is to familiarize them with the management and treatment of acquired data and its interpretation. In Table A, the results of a hypothetical microthermometric study of fluid inclusions are summarized. It can be supposed that the petrographic characteristics of these fluid inclusions suggest that all fluid inclusions belong to a unique population (primary two-phase fluid inclusions with a very similar degree of fill throughout). The following questions are proposed:

1. Which chemical composition can be assumed for the studied fluid? From which of the parameters studied can this be deduced?
2. Make a histogram of frequencies for the values of temperature for: (A) melting of the last crystal of ice, (B) melting of hydrohalite, and (C) homogenization.
3. Represent fluid inclusions from Table A on a diagram of Borisenko (1977, -in Shepherd et al. 1985-), and calculate the salinity and the Na/Ca relationship for each inclusion using the aforementioned diagram.
4. Make new salinity calculations using formulae proposed by Potter et al. (1978) and Bodnar (1993). What conclusions do you reach by comparing the results obtained by the three methods?
5. Represent data on a T_H vs. salinity diagram, using different symbols according to the Na/Ca relationship of each inclusion. Which conclusions can be reached from this diagram?
6. From the histograms obtained in paragraph 2 and the graphs obtained in paragraphs 3 and 5, can we say that the number of measures is sufficient, or is it necessary to continue the process of data acquisition? What geological interpretation can be “invented” from these graphs?
7. Choose a fluid inclusion that is considered to be representative and calculate the isochore using the formula proposed by Zhang and Frantz (1987). If a formation temperature of 450°C is assumed for the host mineral of fluid inclusion, at what pressure could fluid be trapped?

⁶ Answer to these questions and more information for interested persons to go more deeply into this kind of exercises will be sent if you write an e-mail to smorales@ugr.es

Table A. Microthermometric values obtained from a hypothetical study of fluid inclusions.

Ref.	T _{FM}	T _M	T _{MH}	T _H	Ref.	T _{FM}	T _M	T _{MH}	T _H
1	-52.0	-16.5	-35.0	402	16	-49.8	-11.1	-29.1	381
2	-53.0	-12.5	-33.0	385	17	-50.0	-10.9	-28.1	378
3	-50.2	-13.5	-32.0	391	18		-9.7	-29.1	373
4	-49.7	-13.0	-30.0	384	19		-8.8	-29.9	370
5	-52.1	-16.0	-31.5	396	20	-49.5	-10.1	-27.2	377
6	-50.4	-11.5	-32.4	385	21	-48.8	-8.8	-25.9	366
7	-49.7	-14.6	-30.4	392	22	-47.6	-8.1	-28.2	362
8	-47.8	-11.3	-32.6	381	23		-7.5	-28.1	363
9	-48.7	-14.7	-33.9	397	24		-8.1	-25.5	361
10	-52.1	-12.2	-29.1	381	25		-7.5	-25.4	358
11	-51.5	-11.2	-30.3	383	26	-48.9	-2.0	-24.1	301
12	-50.4	-15.4	-32.6	398	27	-46.9	-9.2	-32.2	371
13	-49.9	-12.6	-31.1	387	28	-48.9	-7.2	-26.1	358
14	-48.8	-10.4	-30.3	380	29		-6.4	-25.2	344
15	-47.9	-9.6	-30.7	377	30		-6.0	-25.0	348

Calculation for salinity

$$\text{Salinity (\% wt.)} = 1.76958T_m - 4.2384 \cdot 10^{-2}T_m^2 + 5.2778 \cdot 10^{-4}T_m^3 \quad (\text{Potter et al., 1978})$$

$$\text{Salinity (\% wt.)} = 1.78T_m - 0.0442T_m^2 + 0.000557T_m^3 \quad (\text{Bodnar, 1993})$$

Calculation for isochores (Zhang and Frantz, 1987)

$$P = A_1 + A_2T$$

$$A_1 = 6.100 \cdot 10^{-3} + (2.385 \cdot 10^{-1} - a_1)T_h - (2.855 \cdot 10^{-3} + a_2)T_h^2 - (a_3T_h + a_4T_h^2)m$$

$$A_2 = a_1 + a_2T_h + 9.888 \cdot 10^{-6}T_h^2 + (a_3 + a_4T_h)m$$

ABBREVIATIONS

T_{FM}: Eutectic temperature
T_M: Temperature of melting of last crystal of ice
T_{MH}: Temperature of melting of hydrohalite
T_H: Homogenization temperature
m: Molality
a₁, a₂, a₃, a₄ → Constants

	a ₁	a ₂	a ₃	a ₄
H ₂ O	2.857*10 ⁻¹	-6.509*10 ⁻²		
CaCl ₂	2.848*10 ⁻¹	-6.445*10 ⁻²	-4.159*10 ⁻¹	7.438*10 ⁻³
KCl	2.846*10 ⁻¹	-6.403*10 ⁻²	-2.306*10 ⁻¹	3.166*10 ⁻³
NaCl	2.873*10 ⁻¹	-6.477*10 ⁻²	-2.009*10 ⁻¹	3.186*10 ⁻³

INDEX

**Electron back-scattered diffraction (EBSD) in the SEM:
applications to microstructures in minerals and rocks and
recent technological advancements..... 7**

Elisabetta Mariani

TEM in Geology. Basics and applications21

Fernando Nieto García

**X-ray absorption spectroscopy in Mineralogy and in
the Earth and Environmental Sciences 43**

Jesús Chaboy Nalda

**Raman, conventional infrared and synchrotron
infrared spectroscopy in Mineralogy and Geochemistry:
Basics and applications57**

Biliana Gasharova

**Alike as two water drops: distinguishing one source of
the same substance from another83**

Clemente Recio Hernández

**Radiogenic isotopes and their applications within a
range of scientific fields111**

Kjell Bilström

**Analytical techniques applied to fluid inclusion studies:
Basics and applications133**

Salvador Morales Ruano

